STUDIES ON THE PHOTOCATALYTIC ACTIVITY OF TITANIUM DIOXIDE

Ian Muir Fraser

A Thesis Submitted for the Degree of PhD
at the
University of St Andrews

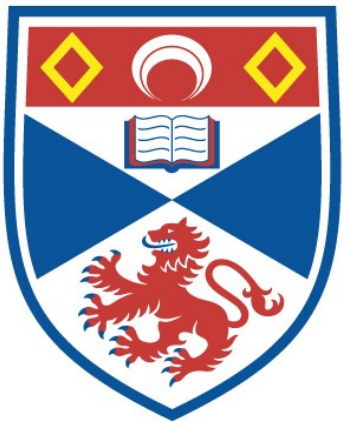

1986

Full metadata for this item is available in
St Andrews Research Repository
at:
http://research-repository.st-andrews.ac.uk/

Please use this identifier to cite or link to this item:
http://hdl.handle.net/10023/15530

This item is protected by original copyright

STUDIES ON THE PHOTOCATALYTIC ACTIVITY OF TITANIUM DIOXIDE

A Thesis

presented for the degree of

DOCTOR OF PHILOSOPHY

in the Faculty of Science of the

University of St. Andrews

by

Ian Muir Fraser, B.Sc.

United College of

St. Salvator and St. Leonard,

St. Andrews.

August 1985

ProQuest Number: 10170727

All rights reserved

INFORMATION TO ALL USERS
The quality of this reproduction is dependent upon the quality of the copy submitted.

In the unlikely event that the author did not send a complete manuscript and there are missing pages, these will be noted. Also, if material had to be removed, a note will indicate the deletion.

ProQuest 10170727

Published by ProQuest LLC (2017). Copyright of the Dissertation is held by the Author.

All rights reserved.
This work is protected against unauthorized copying under Title 17, United States Code
Microform Edition © ProQuest LLC.

ProQuest LLC.
789 East Eisenhower Parkway
P.O. Box 1346
Ann Arbor, MI 48106 – 1346

Th A341

DECLARATION

I declare that this thesis is my own composition, that the work of which it is a record has been carried out by me, and that it has not been submitted in any previous application for a Higher Degree.

This thesis describes results of research carried out at the Department of Chemistry, United College of St. Salvator and St. Leonard, University of St. Andrews, under the supervision of Dr. J.R. MacCallum since 1st October, 1982.

Ian M. Fraser

CERTIFICATE

I hereby certify that Ian Muir Fraser has spent twelve terms of research under my supervision, has fulfilled the conditions of Ordinance No. 12 and Resolution of the University Court 1967, No. 1, and is qualified to submit the accompanying thesis in application for the degree of Doctor of Philosophy.

Dr. J.R. MacCallum

ACKNOWLEDGEMENTS

I would like to express my gratitude to Dr. J.R. MacCallum for the enthusiastic support and encouragement which he has given to me during my period of study at St. Andrews.

Sincere thanks are due to my wife and my parents for their patient understanding and support which I have enjoyed throughout my university studies, both at Edinburgh and St. Andrews.

I would also like to thank the Science and Engineering Research Council and Tioxide International for the award of a Research Studentship over the period 1982 - 1985. In addition, I am indebted to Professor P.A.H. Wyatt and Professor Lord Tedder for the provision of research facilities. Thanks are also due to Mr. R.D. Murley and Dr. T.A. Egerton of Tioxide for many interesting discussions.

Several members of the technical staff deserve special mention, namely Mr. C. Smith (Glassblower), Mr. D. Wilkie (Electronics Workshop) and Mrs. M. Smith (NMR Technician), whose assistance was much appreciated.

CONTENTS

CONTENTS

T O E L A I N E, M U M A N D D A D

For moments shared, for joys untold.

SUMMARY

A novel technique for determining the photoactivity of anatase and rutile forms of TiO_2 has been developed. This involves measurement of the rate of oxygen-uptake in the propan-2-ol/propanone dehydrogenation system, which is photocatalysed by TiO_2 particles maintained in suspension. The system has been studied under several experimental conditions, including the variation of incident light intensity and sample temperature.

The effect of varying the alcohol concentration on the oxygen-uptake rate has been studied and found to be related to the self-association properties of the alcohol, as determined from a series of NMR studies. In addition, strong organic bases have been shown to be effective in reducing the oxygen-uptake rate and a mechanism involving the blocking of surface sites on TiO_2 is proposed.

The generation and participation of H_2O_2 in the alcohol to ketone conversion has been studied and, in particular, a technique has been developed to enable the luminescence, which has been observed to emanate from the vortex of the irradiated suspension, to be studied under various experimental conditions. This technique revealed the rapid nature of the interaction of H_2O_2 at the TiO_2 surface. The overall mechanism of the photocatalysed dehydrogenation is discussed in terms of two interdependent pathways: one involving oxygen, the other H_2O_2.

Photoluminescence from dry, powdered samples of anatase and rutile has been observed at low temperatures upon excitation with a pulsed nitrogen laser. The decay kinetics of the photoluminescence have been modelled via computer fitting techniques and the participation of two sets of trapping sites is postulated for anatase and rutile.

The photophysical behaviour of benzophenone in poly(methylmethacrylate) films has been studied and a dual pathway for triplet deactivation, involving delayed fluorescence and triplet-triplet annihilation put forward.

CHAPTER 1

1 OXYGEN-UPTAKE STUDIES OF TITANIUM DIOXIDE SYSTEMS

1.1 Introduction

Titanium dioxide (TiO_2) is used extensively as an inorganic pigment in the paint and plastics industries. Pigments, which may be organic or inorganic in origin, may be defined as solid materials, in the form of small discrete particles, which are incorporated into, but remain insoluble in, the paint or plastic media.

A pigment functions in two main ways to improve the appearance of the polymeric material into which it is dispersed. Firstly, it can impart colour into the system and secondly, the pigment, being a particulate dispersion, can render the material opaque. The degree of opacity conferred depends on the light scattering properties of the pigment, which in turn are influenced largely by particle size.

Due to its inherent compact crystal structure, TiO_2 possesses a high refractive index (2.55-2.71 depending on crystal form). The higher the refractive index, the greater the opacifying power of the pigment. Thus, TiO_2 compares highly favourably with other white, inorganic pigments eg. zinc oxide (2.0) and white lead (2.0).

The health problems associated with the use of certain pigments, notably white and red lead, have caused increasing concern in recent years. Since TiO_2 is a fairly inert material, it is relatively non-toxic. As a result, this pigment is finding increasing use in the food packaging industry in addition to superseding the use of more toxic pigments in paint media. It is clear, therefore, that TiO_2 possesses several advantages over alternative pigment materials and this is borne out by an examination of the TiO_2 consumption by the USA plastics industry shown in Table 1.1.

Table 1.1: Pigment and Dye Consumption in Plastics by USA (1981)[1]

	Colourant	Consumption (tonnes)
INORGANIC	Titanium Dioxide	102,000
	Iron Oxide	3,500
	Others	7,500
ORGANIC	Carbon Black	30,000
	Others	5,000
	Dyes	2,500
TOTAL		150,000

1.1.1 Preparation of Titanium Dioxide

Pigmentary grade TiO_2 can be prepared in two ways, namely by the sulphate or the chloride processes. In the sulphate process (1918), the ore ilmenite, $FeO.TiO_2$, is dissolved in sulphuric acid and the resultant solution of titanium sulphate is hydrolysed by boiling to produce a hydrated oxide, with the iron remaining in solution. The oxide is then calcined at approximately 1300 K to form the TiO_2 pigment. By careful control of the precise calcination conditions, both the crystal type and particle size can be tailored to suit particular requirements.

The chloride process is the more modern production method (1949), although manufacturing aspects make it the more technically difficult of the two routes. With this process mineral rutile, an impure form of TiO_2, is reacted with chlorine to form the liquid titanium tetrachloride ($TiCl_4$) and this, after purification, is oxidised under carefully controlled conditions to produce TiO_2. By adjusting the oxidation conditions, both the crystal form and the particle size of the pigment can be controlled.

1.1.2 Structure of Titanium Dioxide

Three crystalline forms of TiO_2 have been identified. These are: rutile, anatase and brookite. All three are found in nature. Both anatase and rutile possess crystal structures which consist of titanium ions octahedrally coordinated to six oxygen ions, as shown in Figure 1.1.

The main structural difference between anatase and rutile lies in the fact that the axial bond length ("a" in Figure 1.1) is slightly shorter in anatase than in rutile (196 pm and 198 pm respectively)[2]. The packing arrangements have been identified as being hexagonal for rutile and cubic for anatase[3].

1.1.3 The Photochemical Behaviour of Rutile and Anatase

Despite the great advantages of using TiO_2 pigments in paint and plastics systems, they possess one major detrimental feature. Through the passage of time, pigmented polymer materials exposed to the atmosphere undergo a chemical breakdown. It is widely accepted that the presence of the TiO_2 can enhance this degradation process in which the surface of the polymeric material is gradually eroded to expose the pigment particles[4]. This phenomenon is known as "chalking". Surface erosion can proceed by washing the pigment away from the

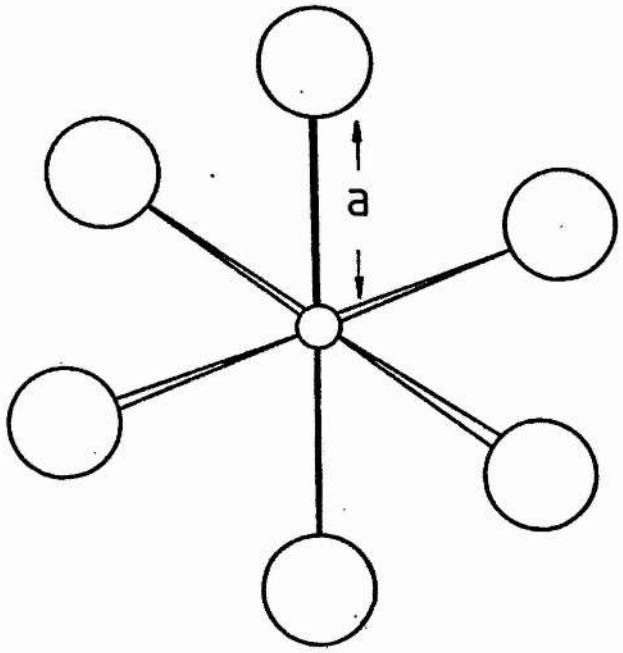

Figure 1.1 Co-ordination of ions in TiO_2

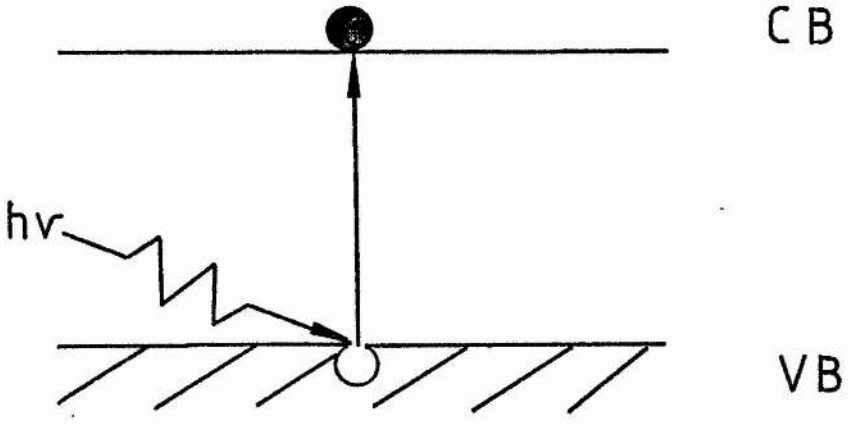

Figure 1.2 Semiconductor photoexcitation

○ = hole ● = electron

VB = Valence Band

CB = Conduction Band

surface as a result of atmospheric precipitation. The degradation process can then continue, leading to further breakdown of the freshly exposed surface. In the case of painted surfaces, therefore, the appearance would suffer considerably and, more importantly, the material which the paint was supposed to be protecting could eventually be exposed to the atmosphere itself. Plastic materials on the other hand, could have their mechanical properties seriously affected in the event of extreme surface erosion.

A great deal of effort has been expended in recent years in order to gain an understanding of the factors responsible for the chalking process, so as to minimise its effects[5]. It has become clear that several features must be present for the chalking process to occur. These are as follows:

1) Exposure by Light of a Suitable Wavelength

It has been shown that light must be present in order for the enhanced degradation of the surface, mediated by TiO_2, to occur. Further, the wavelength range of the impinging light is crucial. Only light of wavelength less than a certain value (ca. 385 nm for anatase and 415 nm for rutile) is effective. Use of light of greater wavelengths has been shown to result in a dramatic tailing-off in the rate of chalking[6]. This wavelength dependence relates directly to the semiconductor properties of TiO_2 and, in particular, to the absorption band edge of the material. The absorption edge of anatase is greater than that of rutile and this is consistent with the higher energy photons required to initiate the chalking process with anatase

pigment. A simplified energy level diagram is shown in Figure 1.2. It is now generally accepted that photon capture and subsequent exciton formation are necessary prerequisites for the chalking process.

2) The Presence of Oxygen

Experiments have been carried out by several groups to examine the effect of excluding oxygen from irradiated polymer materials[7]. It was found that exclusion of oxygen - effected by irradiating the samples in a nitrogen atmosphere - led to the cessation of the chalking process. On subsequent admission of oxygen, the surface erosion commenced. The extent of chalking observed in these cases was determined by weight loss measurements.

3) The Presence of Water

Volz et al.[8] were the first workers to establish that the presence of a trace of water is essential for the chalking mechanism to operate. They found that water vapour was able to diffuse readily into their pigmented test samples and hence care had to be exercised in order to permit only air (or oxygen) into their weathering instrument. These workers showed that if water vapour was completely excluded, then the chalking did not occur - even in the presence of oxygen.

1.1.4 Differences in Photoactivity Between Anatase and Rutile

In all cases, when considering pigmented polymer systems, the anatase form of TiO_2 has been found to be more photoactive - ie produces chalking at a higher rate - than rutile. In order to understand how this difference affects the structure of the pigmented polymer surface, it is necessary to consider the different degradation processes occurring.

If a polymer sample containing no pigment is exposed to near UV radiation (ie of wavelength less than ca. 400 nm), it will undergo a slow photodegradative breakdown. Many proposals have been put forward as mechanisms for this process, suggesting the presence of carbonyl impurities[9], free radicals[10], singlet oxygen[11,12] and catalyst residues[13,14]. As an example, a generally accepted mechanism for the photo-induced degradation of PVC is shown in Figure 1.3. It is clear, however, that the UV degradation of polymers in general is a complex process.

On introducing TiO_2 as a pigment dispersed in a polymer, the photodegradative behaviour becomes more complicated. In this situation, the UV degradation process mentioned above will still apply. In addition, however, there will be an extra contribution to the overall extent of photodegradation attributable to the pigment itself.

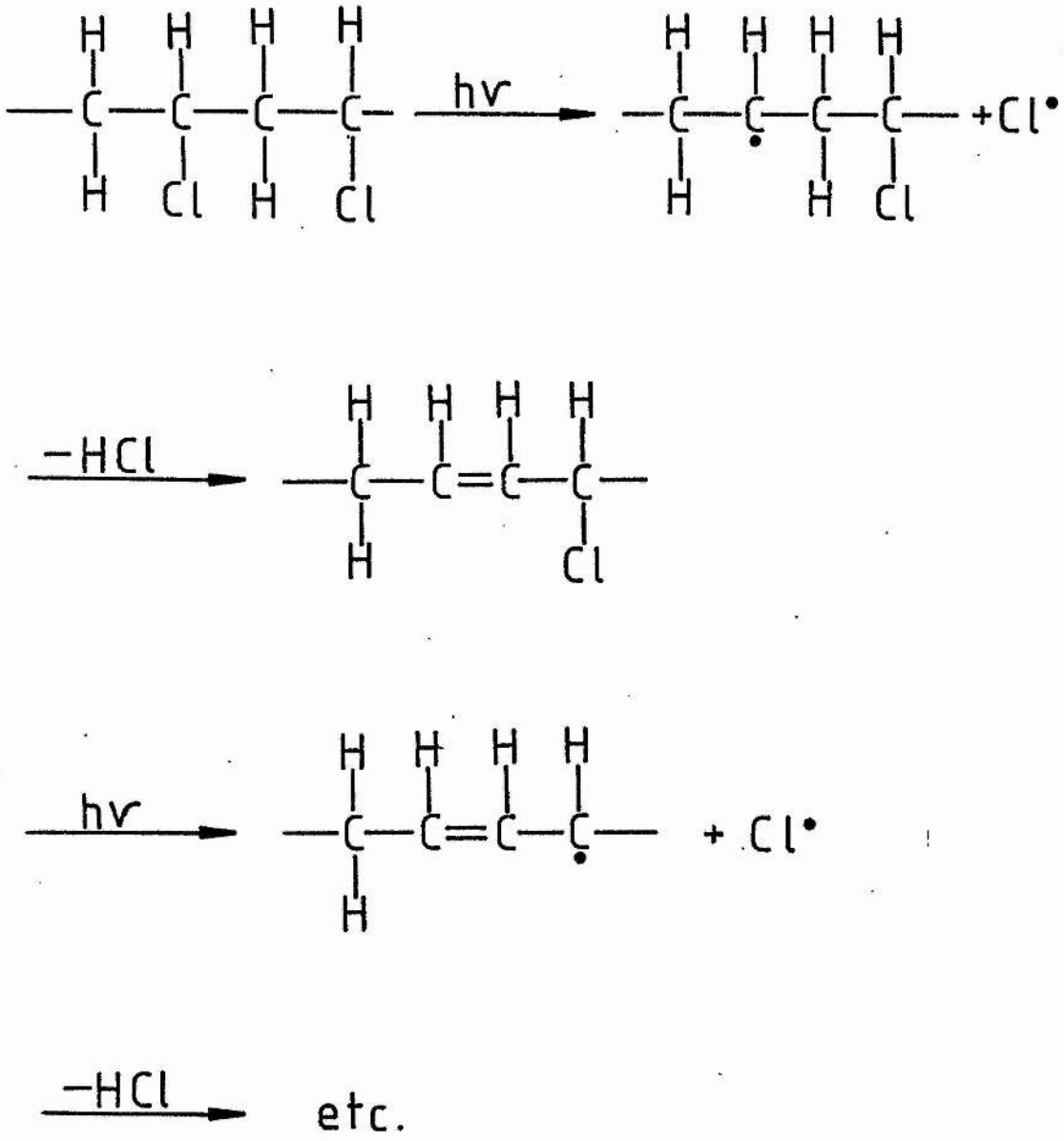

Figure 1.3 Photodegradation of PVC

For polymer systems incorporating anatase pigments, it has been found that the degradation induced by the pigment particles proceeds at a higher rate than that due to the "normal" UV degradation[15,16]. In this case, therefore, the polymeric material in the immediate vicinity of the pigment particles degrades faster than the adjacent regions of polymer which have no anatase in their immediate vicinity. The combined effects of these processes manifests itself in a surface "pitting" of the material. This is illustrated in Figure 1.4.

The use of rutile leads to a different pattern of surface erosion in polymer systems to that experienced with anatase. With rutile, the rate of photocatalysed degradation is generally less than that of the "normal" UV degradation acting on the polymer directly[17]. Hence, in this case, the polymeric material surrounding a particle of rutile may actually be screened from the relatively more destructive effects of direct UV exposure. By contrast, those polymer regions which are free of any nearby particles will be degraded to a greater extent. In terms of the pigmented polymeric surface, the topography takes on a "pedestal" structure, as shown in Figure 1.5. The regions of polymer underneath each exposed pigment particle is protected to a certain extent by the shadow which it casts.

As a consequence of their different photocatalytic behaviour, it is clear that anatase pigments are unsuitable for plastics or paint applications in situations in which they are exposed to strong sunlight. In practice, rutile pigments are now used almost exclusively in exterior paint applications. However, because of its

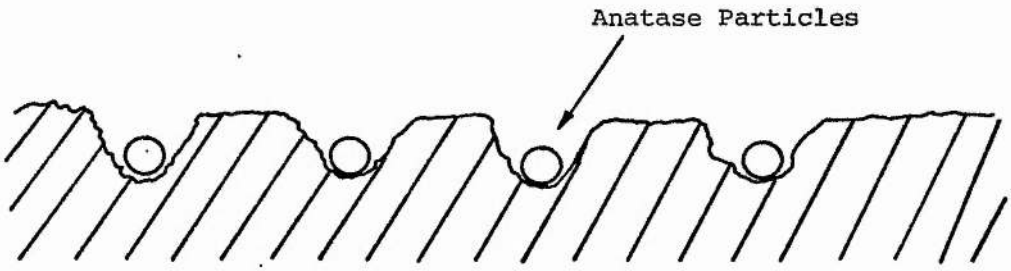

Figure 1.4 Pitting of Polymer Surface mediated by anatase

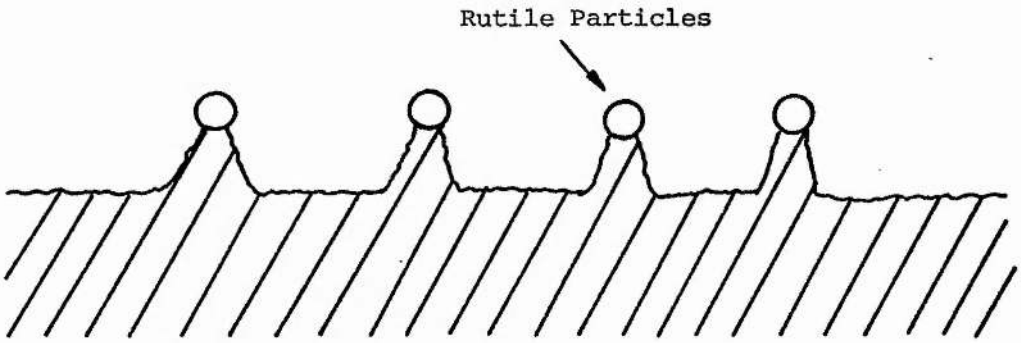

Figure 1.5 Pedestral structure of Polymer Surface incorporating rutile

high level of brightness, anatase is still widely used - chiefly in the fibre, paper and printing ink industries.

1.1.5 Measuring the Extent of Polymer Photodegradation

Many different chemical and physical methods have been applied in the determination of the extent of degradation. The simplest approach consists of visual observations of the features associated with a photodegraded polymer surface and given as the extent of degradation per unit surface area[18]. Examples are shape and size of surface cracking; size and frequency of blistering and loss of gloss (particularly relevant to paint samples).

Clearly, any assessment of the extent to which TiO_2 pigment is involved in polymer photodegradation is a complicated process. This is because the polymer itself can undergo photochemical breakdown in the absence of any pigment, due to direct action of near UV light. Furthermore, as mentioned previously, rutile can act as a photostabiliser in a polymer under certain circumstances. Hence the effect of the TiO_2 itself in the degradation of a particular material must be assessed by applying the visual tests mentioned above to two samples of the same polymer - with one containing the pigment. The difference in the extent of photodegradation, between the test samples after exposure, thus gives a measure of the degree of sensitisation (or stabilisation) exerted by the pigment alone. However, this is

clearly a very rudimentary and qualitative approach.

Pigmented polymer samples may be tested to determine the extent of chalking. One simple, standardised, method is the so-called "chalk retention" test. In this technique, a section of black cloth is drawn over an exposed sample of pigmented polymer. The more extensive the white stain, the greater the amount of chalking. The cloth can then be compared with photographic standards and a chalk retention rating assigned (ASTM D659-74).

1.1.6 Monitoring the Photodegradation of Pigmented Polymers

it is clear that with the widespread, ever-increasing number of uses to which polymers are being introduced and the extensive use of TiO_2 as the most important pigment in these systems, there has been and remains, a strong need to study and understand the behaviour of these materials. The aims of monitoring the pigmented polymer materials are two-fold. Firstly, an effective experimental method developed to monitor the deterioration in a sample may yield information regarding the mechanism of the various processes involved. Secondly, information may be gained which could be used to predict the behaviour of the sample on exposure to certain atmospheric conditions, over a long period of time. Techniques used to follow the photodegradation of polymer samples fall into two categories:

(1) Outdoor Testing Methods

One of the major problems associated with the exterior testing of weatherability is that the extent of degradation depends very strongly on the geographical location and the elevation above sea level of the sample. In addition, consistency of weathering results is difficult to achieve unless long periods of exposure (ca. 3-5 years) are employed. The reason for this is that climatic conditions can vary to a very large extent and hence, only through prolonged exposure can any averaging-out of the environmental effects be observed.

An alternative method of testing the weatherability of pigmented polymer samples is to place them in a relatively constant atmospheric environment experiencing strong sunlight, eg. desert regions. The advantage here is that the severe conditions lead to an accelerated photodegradation and hence the testing need not be over such a long period of time.

In recent years, a system has been developed for rapid evaluation of sample photodegradative performance[19,20]. This device is capable of tracking the path of the sun and focusing its radiation onto the polymeric test samples by means of a series of angled mirrors. Intensity enhancements of up to ten fold, relative to conventional exposure, have been achieved and simulation of the effects of precipitation can be obtained by a series of water sprays. However, an important limitation to the use of accelerated weathering equipment is that due to the extreme conditions, photodegradation may occur via

a different mechanism to that observed in natural conditions.

(2) Indoor (laboratory) Testing Methods

Several devices have been developed to mimic the natural atmospheric environment in the laboratory. In general, these provide for the accelerated weathering of pigment containing polymer samples. In the case of the "Weather-Ometer", for example, samples are coated onto slides which are then suspended around the inside of a large cylindrical drum[21]. A carbon-arc discharge, contained in a pyrex sleeve, is used as the source of strong, near UV radiation. Provision is made for spraying the samples with water at variable time intervals to produce rainfall simulation. Finally, the drum can be rotated, to produce an averaged weathering environment for the slide samples.

Because of the difficulties associated with controlling the various weathering parameters exactly and since the intensity of the carbon arc source may alter through time, the same sample tested on two different machines may lead to differing extents of degradation. A further complication is the fact that the spectral distribution of the carbon arc is only an approximation to that of natural sunlight. To circumvent this problem, the xenon lamp has been adopted in many weathering devices. The output of this lamp follows the wavelength range of the sun at ground level and has the additional advantage of requiring much less power to operate than a carbon arc light source[22].

1.1.7 Direct Measurement of TiO_2 Photoactivity

The techniques mentioned in the previous section can provide data of a general nature regarding the useful lifetime of a given polymer sample containing a certain pigment type. However, these techniques can yield little information regarding the mechanism of the photocatalysed degradation. In addition, the complicated structure of the artificial weathering devices with the large number of parameters under control means that reproducible results are difficult to achieve. To overcome these problems, a departure was made from the conventional weathering techniques. It was established by G. Irick[23] that a good correlation existed between photodegradation rates of pigmented polymers and the rates of dehydrogenation of propan-2-ol to form propanone, photocatalysed by TiO_2. More specifically, this researcher found that the activity series of several different TiO_2 grades (including rutile and anatase forms) was the same for both alcohol conversions and polymer photodegradations.

The propan-2-ol/TiO_2 photocatalytic system has been the subject of a great deal of research in recent years. Most of this work has been carried out by studying the vapour phase adsorption/desorption behaviour of species on the TiO_2 surface using infrared spectroscopy to monitor the progress of the reaction[24]. G. Munuera and F.S. Stone[25] used the technique of temperature programmed desorption (TPD) to study the relative strengths of adsorption of the vapour phase reactant and product (propan-2-ol and propanone respectively). These workers were thus able to show that the alcohol was much more tightly

bound to the TiO_2 surface than the ketone, suggesting that once formed, this species would be readily displaced by an incoming alcohol molecule. In reality this situation would have to apply, otherwise a cessation of the photocatalysed conversion would be observed after the TiO_2 surface became covered with acetone molecules.

Several recent studies have been undertaken on the liquid phase photoconversion of propan-2-ol to propanone mediated by TiO_2[26-28]. The advantage with this system is that it is a closer model of the photocatalytic behaviour of the pigment in a polymeric environment than the vapour phase system. However, the direct adsorption/desorption techniques mentioned above can no longer be applied to the liquid phase studies and hence different methods have been adopted to gain kinetic and mechanistic information on the progress of the reaction.

The experimental apparatus in general use by the liquid phase experimentalists employs a mercury arc lamp excitation source. By using filters and/or a pyrex reaction vessel (which passes only light of wavelength greater than ca. 310 nm) it can be so arranged that only light down to the near UV range can impinge on the sample. Since pure propan-2-ol absorbs at much shorter wavelength, this ensures that the exciting light is absorbed only by the TiO_2 dispersed in the liquid medium.

The course of the liquid phase reaction has been monitored in the past by analysing the irradiated suspension at various time intervals, to establish the relative propanone concentration. These data are then used to determine kinetic information on the rate of propanone formation. Techniques adopted to ascertain the amount present have centred, almost exclusively, on the use of spectroscopic and/or chromatographic analytical methods[26-28]. Of the spectroscopic techniques, that which has been most commonly applied has been infrared spectroscopy. Aliquots of the slurry can be removed and, after centrifugation to separate the liquid from the TiO_2, the concentration of propanone may be determined by measuring the intensity of the carbonyl stretching vibration at ca. 1650 cm^{-1}.

Major limitations do, however, exist in the studies which have involved the analysis of propanone. Firstly, information gained centres around the final process in the reaction seqûence, namely that forming the propanone. The data would be of greater value if a reaction participant which was involved at an early stage of the photoconversion, could be monitored. Secondly, and more importantly, the extraction of samples from the irradiated suspension introduces a restriction on the amount of information which can be obtained in the early time period of the process; due to the finite amount of time required to remove the sample. Thirdly, the extraction of the sample involves disturbing the system and a dilemma must be overcome, since removal of a large number of samples will yield more data but this would in turn introduce a large volume change which could alter the efficiency of the system eg. light utilisation. In the light of the

limitations imposed by the propanone monitoring methods, it was decided to develop a technique for studying this system in a different and more efficient fashion.

As mentioned previously, one of the essential requirements in the photoprocesses catalysed by TiO_2 is the presence of oxygen. Measurement of the rate at which the propan-2-ol/TiO_2 system consumed oxygen would, it was hoped, yield significant mechanistic information; since esr studies on the vapour phase system have revealed that oxygen participation occurs at an early stage in the photoconversion[29]. In addition, the monitoring of oxygen-uptake affords the opportunity to study the system in a continuous and non-intrusive manner. Thus, many readings of oxygen consumption could be made after switching on the excitation source and over a short period of time.

Oxygen-uptake monitoring has been widely applied in the polymer photodegradation field after the first studies carried out by N. Grassie and N.A. Weir[30]. In this system, polymer samples - usually in the form of films - were irradiated at a constant temperature and the oxygen consumption monitored by a differential pressure manometer. It was decided, therefore, to adapt the oxygen- uptake technique to study the liquid phase propan-2-ol/TiO_2 system under various experimental conditions and using several TiO_2 grades (both anatase and rutile). It was hoped that this would lead to detailed information regarding the nature of TiO_2 involvement in this system and by inference, to practical polymeric environments. A second aim of the study was to develop a fast, refined experimental test for the photoactivity of a given TiO_2 grade.

1.2 Experimental

1.2.1 Description of the Oxygen-Uptake Apparatus

The experimental arrangement is shown in Figure 1.6. The various sections of the apparatus comprised the following:

1) Excitation

The lamp used was a medium pressure mercury arc lamp (Engelhard Hanovia, 500W) connected to one of two stabilised power supplies (Engelhard Hanovia). A ventilation system ensured adequate removal of any ozone produced as a result of oxygen photolysis. Power supply 2 produced a greater lamp intensity than power supply 1, although no attempt was made to quantify the actual difference. The power supply units compensated for the gradual fall-off in lamp output through time by supplying the lamp with a slowly increasing current. The ideal situation would thus be that in which the output of the lamp could remain constant throughout its working life.

A cylindrical housing, equipped with two sidearm excitation ports, was used to enclose the lamp. One of these was used to supply radiation to the uptake cell, whilst the other was associated with lamp intensity measurement. The intensity of lamp emission was

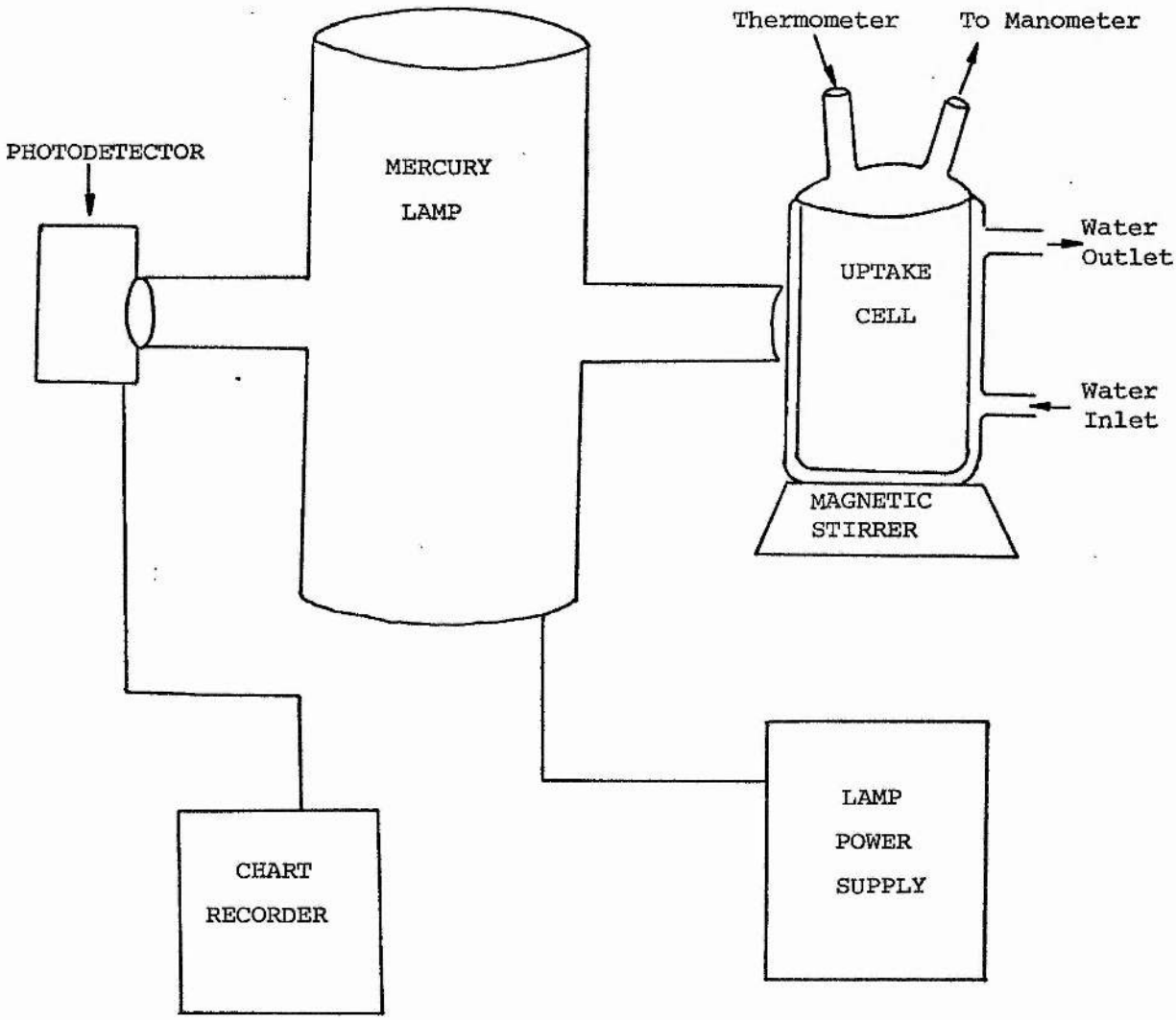

Figure 1.6 Oxygen Uptake Apparatus

directly and continuously monitored by attaching the housing output arm directly to a vacuum photodiode (RCA Type 935). The output of this device was connected to a chart recorder (Beckman) operating in the timebase mode. Hence the relative intensity of the excitation source could be continuously measured during the course of an oxygen-uptake experiment. In practice, the intensity was found to vary by less than +/- 2%.

2) Oxygen-Uptake Cell

The vessel itself was constructed of pyrex; thus only radiation of wavelength greater than ca. 305 nm could reach the slurry. One of the most important considerations in constructing a device which utilises the measurement of pressure is the optimisation of temperature stability. To this end, the cell was fitted with an integral pyrex water jacket. Circulating water was supplied from a thermostatic bath (Grant Instruments Ltd.). To prevent the accumulation of dust particles inside the water jacket - thus decreasing the efficiency of transfer of radiation into the cell - a glasswool filter was placed in the water input hose feeding the jacket.

Temperature regulation of the slurry to be tested was controlled by adjusting the thermostatic bath temperature. A magnetic stirrer (Voss Instruments Ltd.), operating at a constant 1700 rpm, provided for efficient heat transfer between the water jacket and slurry and activation of the slurry itself. In addition, the stirring ensured equilibration of oxygen molecules between the gas and liquid phases.

Once thermal equilibration was achieved, the sample temperature could be maintained with an uncertainty of ca. +/- 0.5 K. In addition, the control on the water bath was calibrated such that any temperature within the range 318 K down to room temperature could be attained.

Sample components were added to the uptake cell via a B14 size ground glass socket (Quick-Fit). A mercury thermometer was then inserted into this socket, in order that the slurry temperature could be obtained directly.

1.2.2 Oxygen-Uptake Measurement

The manometer system consisted of a U-tube, the length of each arm being ca. 80cm. The diameter of the capillary inside the tube was 0.2cm. Thus small changes in volume could produce large deflections in manometer level.

The fluid used in the manometer, throughout the series of oxygen-uptake experiments, was analytical grade propan-2-ol (Fisons). One arm of the U-tube was connected to a B10 size ground glass socket (Quick-Fit), while the other was attached to a tap. This was opened prior to an experiment, in order to level the manometer fluid in each arm of the U-tube. During the uptake run, the tap remained closed. Air was used as the oxygen source for the manometer system. Finally, the U-tube itself was attached to a wooden ruler to facilitate

manometer fluid level measurement.

1.2.3 Materials Used in Oxygen-Uptake Experiments

The pigments used in all cases were uncoated anatase or rutile grades. The main reason for this was that if coated pigments had been used, then experimental observations might have been dependent on the coating and not on the intrinsic nature of the TiO_2 itself. The anatase samples used were supplied by Tioxide International Ltd. (code CLD 1729/F) and by Aldrich. Rutile was also supplied by Tioxide (code CLD 1729/A). Propan-2-ol was of analytical grade (Fisons), while "spectrograde" cyclohexane (Fisons) was used in the alcohol dilution experiments. The surface blocking agents used were Tinuvin-770 (Ciba-Geigy Ltd.) and 1,4-diazabicyclo[2.2.2]octane (DABCO) (Aldrich).

1.2.4 Oxygen-Uptake Experimental Procedure

It was important to adopt a standardised procedure for the oxygen-uptake runs from the outset. The volume of liquid used in all cases was 100 cm^3. This meant that the gas volume above the liquid in the cell was kept very small and the liquid level maintained well

above the lamp housing arm outlet; continuous irradiation of the suspension was thus assured. The mass of the appropriate pigment used was fixed at 1g in each case. The importance of adopting standardised pigment mass:volume ratios has been emphasised by P.R. Harvey et al.[27].

The components of the sample to be tested were added to the uptake cell, with the magnetic stirrer in operation to ensure efficient suspension activation. Connection was then made between the cell and the thermostatic bath which was set at the required sample temperature. The cell itself was then covered to allow thermal equilibration in the dark. At this stage, the manometer system was levelled and connected to the cell. The mercury lamp was allowed ca. 2 hours to warm up and fully stabilise. During this period, the intensity was monitored at intervals using the arrangement mentioned previously.

At the commencement of the experiment, the cover surrounding the uptake cell was removed, thus connecting it with the lamp. Simultaneously, a stop-watch was started and readings of the manometer level were taken at approximately four minute intervals. These values were converted to give the number of moles of oxygen consumed. The experimental run was continued for a total time of sixty minutes.

1.3 The Nature of an Oxygen-Uptake Isotherm

It was established at an early stage that the appearance of the plot of oxygen-uptake with time, for a given pigment, depended on the temperature at which the experiment was carried out. Thus a series of oxygen-uptake isotherms could be obtained. A typical isotherm is shown in Figure 1.7. Each isotherm profile resolved itself into three parts:

1) Equilibration Phase (0 to ~4 mins.)

This constituted the initial region of the uptake isotherm. During this phase, the oxygen-uptake actually became negative, thus indicating an apparent increase in cell pressure. This appeared to be due to a slight heating effect, created by the infrared component of the mercury lamp. A slight rise of *ca.* 0.5 K was observed on the thermometer.

It was found that the extent of this equilibration region could be minimised by using a finer water filter. Thus the heating effect of the lamp was reduced by the resulting increase in flow rate of the water circulating in the cell jacket. However, a compromise was reached regarding the size of the filter since, if it was made too

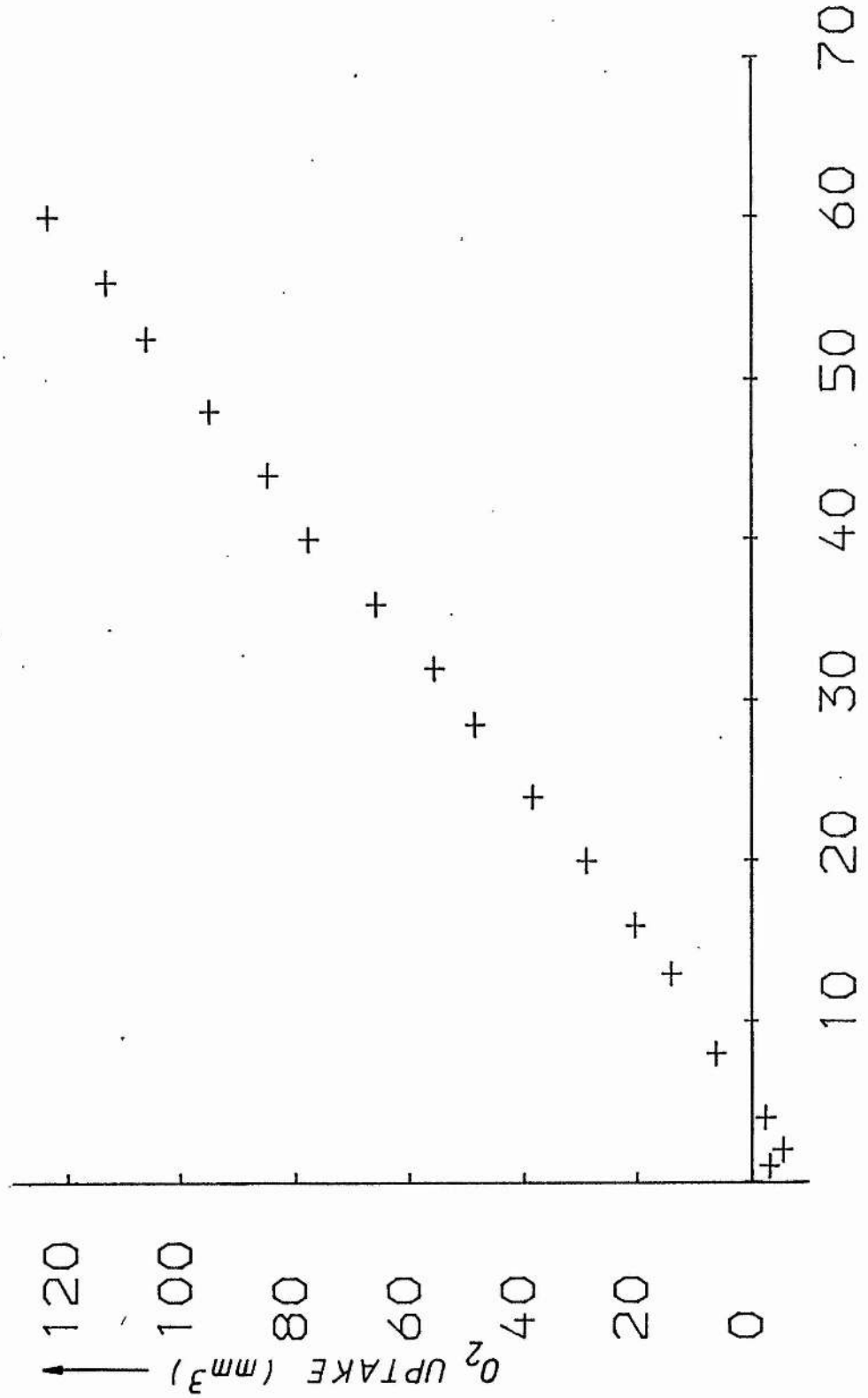

Figure 1.7

small, there was a much greater chance of contamination of the cell with dust/dirt particles from the thermostatic bath.

2) Stabilisation Phase (~4 to ~14 mins.)

This region of the isotherm was associated with a steadying of the cell temperature. From this point on, the temperature remained within the uncertainty mentioned previously. A fast increase in the rate of oxygen consumption was observed during this phase.

3) Linear Phase (~14 to 60 mins.)

Once the stabilisation of the cell temperature had been achieved, a highly linear relationship between oxygen-uptake and time was observed. This corresponds to zero order kinetics[31], ie.

$$\frac{-d[O_2]}{dt} = k \qquad (1.1)$$

More correctly, this is an apparent zero order situation, since the volume changes involved are so small that the oxygen concentration may be considered to be constant.

Thus it can be seen that the slope of an oxygen-uptake isotherm plot is directly related to the rate constant for the process. This remains true for the particular experimental parameters (lamp intensity, temperature, etc.) applicable during the uptake experiment. To standardise the analysis of the data, the slope of the uptake isotherm in the 20 - 60 min. period was chosen as the rate.

It is apparent from Figure 1.7 that the linearity of this time region is excellent and the rate was calculated by applying linear regression analysis to the slope data (see Appendix I). The correlation coefficient, r, for the linear region was always greater than 0.99. For example, the analysis of the data corresponding to the isotherm of Figure 1.7 gives:

Slope = Rate = 1.61×10^{-9} mol O_2 s^{-1};

Correlation Coefficient (r) = 1.00

(Strictly speaking, this rate applies to the experimental conditions employed - ie. 100 cm^3 of propan-2-ol per 1g of TiO_2. However, since the same pigment : volume ratio was employed throughout this work, the rate may be taken to apply to these conditions from this point on).

In addition, it was found that the same slurry sample could be used repeatedly, over a period of several days, without any significant change in the uptake rate - experimental runs being reproducible to within ca. 12%.

1.4 Variation of Oxygen Concentration

Qualitative experiments were carried out to establish the effect of variation of oxygen partial pressure on the oxygen-uptake rate for anatase. This was achieved by thoroughly purging the slurry with oxygen prior to cell equilibration. However, there were two constraints which had to be accommodated. Firstly, the nature of the cell construction made it difficult to ensure complete removal of air from the manometer system and secondly, there was no way of knowing the actual oxygen partial pressure in the cell.

A propan-2-ol/anatase (Tioxide) slurry was prepared in the usual way and an uptake run carried out in air at 298 K. The reaction was then terminated and oxygen flushed through the cell for *ca.* 15 minutes. The manometer was reconnected and the entire system left to re-equilibrate. An uptake experiment undertaken on this oxygen enriched suspension showed virtually no change in uptake rate with respect to the previous run in air (a difference of only ~1%). Figure 1.8 illustrates the lack of effect of oxygen partial pressure on the rate of uptake. The relevant rate data derived from these isotherms is given in Table 1.2. It is interesting to note that R.B. Cundall et al.[26] observed no change in the rate of propanone formation on increasing the partial pressure of oxygen with propan-2-ol/anatase slurries under similar experimental conditions.

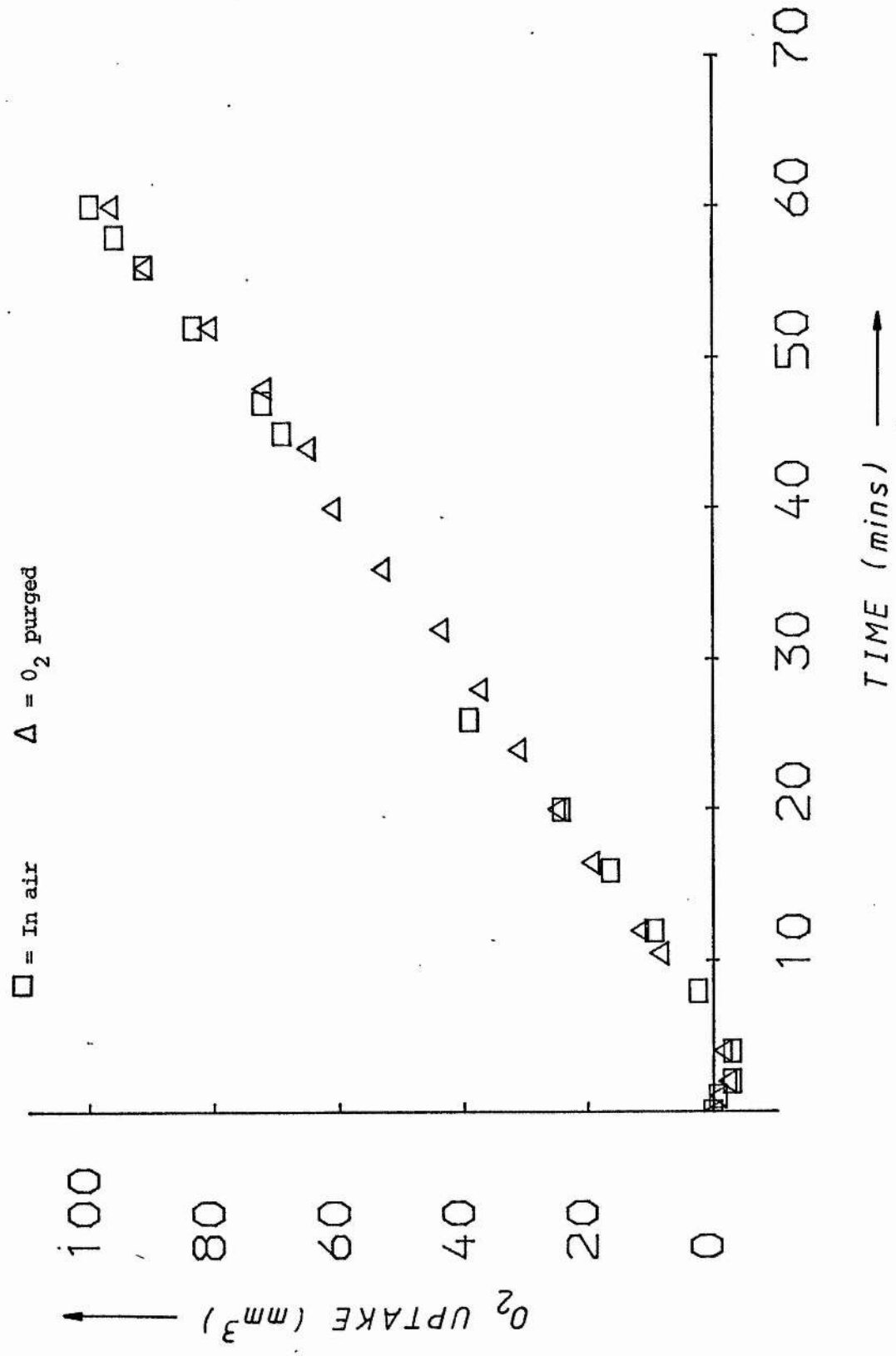
□ = In air
Δ = O_2 purged
O_2 UPTAKE (mm^3)
0
20
40
60
80
100
10
20
30
40
50
60
70
TIME (mins)

Figure 1.8

Table 1.2: Effect of O_2 Partial Pressure on Uptake Rate For Propan-2-ol/Anatase (Tioxide) Suspension at 298 K

CONDITIONS	CORR. COEFF. (r)	UPTAKE RATE (mol O_2 s^{-1})/10^{-9}
IN AIR	1.00	1.24
O_2 PURGED	1.00	1.23

1.4.1 Zero Order Kinetics

The experimental observation established in the previous section was that the rate of consumption of oxygen followed "apparent" zero order kinetics, due to the very small change in oxygen concentration during an uptake experiment. A parallel can be drawn here with the reaction of iodine in acidic aqueous acetone[32], ie.

$$CH_3COCH_3 + I_2 \longrightarrow CH_3COCH_2I + HI \qquad (1.2)$$

It has been established for this system, that if the concentration of acid catalyst is considerably greater than that of the iodine solution, the reaction is zero order - with the rate of reaction remaining constant with time and not depending on the

concentration of iodine or acetone.

1.5 The Dependence of Temperature on Oxygen-Uptake Rates

Variation of the temperature of the circulating water in the reaction vessel jacket meant that oxygen-uptake rate determinations could be carried out (after complete thermal equilibration) at any desired temperature in the range ~295 K up to ~318 K. P.R. Harvey et al.[27] studied the effect of temperature variation on the rate of propanone formation in the propan-2-ol/TiO_2 system for the temperature range 283 K - 313 K. They determined the ketone concentration at a given time by analysing 0.2 cm^3 aliquots via gas-liquid chromatography. These workers were able to determine activation energies for propanone formation of 31 kJ mol^{-1} for uncoated anatase and a large variation in activation energy values for rutile (from ~27 to ~54 kJ mol^{-1}, depending on surface treatment).

In order to determine the temperature dependence on oxygen-uptake, experiments were carried out at several temperatures for each of the uncoated TiO_2 samples, ie. the anatase (Tioxide and Aldrich) and rutile (Tioxide). In the case of the Aldrich anatase sample, power supply 1 was used with the medium pressure mercury arc lamp. As mentioned in the experimental section, this resulted in a much lower lamp output than that obtained when using power supply 2, which was used with the other two TiO_2 samples. A distinct increase

in O_2 consumption rate with temperature was observed for each TiO_2 sample. Figure 1.9 illustrates the Arrhenius plots for each TiO_2 sample, with the relevant activation energy data given in Table 1.3. Since the Arrhenius plots shown are highly linear in character, this implies the action of a single rate determining process, giving a single valued activation energy.

It is interesting to note the close similarity between the values for the activation energy obtained from the oxygen-uptake and the propanone formation rates. It thus appears that the rate determining step for both these processes is the same. A further observation which is worthy of note relates to the effect of the low lamp intensity on results obtained for the Aldrich anatase sample. Although the variation of lamp intensity will be considered in detail in a later section, it is clear at this stage that while dramatically lowering the absolute oxygen-uptake rate, the use of the lower lamp intensity gave the same activation energy (within experimental error) as the Tioxide anatase. Hence the rate determining step in the oxygen-uptake process does not appear to alter on changing the incident light intensity.

An important consideration which must be taken into account, in relation to the variable temperature oxygen-uptake rates, is the possible change in solubility of oxygen with temperature. The significance of this physical process lies in the fact that if the solubility were to vary markedly with temperature, then any apparent "activation energy" could be entirely due to the temperature profile of oxygen solubility. However, R.J. Wilcock and R. Battino[33]

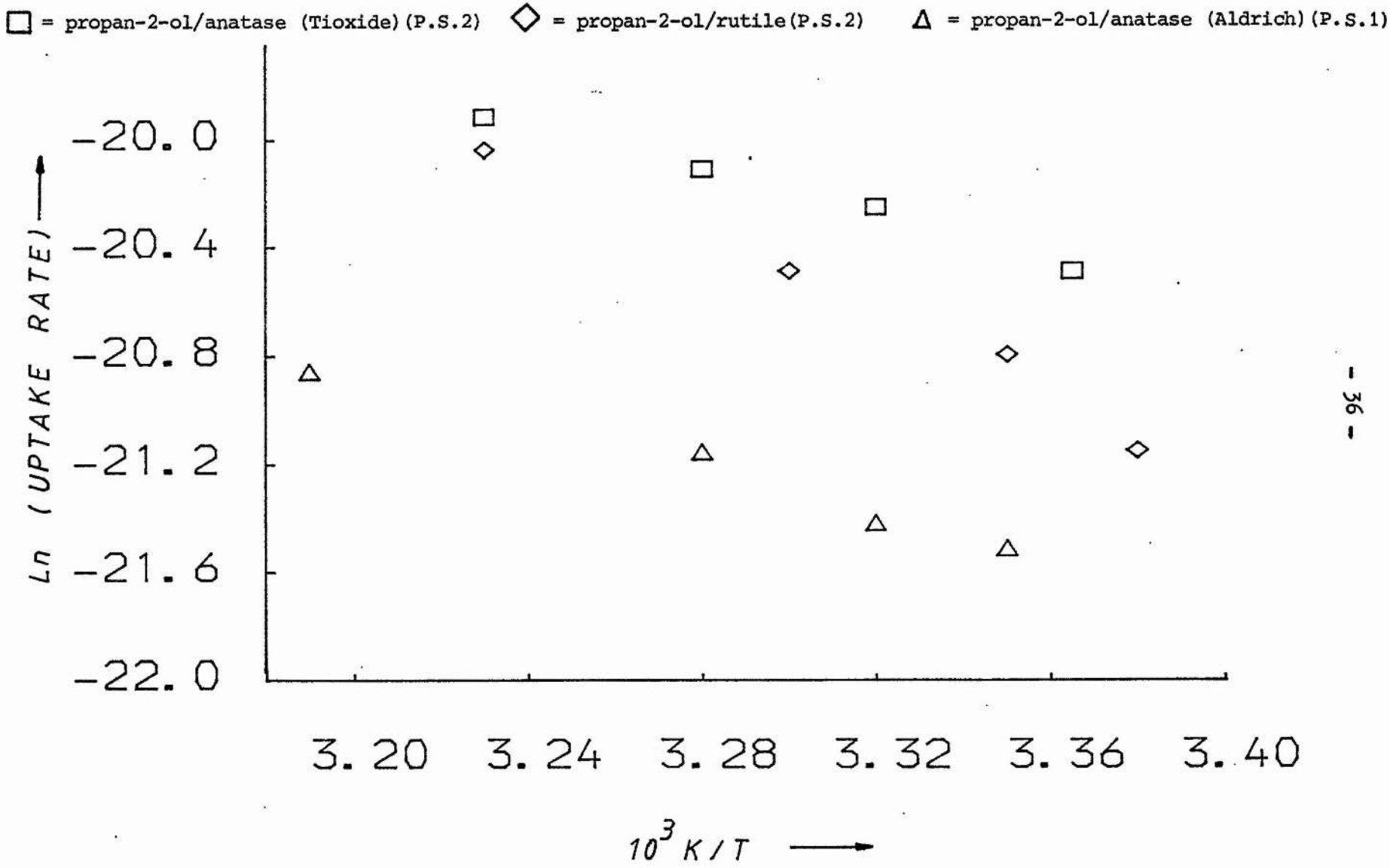
□ = propan-2-ol/anatase (Tioxide) (P.S.2)
◇ = propan-2-ol/rutile (P.S.2)
Δ = propan-2-ol/anatase (Aldrich) (P.S.1)
Ln (UPTAKE RATE) ⟶
-20.0
-20.4
-20.8
-21.2
-21.6
-22.0
3.20
3.24
3.28
3.32
3.36
3.40
10³ K/T ⟶

Figure 1.9

studied the solubility of oxygen in 1-octanol and 1-decanol and found that it varied only slightly throughout the range 283 K - 313 K. Furthermore this slight trend was such that the oxygen solubility decreased with increasing temperature. The specific values which these workers obtained were in terms of equilibrium mole fractions, which varied from 1.16×10^{-3} to 1.13×10^{-3} for 1-octanol, over the range 283.35 K to 298.13 K and from 1.26×10^{-3} to 1.24×10^{-3} for 1-decanol (over 282.74 K to 313.56 K). It is reasonable to conclude from this, therefore, that any errors in isotherm rate values due to oxygen solubility effects would be well within the experimental error.

Table 1.3

(a) Propan-2-ol/Anatase (Tioxide) (power supply 2)

TEMP (K)	10^3 /T (K^{-1})	RATE/10^{-10} (mol O_2 s^{-1})	ln(RATE)
297.2	3.37	12.7	-20.48
301.2	3.32	16.1	-20.25
305.2	3.28	18.5	-20.11
310.0	3.23	22.5	-19.91

Correlation Coefficient = -1.00; Activation Energy = 33.5 kJ mol^{-1}

(b) Propan-2-ol/Anatase (Aldrich) (power supply 1)

TEMP (K)	10^3 /T (K^{-1})	RATE/10^{-10} (mol O_2 s^{-1})	ln(RATE)
298.2	3.35	4.55	-21.51
301.2	3.32	5.01	-21.41
305.2	3.28	6.51	-21.15
313.2	3.19	8.79	-20.85

Correlation Coefficient = -0.99; Activation Energy = 35.0 kJ mol^{-1}

(c) Propan-2-ol/Rutile (Tioxide) (power supply 2)

TEMP (K)	10^3 /T (K^{-1})	RATE/10^{-10} (mol O_2 s^{-1})	ln(RATE)
295.5	3.38	6.54	-21.15
298.6	3.35	9.35	-20.79
303.0	3.30	12.7	-20.48
309.9	3.23	19.9	-20.04

Correlation Coefficient = -0.99; Activation Energy = 59.2 kJ mol^{-1}

1.6 The Effect of Light Intensity Variation on Oxygen-Uptake Rates

As mentioned previously, it has been established that the presence of light in the near UV region - specifically of bandgap energy or greater - is required for photocatalytic activity of TiO_2 to be observed. In order to confirm that this is also an essential requirement for the observation of oxygen-uptake by the system, an experiment was undertaken in which the cell was isolated from the mercury lamp. The experiment was carried out using lamp power supply 1, with anatase (Aldrich) at 298 K.

As a first stage in the experiment, thermal equilibration was allowed to proceed in the usual manner. The lamp was permitted to impinge on the sample cell and oxygen- uptake was observed to proceed normally. After 60 mins., the lamp was covered and further readings were taken. The rate of oxygen- uptake slowed down and effectively ceased after ca. 10 mins. The cell was left in the dark for a further 30 mins., during which time the manometer level remained fairly steady. On subsequent re-equilibration by the lamp on the cell, a resumption of oxygen- uptake was observed, with a rate very close to that obtained initially. The complete uptake profile for the experiment is shown in Figure 1.10 , with the corresponding relative lamp intensity - as measured on the chart recorder - superimposed.

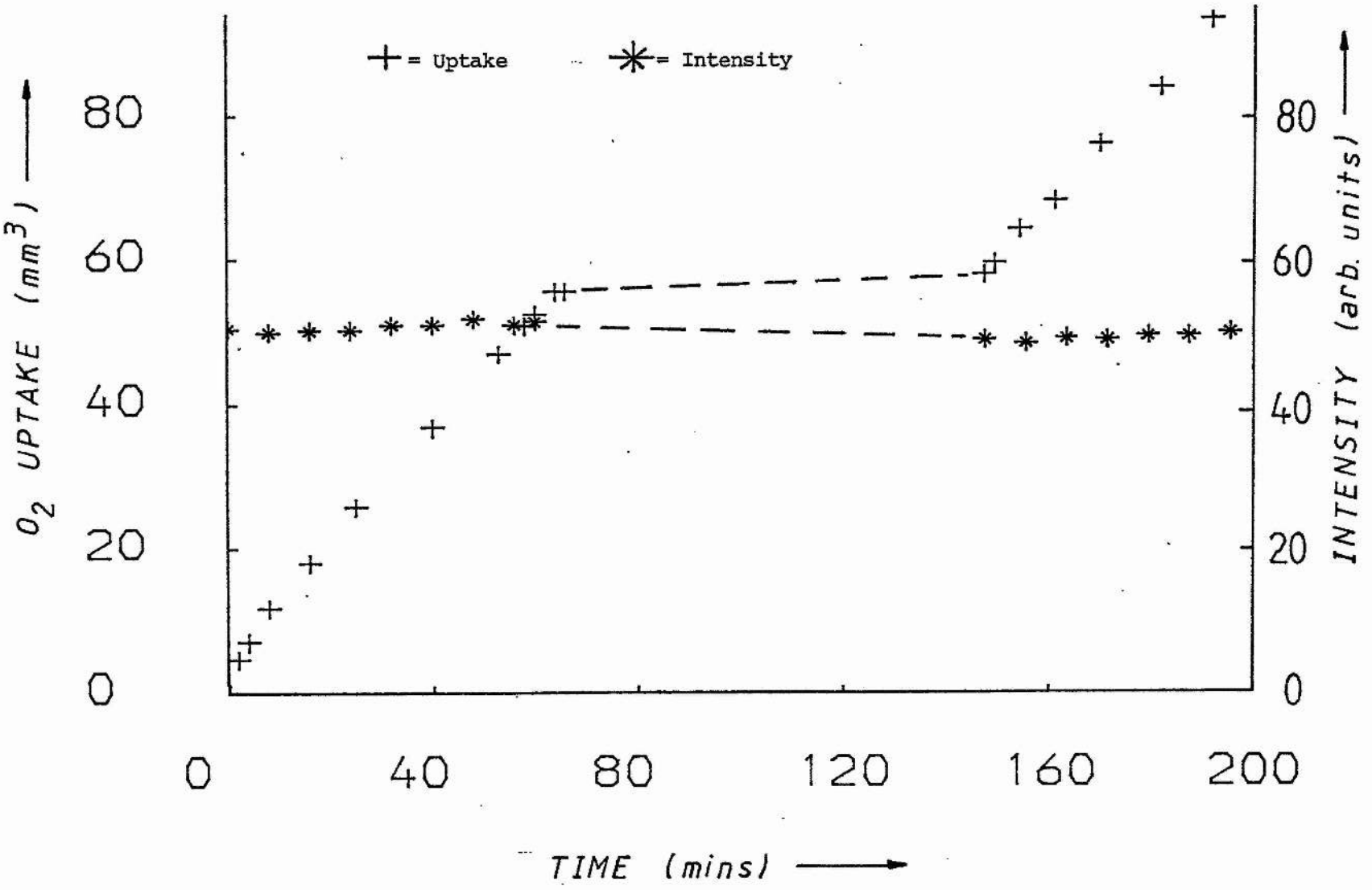
+ = Uptake
* = Intensity
O_2 UPTAKE (mm^3)
INTENSITY (arb. units)
0
20
40
60
80
0
40
80
120
160
200
TIME (mins)

Figure 1.10

Rates of oxygen-uptake, obtained from the slopes of the two separate regions of the isotherms are shown in Table 1.4.

Table 1.4: Oxygen-Uptake Rates Before and After Lamp Isolation Period

TIME REGION (Mins)	CORRELATION COEFF (r)	UPTAKE RATE (mol O_2 s^{-1})
20 - 60	0.999	5.27×10^{-10}
152 - 196	0.998	5.17×10^{-10}

Having established that near UV light is essential for the observation of oxygen-uptake by anatase, it was decided to carry out several separate experiments in which the lamp intensity was varied by a known amount, in order to gain more detailed information regarding the oxygen-uptake rate dependence on the intensity itself.

The reduction in intensity was effected by placing one of three neutral density filters (Barr and Stroud Ltd.) between the lamp and cell, normal to the incident beam. Hence four different uptake rates could be obtained (corresponding to the three filters plus a run with the full lamp intensity). However, two practical considerations had to be taken into account.

1) Heating Effect

As mentioned in the experimental section, the circulating water in the jacket surrounding the uptake cell compensated for the heating effect due to the infrared (IR) components of the mercury lamp output. This compensation accounts, at least in part, for the equilibration phase in the uptake isotherm. On placing a filter between the lamp and cell, a large proportion of the IR is absorbed by the filter itself. The effect of this on an uptake experiment was to induce a sudden drop in temperature (of ca. 0.5 K) which, in turn, produced an erroneous manometer volume change. Thermal re-equilibration of the system, initiated by the thermostatic bath, generally took ca. 3 - 5 mins. and hence this early period after insertion of the filter was excluded from uptake rate calculations.

2) Filter Non - Linearity

The neutral filters used were rated by the manufacturers as being 0.2, 0.3 and 0.5 absorbance values. From the Beer - Lambert Law, the absorbance may be given by the following expression:

$$\mathrm{Log}_{10}\left(\frac{I_o}{I}\right) = \epsilon cl = D \qquad (1.3)$$

where: I_o = Intensity of light of wavelength λ incident on a sample.

I = Intensity of light of wavelength λ after passing through

a sample.

ϵ = The molar extinction coefficient ($dm^3\ mol^{-1}\ cm^{-1}$)

c = Sample concentration ($mol\ dm^{-3}$)

l = Path length of sample (cm)

D = Absorbance (dimensionless quantity)

Obviously, in the case of glass composition filters, both the "concentration" and path length are fixed, the extinction coefficient being the only variable determining the absorbance at a particular wavelength.

The percentage transmittance through a sample (filter, solution etc.) can be obtained by rearrangement of equation (1.3):

$$\%Trans = ((10^{D})^{-1}) \times 100 \qquad (1.4)$$

In this way, the 0.2, 0.3 and 0.5 filters correspond to %Trans values of 63.1, 50.1 and 31.6 respectively. It was found that when UV/visible absorption spectra were obtained for the filters, these transmittance values held constant only for wavelengths greater than ca. 400 nm for the 0.2 and 0.5 filters and ca. 490 nm for the 0.3 case. Below these wavelength thresholds, the absorbance of the filters increased - correspondingly the %Trans decreased - in a markedly non-linear fashion. To illustrate this, the absorption

spectrum of the 0.2 filter is shown in Figure 1.11.

The region of photochemical significance, as far as the oxygen-uptake cell is concerned, is the near UV region (of ca. 300 - 420 nm). With anatase, however, the wavelength region of 390 - 420 nm is of too low an energy to induce exciton formation. In addition, from Figure 1.11 it is clear that very little radiation below ca. 320 nm will enter the uptake cell - the pyrex of the cell itself imposing a similar cut-off. Within the useful range, there are only two significant excitation lines in the medium pressure mercury lamp output: at 334 nm and 366 nm, with relative intensities of 9.3 and 100.0 respectively[34]. Thus if any dependence regarding the rate of oxygen-uptake on intensity could be found, it was thought reasonable that the variation would be with the intensities of these two lines.

Because of the problem of filter non-linearity, the genuine absorbance - and hence percentage transmittance values - had to be obtained for each of the three filters at 334 nm and 366 nm. The absorption properties of the filters, obtained from the spectrophotometer, are listed in Table 1.5.

Figure 1.11 Absorption Spectrum of "0.2" Neutral Filter

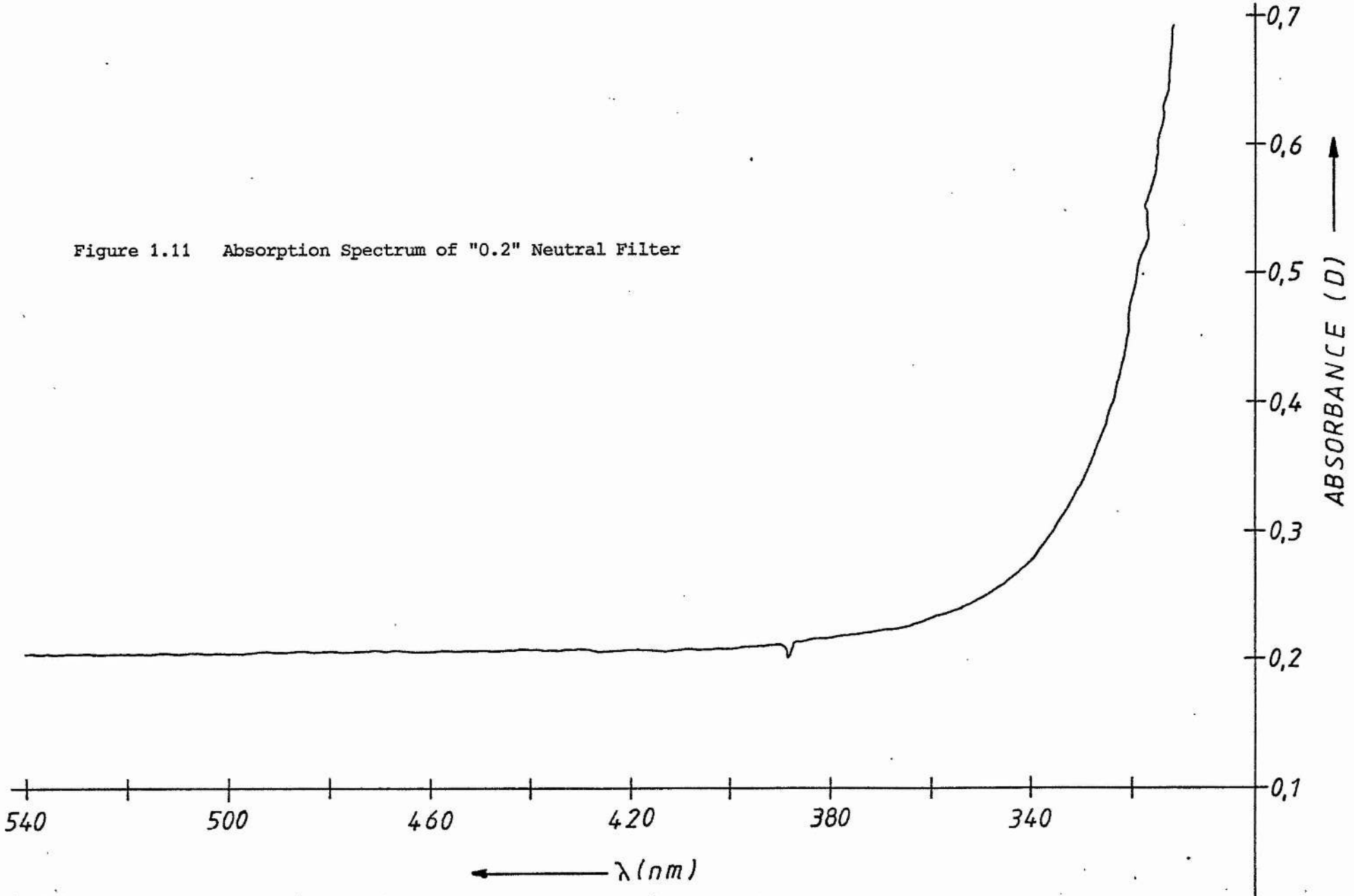

Table 1.5: Absorption Data for Neutral Filters

FILTER TYPE	ABSORBANCE		%TRANSMITTANCE	
	334 nm	366 nm	334 nm	366 nm
0.2	0.305	0.225	49.5	59.6
0.3	0.600	0.440	25.1	36.3
0.5	0.600	0.514	25.1	30.6

Absolute lamp intensity, when no filters were employed, was unknown but the relative intensity reduction on introducing a filter can be calculated; firstly by making the following assumption:

$$I_{tot} = (I_{334} + I_{366}) \qquad (1.5)$$

where I_{tot} is the total intensity of radiation incident on the uptake cell which is effective in inducing exciton formation in anatase. I_{334} and I_{366} are the intensities of radiation reaching the cell at 344 nm and 366 nm respectively. Furthermore, if a superscript of "a" is used to indicate the full lamp intensity and superscript "b" used to signify reduced intensity, after passing through a certain filter then, for example, in the case of the 0.2 filter:

$$^{b}I_{334} = {}^{a}I_{334} \times 0.495 \qquad (1.6)$$

$$ {}^{b}I_{366} = {}^{a}I_{366} \times 0.596 \qquad (1.7) $$

The next stage in the analysis of the intensity data is to take account of the greater weight attributable to the intensity at 366 nm, since this is much more intense than the line at 334 nm. Assume that the total intensity without the filters is 1.00, thus:

$$ {}^{a}I_{tot} = ({}^{a}I_{334} + {}^{a}I_{366}) = (0.09 + 0.91) \qquad (1.8) $$

Hence, again using the 0.2 filter as an example, the ratio of effective radiation intensities, before and after insertion of the filter, may be obtained from:

$$ \frac{{}^{a}I_{tot}}{{}^{b}I_{tot}} = \frac{{}^{a}I_{344} + {}^{a}I_{366}}{{}^{b}I_{334} + {}^{b}I_{366}} $$

$$ = \frac{0.09 + 0.91}{(0.09 \times 0.495) + (0.91 \times 0.596)} = 1.70 \qquad (1.9) $$

The estimated uncertainty in the final value is ca. 3%; the only error source of any significance being the absorbance values, obtained from the UV/visible spectrophotometer. The value of 1.70 corresponds to a reduction of 41% in effective radiation intensity reaching the uptake cell, after inserting the 0.2 filter into the path of the beam.

Using an identical approach to that adopted above, intensity reductions can be calculated for the 0.3 and 0.5 filters. The complete data are presented in Table 1.6.

Table 1.6: Relative Intensity Reductions for Neutral Filters

FILTER TYPE	$^{a}I_{tot}/^{b}I_{tot}$	% INTENSITY REDUCTION	RELATIVE INTENSITY
NONE	1.00	0	1.00
0.2	1.70	41	0.59
0.3	2.83	65	0.35
0.5	3.32	70	0.30

The variable intensity oxygen-uptake experiments were carried out at 301 K using anatase (Tioxide). Lamp power supply 2 was used throughout the series and hence the lamp intensity, incident on the uptake cell, was correspondingly greater than that of the previous experiment in which the lamp was isolated from the sample. In each case, oxygen-uptake measurements were taken over a ca. 45 min. period with no filter present, in order to establish the "full" uptake rate. The appropriate filter was then inserted and, after allowing re-equilibration to take place, further readings were obtained in order to determine the new rate. Separate experiments were employed for each of the three filters and, in addition, a complete run was carried out without using any of the filters. Table 1.7 lists the

results of the various uptake rate determinations, with the rates expressed both in the initial units, as observed during the experiment (mm^3 O_2 min^{-1}) and after conversion to the S.I. units of mol O_2 s^{-1}. In each case, the slopes before addition of the appropriate filter agreed to within 10% of each other.

Table 1.7: The Effect of Intensity on Oxygen-Uptake Rate

FILTER EXPT.	RATE (mm^3 O_2 min^{-1})	RATE (mol O_2 $s^{-1}/10^{-9}$)
NONE	2.61	1.78
0.2	1.95	1.33
0.3	1.64	1.12
0.5	1.50	1.02

1.6.1 Comparison of Rates and Intensities

The results above make possible a comparison between the rates of oxygen-uptake and the appropriate intensity, in order to gain detailed information regarding the intensity dependence. As a first stage, let the simplest situation be assumed to apply ie. that the rate is directly proportional to the intensity. Hence, by applying the assumption inherent to equation (1.5), this implies that:

$$\text{Rate} \propto I_{tot} \qquad (1.10)$$

and hence: $$\text{Rate} = cI_{tot} \qquad (1.1)$$

where "c" is a constant of proportionality. By using the superscript notation established in equations (1.6) and (1.7), rate and intensity ratios can be equated to give:

$$\frac{{}^{a}R}{{}^{b}R} = \frac{{}^{a}I_{tot}}{{}^{b}I_{tot}} = \frac{({}^{a}I_{344} + {}^{a}I_{366})}{({}^{b}I_{344} + {}^{b}I_{366})} \qquad (1.12)$$

These intensity ratios are shown in Table 1.6 above.

If, however, the rate of oxygen-uptake exhibits a square-root dependence on intensity, then equations (1.10) to (1.12) must be modified as follows:

$$\text{Rate} \propto (I_{tot})^{0.5} \qquad (1.13)$$

leading to:

$$\frac{{}^{a}R}{{}^{b}R} = \frac{({}^{a}I_{tot})^{0.5}}{({}^{b}I_{tot})^{0.5}} = \frac{({}^{a}I_{334} + {}^{a}I_{366})^{0.5}}{({}^{b}I_{334} + {}^{b}I_{366})^{0.5}} \qquad (1.14)$$

The rate ratios, together with intensity ratios for the linear and square root dependencies, are given in Table 1.8.

Table 1.8: Comparison of Linear and Square Root Intensity Dependence

COL. NO.	(1)	(2)		(3)	
FILTER	$\frac{a_R}{b_R}$	$\frac{a_{I_{tot}}}{b_{Itot}}$	$\frac{\text{COL.(1)}}{\text{COL.(2)}}$	$\frac{(a_{I_{tot}})^{0.5}}{(b_{Itot})^{0.5}}$	$\frac{\text{COL.(1)}}{\text{COL.(3)}}$
NONE	1.00	1.00	1.00	1.00	1.00
0.2	1.33	1.70	0.78	1.30	1.02
0.3	1.52	2.83	0.54	1.68	0.91
0.5	1.83	3.32	0.55	1.82	1.00

The ratios of the appropriately numbered columns (COL. NO.'s) shown in Table 1.8, provide a means of assessing the agreement between the rate ratios and the intensity dependencies. Thus the closer the column ratios are to unity, the better the agreement.

Table 1.8 above clearly indicates that the oxygen-uptake rate follows closely and within experimental error, a square root dependence on intensity. Furthermore, testing the agreement of other powers of dependence cannot improve on the COL.(1)/COL.(3) values shown. The agreement can best be illustrated by a plot of uptake rate against the square root of the relative intensity, derived from Table 1.6. This plot is represented in Figure 1.12. Linear regression analysis of the data yields a correlation coefficient, r, of 1.00.

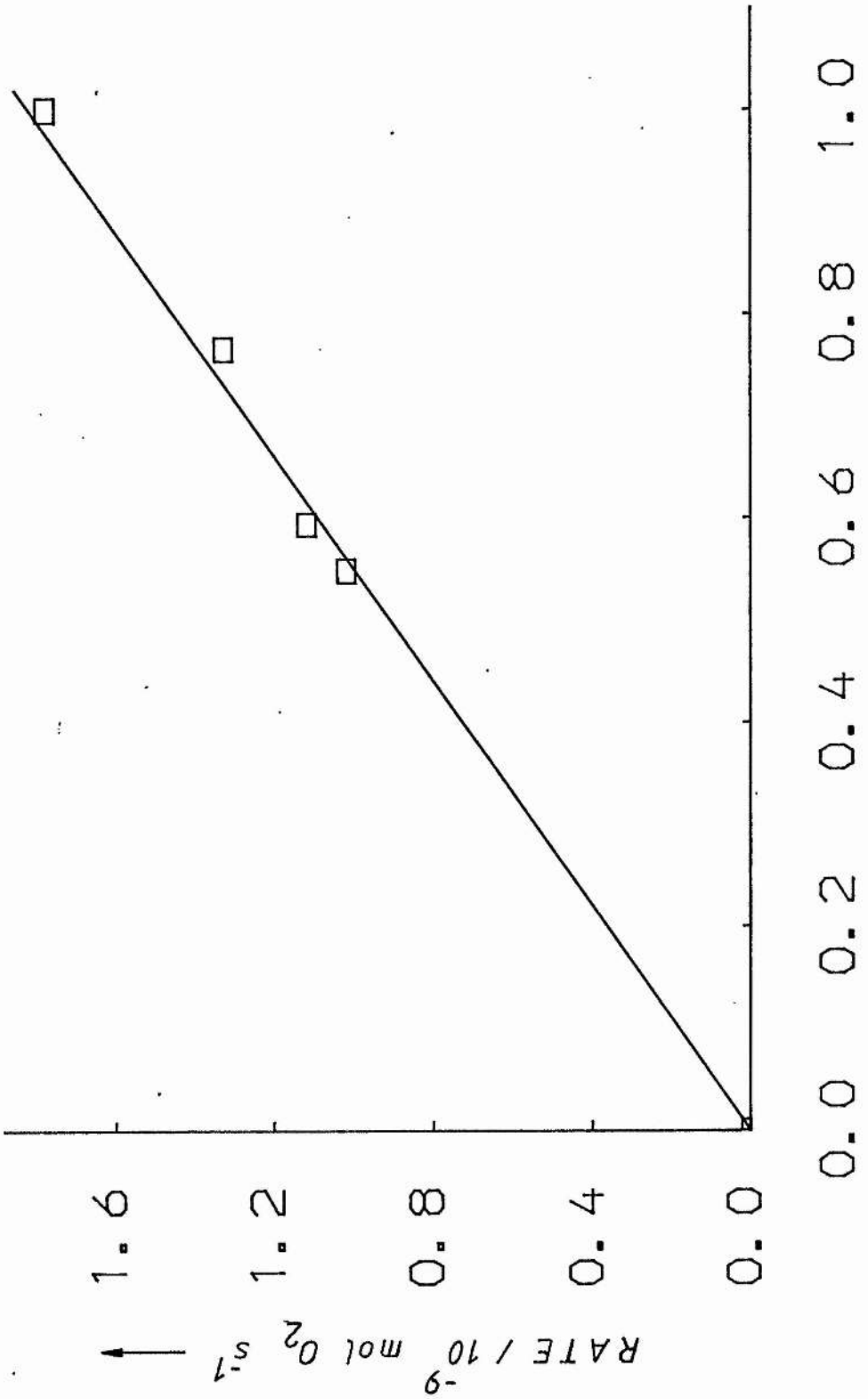

Figure 1.12

1.6.2 Analysis of the Square Root Intensity Dependence

The observation of a square root intensity dependence on the rate of propanone formation for the propan-2-ol/rutile irradiated suspension system, at high intensities, was first reported by T.A. Egerton and C.J. King[35]. The fact that we observed an $I^{0.5}$ relationship for the equivalent oxygen-uptake experiments, albeit using anatase, adds further weight to the assertion that the rate determining process for oxygen-uptake is the same as for propanone formation.

On switching-on the excitation source, excited electron and hole (exciton) formation will occur:

$$TiO_2 + h\nu \xrightarrow{k_1} e + h \qquad (1.15)$$

$$\text{Rate} = k_1 I \qquad (1.16)$$

(where h is Planck's Constant and I is the light intensity). It is generally accepted that exciton migration can then take place and the following trapping processes for the excited electron and hole species have been postulated:

$$e + O_{2\,(ads)} \xrightarrow{k_2} O_{2\,(ads)}^{-} \qquad (1.17)$$

$$h + {}^{-}OH_{(ads)} \xrightarrow{k_3} {}^{\cdot}OH_{(ads)} \qquad (1.18)$$

Competing with these processes, will be thermal electron/hole recombination:

$$e + h \xrightarrow{k_4} \text{HEAT} \qquad (1.19)$$

For the purposes of this model, reaction (1.17) or (1.18) may be considered rate determining, since exciton formation and electron/hole recombination would be expected to proceed rapidly[36]. Furthermore, it was established earlier that the rate of oxygen-uptake was independent of oxygen partial pressure for anatase, in agreement with similar observations by R.B. Cundall et al.[26] for the propanone monitoring anatase system. Thus, it appears that reaction (1.17) is also non-rate determining. By inference, therefore, let it be assumed that reaction (1.18), ie. hole trapping, is rate controlling. In addition, let the concentration of surface hydroxide ions, $[OH^-]_{(ads)}$, be considered large enough relative to the concentration of trapped holes to be treated by pseudo first order kinetics[37]. Hence, let the overall rate of oxygen-uptake be:

$$\text{Rate} = k_3[h] \qquad (1.20)$$

An expression can now be given for the steady state hole concentration:

$$d[h]/dt = 0 = k_1 I - k_3[h] - k_4[h]^2 \qquad (1.21)$$

where the assumption is made that the concentrations of excited electrons and holes are equal.

Under conditions of high intensity (I),

$$k_4[h]^2 >> k_3[h] \qquad (1.22)$$

and hence: $$k_4[h]^2 = k_1 I \qquad (1.23)$$

By rearrangement of equation (1.23), the hole concentration may be given as:

$$[h] = \left(\frac{k_1 I}{k_4}\right)^{0.5} \qquad (1.24)$$

and thus the rate of oxygen-uptake will be:

$$\text{Rate} = \left(\frac{k_3^2 k_1}{k_4}\right)^{0.5} I^{0.5} = k\, I^{0.5} \qquad (1.25)$$

T.A. Egerton and C.J. King[35] applied the treatment shown above to interpret their observed square root intensity dependence on propanone formation rate. In addition, they were also able to carry outt experiments at very low intensities, such that the electron/hole deactivation became a negligible route for exciton depletion. In this set of circumstances,

$$[h] = \frac{k_1 I}{k_3} \qquad (1.26)$$

and hence: $\text{Rate} = k_1 I$ (1.27)

These workers found that at very low lamp intensities, a linear rate dependence on intensity applied, with a square root dependence operating after increasing the excitation flux above a certain transition range.

It is clear, therefore, that a mechanism involving deactivation of holes at surface site traps is consistent with an observed rate dependence on the square root of the incident light intensity. However, this situation presumably operates with the proviso that the intensity must be sufficiently high that thermal electron/hole recombination is the dominant route for hole removal.

1.7 Blocking of Surface Sites on Anatase

In the previous section, mention was made of the participation of sites on the TiO_2 surface at which excitons, the precursors of photocatalytic activity, could be trapped. In addition, it is clear from equation (1.17) that the first stage in the oxygen consumption process may also occur at such sites. An analogy may thus be drawn with the field of enzymology. Here, reactions of a highly specific nature occur at particular sites on the enzyme surface[38]. Enzyme inhibitors, molecules which irreversibly bind at these specific sites, produce dramatic reductions in the efficiency of the enzyme to act as a catalyst.

The identification and characterisation of the nature of surface sites on TiO_2 has received considerable attention in the literature[39,40]. Defect sites on anatase, which are potential exciton traps, have been identified as being acidic[41]. Because of the great advantages to be had from reducing the photocatalytic power of TiO_2, a search was undertaken to find suitable molecules which could act as surface site blocking agents.

The class of compounds selected for this study was that of the strong organic bases. It was hoped that these materials would specifically interact with the acidic sites. Two further criteria were applied to aid the final selection of the most appropriate base. Firstly, the base itself had to be relatively stable, such that once on the surface, it would not readily decompose via any photo-induced processes involving the TiO_2. Secondly, it was very important that the bases chosen would not absorb any of the radiation entering the oxygen-uptake cell. In practice, this meant that the compounds had to possess no absorption band above ca. 315 nm. Obviously, if the bases did absorb in the near UV region, they would be competing with the TiO_2 for the incident radiation. A screening effect would then be in operation. Thus, in the event of any observed reduction in oxygen-uptake rate, it would not be known whether this was attributable to the surface blocking of sites, or simply the reduction in exciton formation due to the reduced available intensity.

Materials eventually chosen were from the hindered amine light stabiliser (HALS) class of basic organic compounds. Further application of the above selection criteria restricted the choice to two molecules: 1,4 - diazabicyclo[2.2.2]octane (DABCO) and Tinuvin - 770. The structure of DABCO is shown in Figure 1.13. T-770 is a commercial material of empirical formula - $C_{28}H_{52}O_4N_2$. These compounds have been shown to be strong chelating agents of transition metal ions[42].

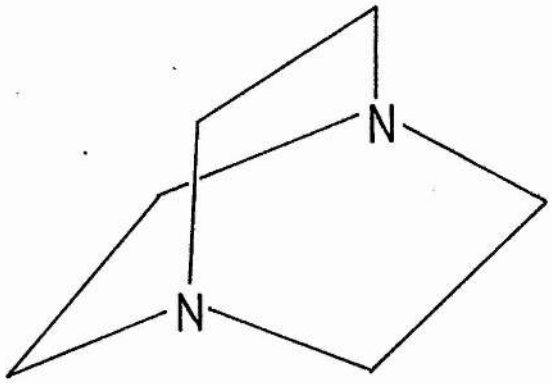

Figure 1.13 Structure of DABCO.

1.7.1 Effect of Strong Bases on Oxygen-Uptake Rates

Throughout this series of experiments, anatase (Tioxide) was used in conjunction with the full lamp intensity ie. with no filters placed between lamp and cell. Lamp power supply 2 was used in all cases. As a first step in the determination of the extent to which site blocking influences TiO_2 photoactivity, a control oxygen-uptake experiment with no added base was performed. In this way the "normal", unperturbed oxygen-uptake rate was obtained in the usual way. Thereafter, the experiment was stopped and a certain quantity of the appropriate base, DABCO or T-770, added so as to give a concentration of 1×10^{-2} mol dm^{-3} in the suspension. Oxygen-uptake measurements were then carried out as before, after full thermal re-equilibration of the system.

Dramatic reductions in the oxygen-uptake rates were observed. Figures 1.14 and 1.15 show the blocking effects on the uptake isotherms for DABCO and T-770, both at 298.5 K. The effectiveness of these bases at reducing the uptake rates can best be expressed as percentage reductions with respect to the unperturbed rate values. Such calculations reveal reductions of 69% and 61% for 1×10^{-2} mol dm^{-3} of DABCO and T-770 respectively. As a check on the reliability of these values, the DABCO experiment was repeated (at 297 K) and a rate reduction of 71% obtained. Hence both bases are capable of producing marked decreases in the photocatalytic capability of anatase, with DABCO appearing the slightly more effective of the two compounds.

To gain an assessment of the concentration dependence of the base on the oxygen-uptake rate, two other concentrations, 1×10^{-3} and 1×10^{-1} mol dm^{-3}, of DABCO were tested in the same fashion as before. These resulted in rate reductions of 46% and 82% respectively - both carried out at 298.5 K. The total results obtained at this temperature are shown in Table 1.9 and it is apparent from this that a logarithmic relationship between DABCO concentration and uptake rate is applicable - although only three data points are available.

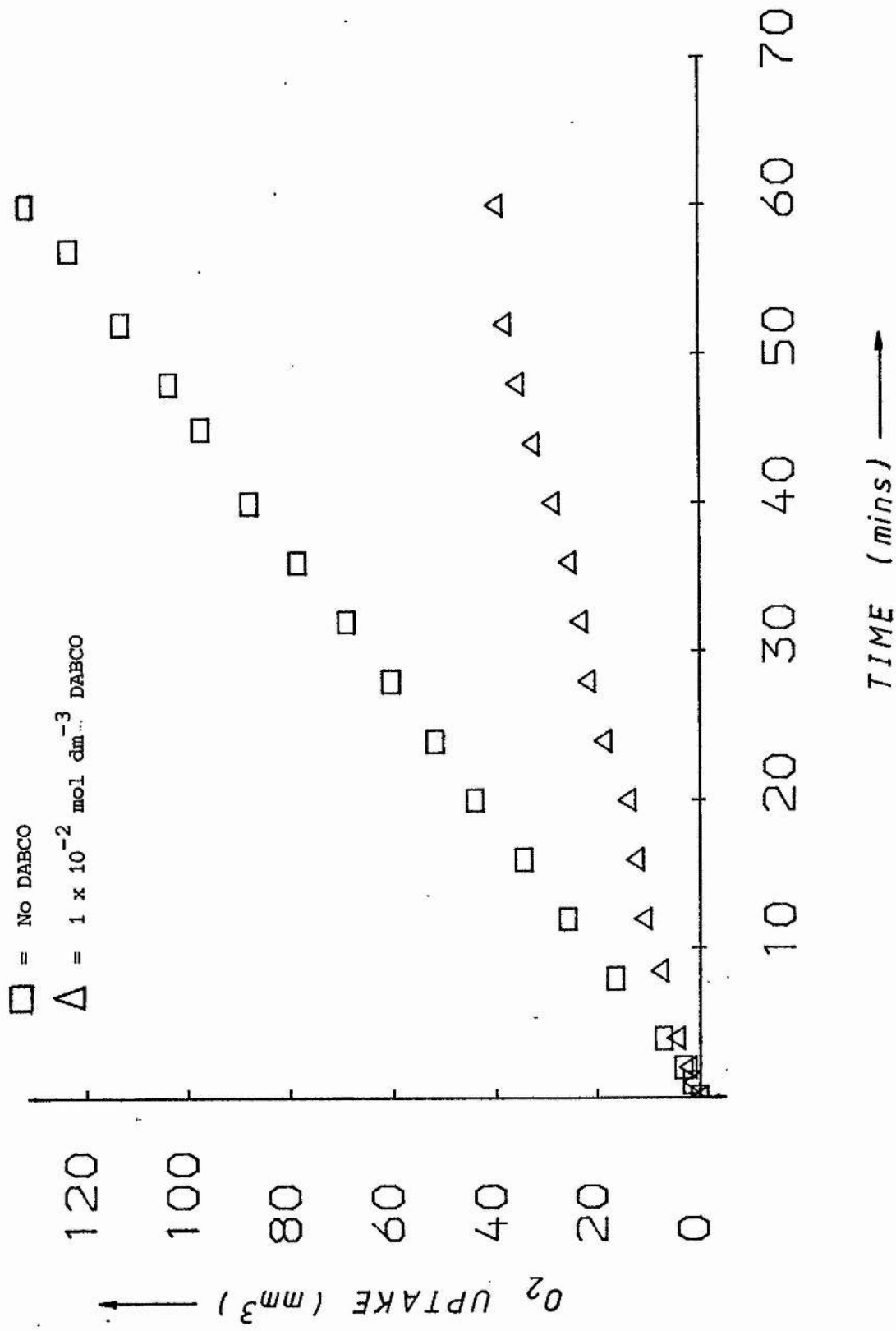
□ = No DABCO
Δ = 1 x 10^{-2} mol dm^{-3} DABCO
O_2 UPTAKE (mm^3) ⟵
0
20
40
60
80
100
120
10
20
30
40
50
60
70
TIME (mins) ⟶

Figure 1.14

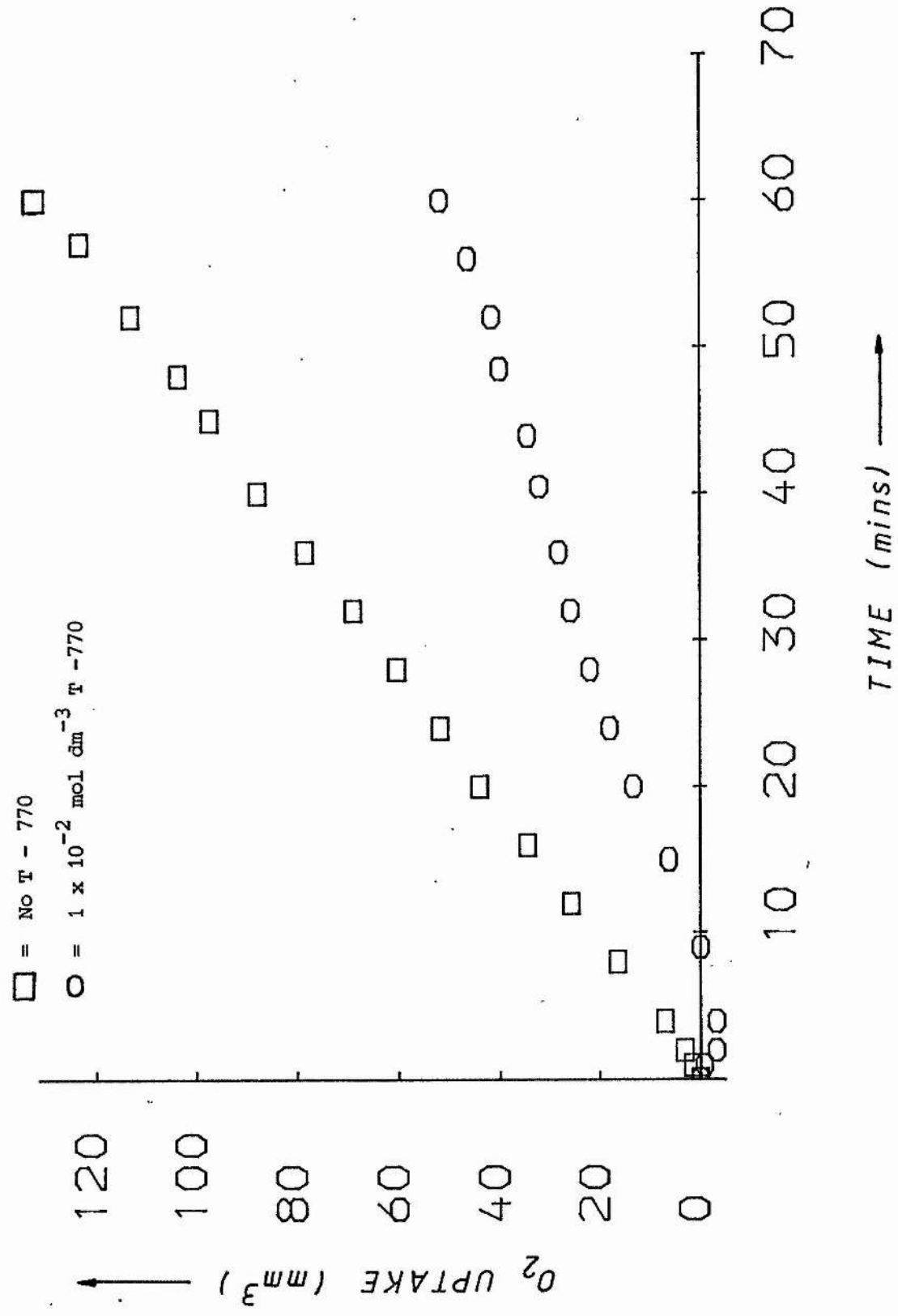
□ = No T - 770
O = 1 x 10^{-2} mol dm^{-3} T -770
O_2 UPTAKE (mm^3)
0
20
40
60
80
100
120
10
20
30
40
50
60
70
TIME (mins)

Figure 1.15

Table 1.9: Effect of Strong Bases on Oxygen-Uptake Rate at 298.5 K

BASE	CONCENTRATION (mol dm^{-3})	UPTAKE RATE (mol O_2 $s^{-1}/10^{-9}$)	% RATE REDUCTION
NONE	0	1.49	0
T-770	$1x10^{-2}$	0.54	61
DABCO	$1x10^{-3}$	0.69	46
DABCO	$1x10^{-2}$	0.46	69
DABCO	$1x10^{-1}$	0.23	82

1.7.2 Influence of Site Blocking on Activation Energy

It has been shown above, that addition of relatively small concentrations of strong organic bases can produce large rate reductions in oxygen-uptake for propan-2-ol/ anatase suspensions. Furthermore, this may be explained by assuming that a strong adsorption of the base on the anatase surface occurs, such that oxygen is inhibited from interacting with any trapped excitonic species. On considering the variation of temperature on the uptake rate with the base also present, one of two possible cases may be expected:

1) The uptake rate may be decreased by the same proportion at each temperature. This would result in no change being observed in the slope of the Arrhenius plot. Thus the activation energy (Ea) for oxygen-uptake would remain the same and the effect of the base would be to slow down the overall rate but would have no influence on the rate determining step (RDS) itself.

2) It could be that the uptake rate varies in a different manner with temperature when the base is present. Such a situation would imply that the base is not only reducing the overall rate but that it is also directly interfering, or indeed altering the RDS. This situation would manifest itself by a change in the slope of the Arrhenius plot, for oxygen-uptake with the base present.

In order to observe which situation would prevail, oxygen-uptake experiments were carried out at various temperatures for suspensions containing 1×10^{-2} mol dm^{-3} of both DABCO and T-770. Once again, the anatase (Tioxide) grade of TiO_2 was used throughout, thus maintaining consistency with the previous runs. The rate data obtained are shown in Table 1.10, while the appropriate Arrhenius plots are illustrated in Figures 1.16 and 1.17.

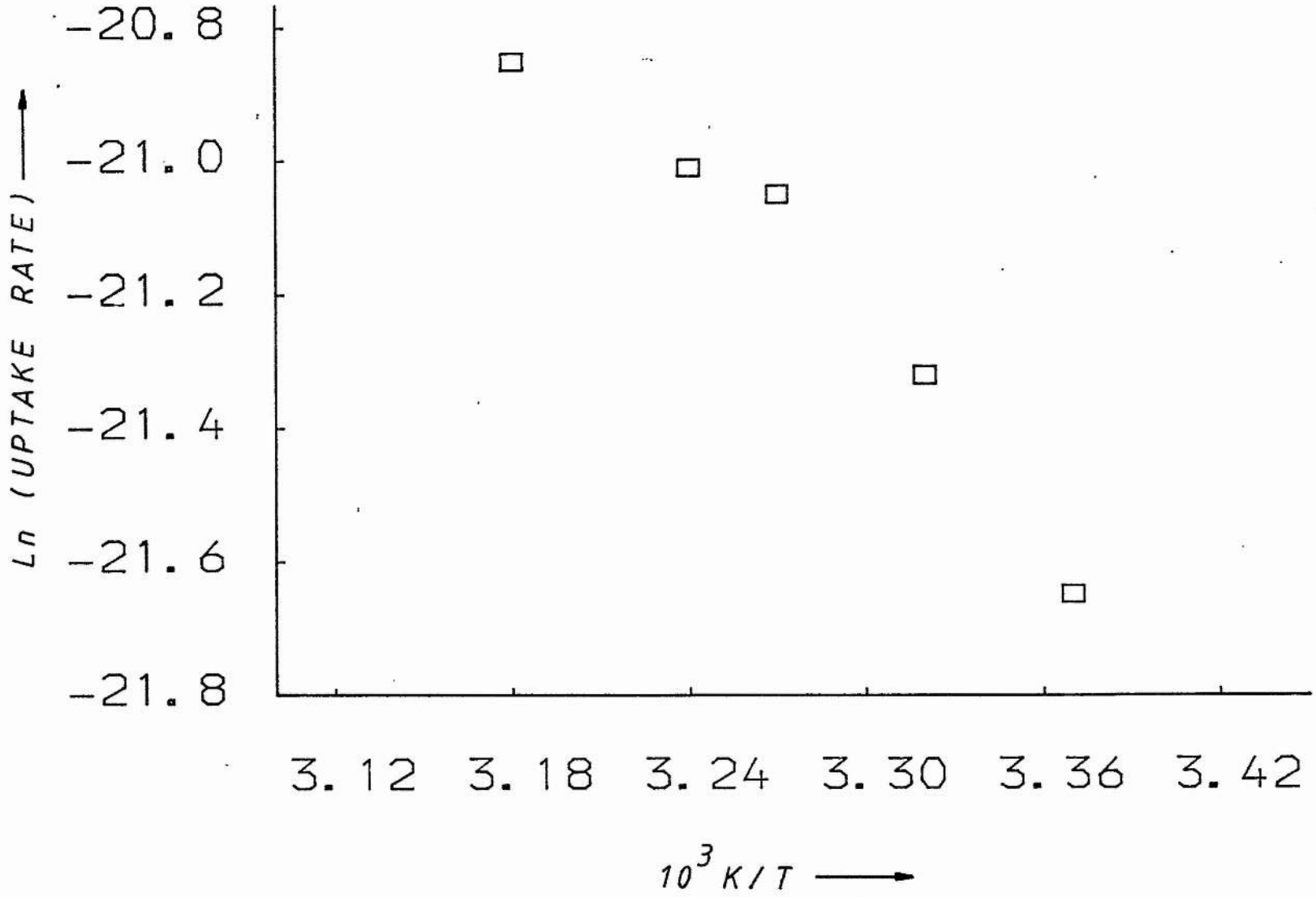
-20.8
-21.0
-21.2
-21.4
-21.6
-21.8
Ln (UPTAKE RATE) ⟶
3.12
3.18
3.24
3.30
3.36
3.42
10^3 K/T ⟶

Figure 1.16

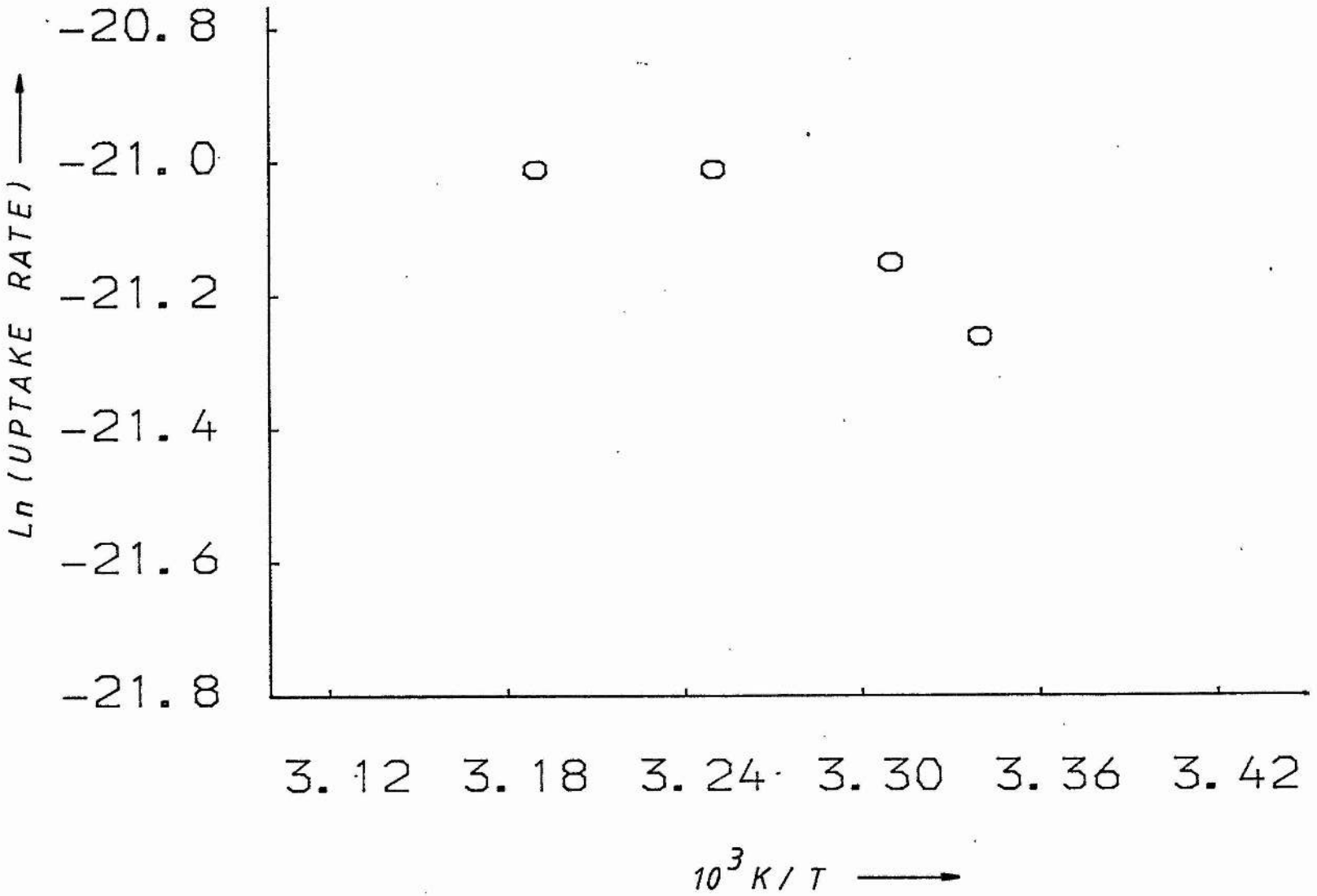
-20.8
-21.0
-21.2
-21.4
-21.6
-21.8
Ln (UPTAKE RATE)
3.12
3.18
3.24
3.30
3.36
3.42
10^3 K / T

Figure 1.17

Table 1.10: Effect of Base on Oxygen-Uptake Temperature Dependence

a) propan-2-ol/anatase (Tioxide)/$1x10^{-2}$ mol dm^{-3} DABCO

TEMP (K)	1/T ($K^{-1}/10^{-3}$)	RATE (mol O_2 $s^{-1}/10^{-10}$)	Ln(RATE)
297	3.37	4.0	-21.65
301	3.32	5.5	-21.32
306	3.27	7.2	-21.05
309	3.24	7.5	-21.01
315	3.18	8.8	-20.85

b) propan-2-ol/anatase (Tioxide)/$1x10^{-2}$ mol dm^{-3} T-770

TEMP (K)	1/T ($K^{-1}/10^{-3}$)	RATE (mol O_2 $s^{-1}/10^{-10}$)	Ln(RATE)
299	3.34	5.86	-21.26
302	3.31	6.51	-21.15
308	3.25	7.48	-21.01
314	3.19	7.48	-21.01

It is clear from Figures 1.16 and 1.17 that the temperature dependence with the bases present is non-linear with respect to the Arrhenius plots. This is in marked contrast to the plot for propan-2-ol/ anatase (Tioxide) alone (refer to Figure 1.9 for comparison). The interpretation of non-linear Arrhenius plots is difficult[37], and since linear regression analysis cannot be applied,

no Ea values can be extracted. Clearly, however, since the profile of the plots change on incorporation of one of the bases, this suggests that the base itself is interfering with the RDS and not just producing a straightforward rate reduction. One possible factor contributing to the curved Arrhenius plots might be that thermally induced desorption of the bases is occurring and that this effect is superimposed on the activated step governing the oxygen-uptake rate.

1.8 Variation of Propan-2-ol Concentration

In order to obtain information of a more detailed nature regarding the mechanism of reactions catalysed on a surface, one general approach is to study the concentration dependence of one of the reactants on the reaction rate[31]. It was therefore decided to apply this technique to the propan-2-ol/anatase (Tioxide) oxygen-uptake system. Here, there are two obvious reactants which could be varied, namely oxygen and propan-2-ol. However, because of the difficulties in determining actual oxygen partial pressures and effective oxygen concentrations (mentioned in a previous Section) this left the alcohol itself as the only possible reactant variable.

From knowledge of the density of propan-2-ol at a particular temperature, it is possible to calculate that the neat concentration is 13.06 mol dm^{-3}, applicable for the temperature range of 273 K up to 313 K, with only a 4% variation due to expansion[43]. Hence dilution to produce solutions of known concentration was undertaken - ranging from 3.25 mol dm^{-3} up to the neat alcohol itself. Clearly however, the selection of the appropriate diluent was of paramount importance. The actual choice of diluent was effected by application of the same criteria used in the selection of the organic bases and mentioned in the section on surface blocking studies. These were that the material

should not undergo any oxygen consuming reactions involving the TiO_2 surface and also that it should be transparent to the radiation entering the uptake cell.

The molecule finally chosen as the inert diluent was cyclohexane and only a very pure spectroscopic grade was employed. The UV/visible absorption spectrum confirmed that there were no impurities present. An oxygen-uptake experiment was carried out in the usual manner, using a slurry of neat cyclohexane/anatase (Tioxide) at 301.5 K. No oxygen-uptake was observed, within experimental error, over the 20 - 60 min. period ie. after full thermal equilibration.

Oxygen-uptake experiments were undertaken at 298 K and 309 K, using propan-2-ol solutions within the concentration range mentioned above. The observed dependence of uptake rate on the alcohol concentration can best be illustrated by a plot of rate against concentration as shown in Figure 1.18. The plots are clearly non-linear, despite possessing fairly high linear correlation coefficients and this is a clear indication as to the limitation of this form of statistical analysis in assessing the degree of linearity of a plot. More importantly, however, Figure 1.18 suggests that on extrapolation back to give zero alcohol concentration (hence neat cyclohexane) there should be an appreciable oxygen-uptake rate; which is known not to be the case. Clearly, therefore, the bulk propan-2-ol concentration dependence is more complicated than one would have intuitively expected.

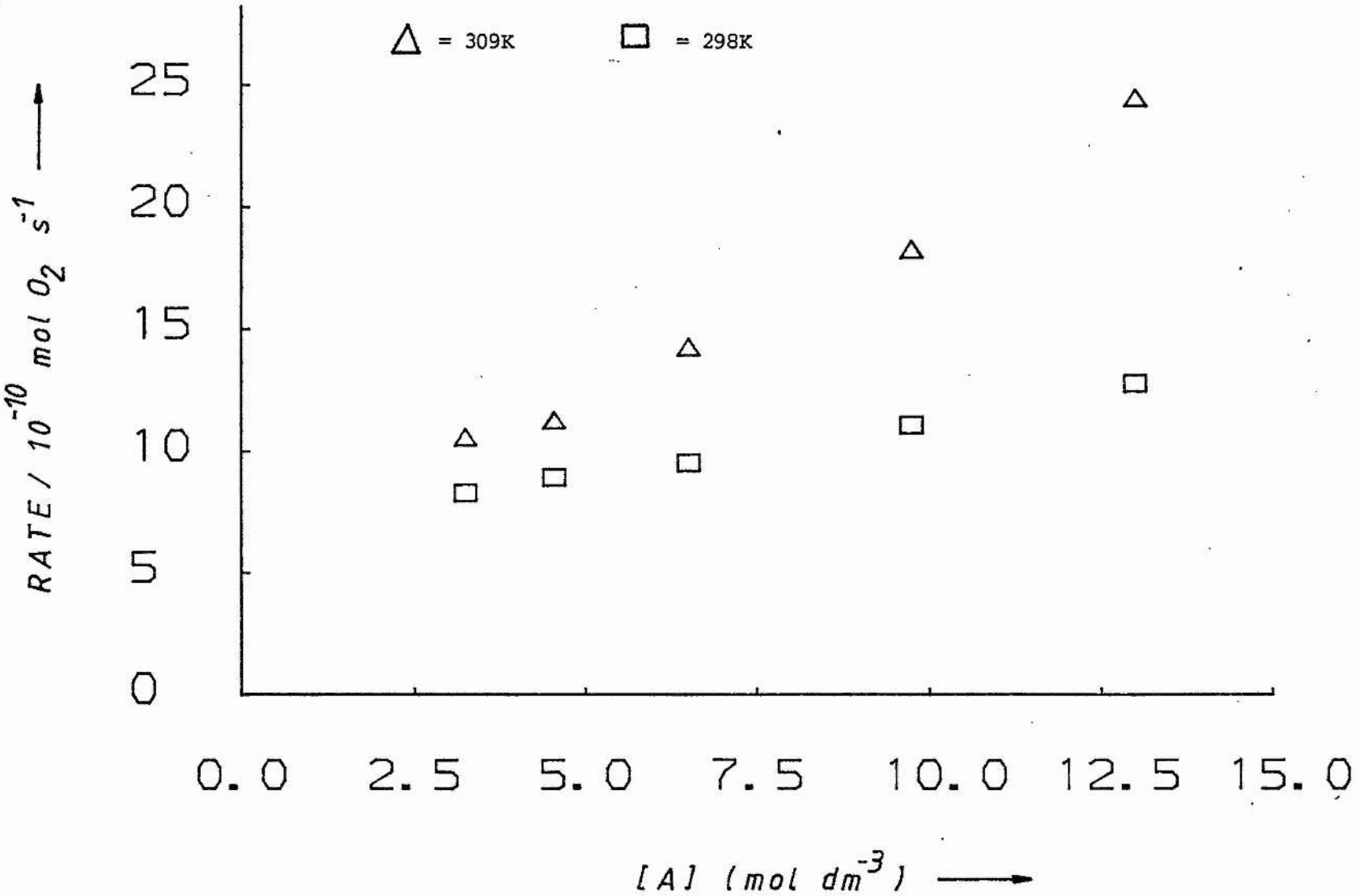
△ = 309K
□ = 298K
RATE / 10^{-10} mol O_2 s^{-1}
0
5
10
15
20
25
0.0
2.5
5.0
7.5
10.0
12.5
15.0
[A] (mol dm^{-3})

Figure 1.18

The above results show that the oxygen-uptake rate varies in a non-linear manner with the bulk alcohol concentration. However, one important reason for this may be that studying the propan-2-ol concentration in terms of solution composition may be a poor model for the processes involving alcohol molecules adsorbed on the anatase surface. In addition, one important physical property of alcohols is their tendency to undergo self association[44]. This process concerns the reversible linking together of alcohol molecules, through weak hydrogen bonds, as follows:

$$ROH + ROH \rightleftharpoons ---O^{R}H-----O^{R}H--- \qquad (1.28)$$

Such associations can result in the formation of chains or cyclic structures[45].

In order to explain the unusual rate dependence on concentration, it was decided to undertake a study on the extent on self association of propan-2-ol and to determine how this association was affected, upon dilution of the alcohol with cyclohexane. From the outset, it was hoped that by determining the concentration of non-associated alcohol molecules and using these values in the oxygen-uptake rate vs. concentration plot, a more clear-cut dependency would emerge. In addition, the propan-2-ol/cyclohexane self association system was worthy of examination in its own right, since no mention of association studies on this alcohol/solvent combination could be found in the literature.

1.8.1 Self-Association in Alcohol Systems

The mechanism and extent by which molecules with certain functional groups, notably -OH and $-NH_2$, undergo self-association to form complexes has received much attention in the literature[46-49]. This attention is well justified since two of the most important phenomena occurring in nature are governed by such associative interactions - namely the structure and formation of ice and the conformation of DNA[50,51].

Studies on the self-association on alcohols have largely centred around the properties of ethanol solutions in carbon tetrachloride[44,52]. However, one important fact was not fully appreciated in earlier work, namely the role of the solvent. This was not taken into account and many early results were marred by the selection of solvents which were themselves either H-bond donors or acceptors. For example chloroform, $CHCl_3$, was used extensively as a solvent in ethanol self-association studies, despite the involvement of the C-H proton. Conveniently, one of the best solvents for use in such studies is cyclohexane which acts neither as proton donor nor proton acceptor.

Techniques which have been applied in the study of self-association processes have mainly involved the use of infrared and Raman spectroscopy[53,54]. These techniques yield characteristic frequencies of molecular vibrations. Such frequencies depend on the masses of the vibrating atoms, the molecular geometry and the restraining forces holding the atoms in their equilibrium positions in the molecule.

H-bond formation gives rise to distortions in the infrared or Raman spectra obtained from a solution under study. Often a separate peak, corresponding to the H-bonded complex, can appear and the concentrations of bound and free alcohol molecules may be calculated from their relative intensities[45]. In other cases, a peak shift is observed, the magnitude of which is related to the extent of association. Concentration dependence measurements on the spectroscopic shift can lead to values for the self-association constant and heat of hydrogen bonding being calculated.

Other experimental methods have been utilised in self-association studies, eg. dielectric constant measurements[55], pressure-volume-temperature studies[56], cryoscopy[57] and surface tension effects[58]. More recently, proton nuclear magnetic resonance spectroscopy, ^{1}H-NMR, has been applied[59,60]. This technique offers far greater sensitivity in detecting H-bond effects in alcohol solutions than that which can be attained by other spectroscopic means. Despite this, however, relatively few complete variable concentration and temperature NMR studies have been carried out for alcohol/hydrocarbon systems. It was

decided, therefore, to apply the NMR technique to the propan-2-ol/cyclohexane system with a view to determining the extent of self-association. Finally, application of this data to the concentration dependent oxygen-uptake results would, it was hoped, reveal whether or not the rate itself is influenced by the self-association properties of the alcohol.

1.8.2 ^{1}H-NMR Self-Association Study of Propan-2-ol in Cyclohexane

1.8.2.1 The NMR Technique

Certain nuclei are said to be "spin active" ie. possess integral or half integral spin quantum numbers (I). For example, ^{1}H is spin active with I = 0.5. In a magnetic field, an isolated ^{1}H nucleus behaves as a minute bar magnet and is permitted to align itself in only two possible ways. These are: alignment with the field (the α state) and against the field (the β state) as illustrated in Figure 1.19.

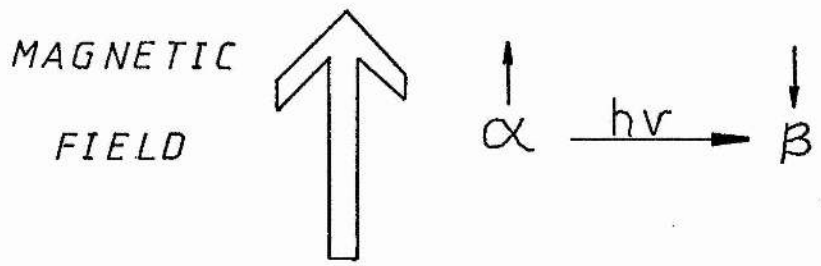

Figure 1.19 Alignment of Nuclei in a Magnetic Field.

Transition from the lower energy α to the higher energy β state may be effected by absorption of electromagnetic radiation of appropriate frequency, v.

The isolated nucleus is, however, an impractical situation since, in reality, all neutral nuclei are surrounded by circulating electrons. When placed in a magnetic field, the electron cloud tends to circulate in such a direction as to produce an induced field opposing that applied, thus:

$$B_{effective} = B_{applied} - B_{induced} \qquad (1.29)$$

where B is the magnetic field strength. The strength of the induced field is dependent on the electron density surrounding the nucleus. Thus for protons bonded to oxygen atoms, as in alcohols, the electron density surrounding the proton will be less than that in which the oxygen is replaced by carbon, due to the greater electronegativity of the former. Hence protons bonded to oxygen experience a greater effective magnetic field (said to be more deshielded) than those attached to carbon. Clearly, therefore, the NMR technique offers a sensitive method of probing the chemical environment of identical types of nuclei such as ^1H.

The frequency of radiation, v, required to promote α state ^1H nuclei to their β state is proportional to the effective magnetic field, B_{eff}. This frequency is known as the resonance frequency and occurs in the radiofrequency region of the electromagnetic spectrum.

The most conventional way of applying the NMR technique is thus to expose the sample to a constant applied magnetic field and irradiate it with radiation of variable frequency until nuclear resonance occurs - detectable by absorption of the radiation.

Since alcohol protons involved in self-association exist in a different environment to the non-associated species, this will be reflected in different resonance frequencies. More specifically, the former type would be more deshielded and hence resonate at higher ν values than the latter. In order to standardise the magnitudes of these chemical shifts, they are generally quoted with respect to a tetramethylsilane (TMS) reference and this practice was adopted throughout the current study. Chemical shifts quoted in this way are, however, dependent on the field strength of the magnet used in the experiments. This problem may be circumvented by expressing the chemical shift in ppm (parts per million), symbol δ, relative to TMS and with respect to the applied field. Hence:

$$\delta = \frac{\text{chemical shift in Hz from TMS} \times 10^6}{\text{spectrometer field strength (in MHz)}} \qquad (1.30)$$

To maintain the consistency of the units, the strength of the magnet used is expressed in MHz. The conversion from the more familiar tesla (T) units may be effected by the following:

$$1 \text{ MHz} \equiv 2.3 \times 10^{-2} \text{ T} \qquad (1.31)$$

However, since the same instrument, with an 80 MHz magnet, was used in

all the propan-2-ol self-association experiments, chemical shifts will be expressed in Hz where possible. These units are more meaningful when comparing samples which differ only slightly in chemical shift.

1.8.2.2 ^{1}H-NMR Data For Self-Association

A fundamental expression, relating an observed chemical shift to a particular alcohol concentration, has been established by J.A. Pople et al.[61]:

$$\frac{(v - v_1)}{(v_p - v)} = \frac{([A] - [A_F])}{[A_F]} \qquad (1.32)$$

where: v is the measured chemical shift of the hydroxyl proton resonance for an alcohol solution of molar concentration [A].

$[A_F]$ is the total molar concentration of non-associated ("free") OH groups.

v_p and v_1 are the theoretical shifts of fully bound and free hydroxyl protons respectively.

Equation (1.32) indicates that the observed OH proton shift represents an averaged shift, balanced by the tendencies of the bound and free OH groups to induce a higher or lower shift respectively. Figure 1.20 illustrates a typical 80 MHz ^{1}H-NMR spectrum of a propan-2-ol/cyclohexane solution of alcohol concentration, [A] = 9.75 mol dm^{-3} at 313 K. The fact that a single OH signal is observed is a clear indication that the associative interaction is a dynamic process, with alcohol molecules alternately linking together and breaking apart.

In order to interpret the NMR data, a self-association model must first be proposed. As with most models, certain assumptions and simplifications must be made, and these constraints borne in mind when interpreting the results. Thus, if only linear association of propan-2-ol molecules to form polymeric chains is assumed, then the association process may be considered as occurring via a series of single steps:

$$A_1 + A_i \rightleftharpoons A_{i+1} \qquad (1.33)$$

where A_i and A_{i+1} represent linear chains of i and i+1 alcohol molecules respectively. A_1 indicates a single alcohol molecule (or monomer unit). A self-association constant corresponding to this process may be expressed as follows:

$$K_i = \frac{[A_{i+1}]}{[A_1][A_i]} \qquad (1.34)$$

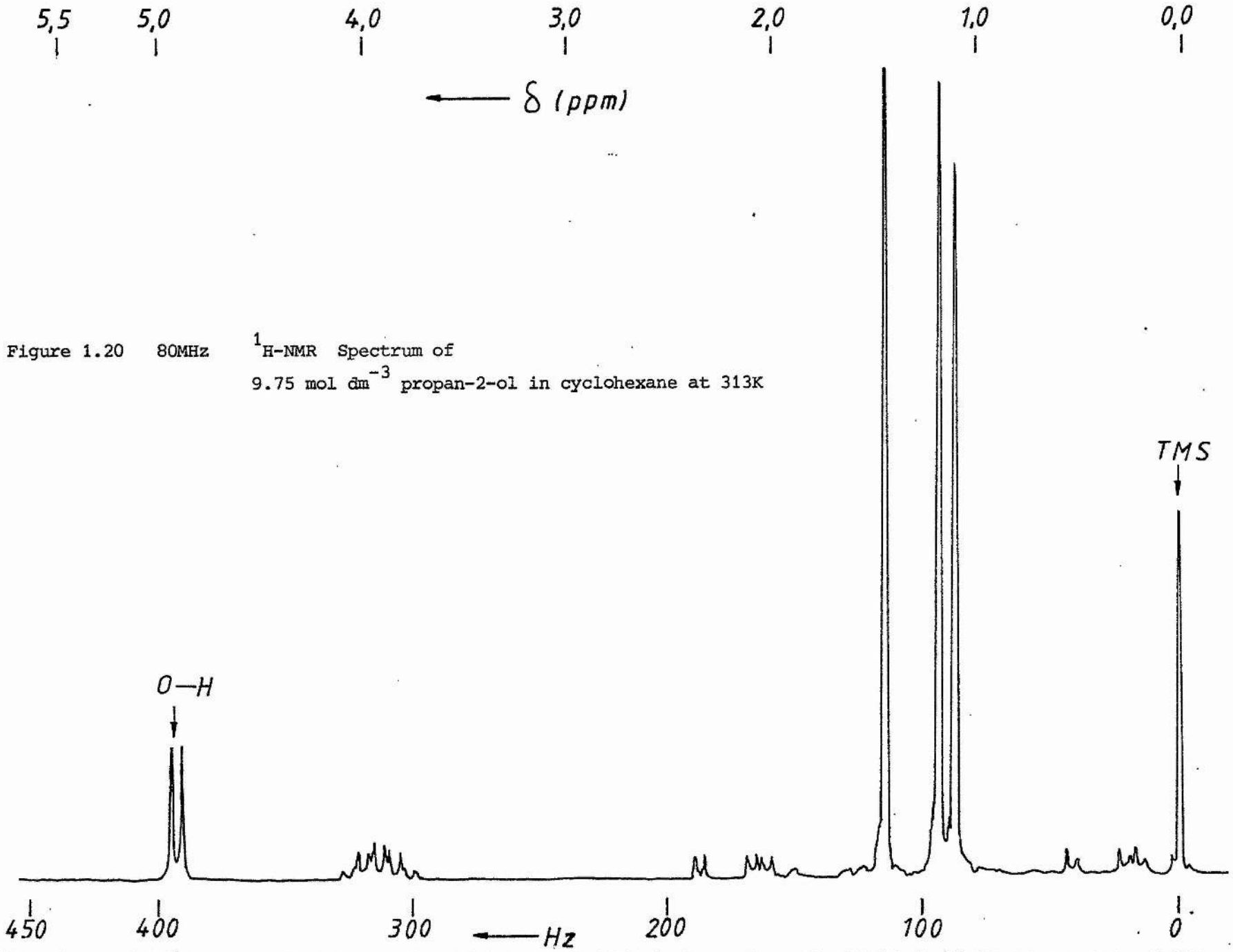

Figure 1.20 80MHz ^{1}H-NMR Spectrum of
9.75 mol dm^{-3} propan-2-ol in cyclohexane at 313K

If the self-association, as represented by equation (1.34), is assumed to be ideal, then the energetics involved in adding a further monomer unit should be independent of the existing chain length. Hence:

$$K_1 = K_2 = K_3 - - - - - - K_i = K \qquad (1.35)$$

A physical interpretation may now be given to the total and free alcohol concentrations, $[A]$ and $[A_F]$ respectively, in terms of the various alcohol chains:

$$[A] = \sum i[A_i] = \sum i[A_1]^i K^{i-1} \qquad (1.36)$$

and $$[A_F] = \sum [A_i] = \sum [A_i]^i K^{i-1} \qquad (1.37)$$

Such expressions may be readily understood by examination of an ideal chain, illustrated in Figure 1.21, for the case in which $i = 4$.

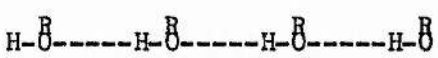

Figure 1.21 Ideal chain association of 4 monomer units.

Clearly, while $[A]$ is concerned with the total number of alcohol molecules per unit volume in each chain, the quantity $[A_F]$ only takes

account of the H atom at the end of each chain which is not involved in association. Hence, irrespective of chain length, each chain will contribute only one OH towards the total $[A_F]$ quantity. This accounts for the only difference between equations (1.36) and (1.37), namely the multiplication factor, i.

The summation expressions in equations (1.36) and (1.37) may be evaluated. For example, in the case of the expansion for [A], the following simplification is made:

$$z = [A_1]K \qquad (1.38)$$

$$\text{Thus} \quad [A] = \sum i[A_1]^i K^{i-1} = [A_1] \sum i[A_1]^{i-1} K^{i-1} \qquad (1.39)$$

$$\text{therefore,} \quad \frac{[A]}{[A_1]} = \sum iz^{i-1} = \frac{d}{dz}\left(\sum z^i\right) \qquad (1.40)$$

$$\text{now,} \quad \sum z^i \sim \frac{z}{(1-z)} \qquad \text{for } z < 1 \qquad (1.41)$$

$$\text{thus,} \quad \frac{[A]}{[A_1]} = \frac{d}{dz}\left(\frac{z}{(1-z)}\right) = \frac{1}{(1-z)^2} \qquad (1.42)$$

$$\text{and so,} \quad [A] = \frac{[A_1]}{(1-z)^2} = \frac{[A_1]}{(1-[A_1]K)^2} \qquad (1.43)$$

By following a similar derivation, it can be shown that:

$$[A_F] = \frac{[A_1]}{(1 - [A_1]K)} \qquad (1.44)$$

Combination of equations (1.43) and (1.44), leads to an expression for the self-association constant, K, in terms of the more useful [A] and $[A_F]$ parameters:

$$K = \frac{[A] - [A_F]}{[A_F]^2} \qquad (1.45)$$

The self-association constant can now be calculated, provided that $[A_F]$ is known. Rearrangement of equation (1.32) enables this latter quantity to be calculated from equation (1.46):

$$[A_F] = \frac{[A](v_p - v)}{(v_p - v_1)} \qquad (1.46)$$

This, in turn, requires that v_p and v_1, the theoretical maximum and minimum self-association limits, be known.

An alternative route to the calculation of K eliminates the need for $[A_F]$ determination as an intermediate step. By combining equations (1.32) and (1.45), the following may be obtained:

$$K[A] = \frac{1 - \{(v_p - v)/(v_p - v_1)\}}{(v_p - v)^2/(v_p - v_1)^2} \qquad (1.47)$$

However, the v_p and v_1 parameters must still be determined before K can be found at a particular temperature.

1.8.2.3 Determination of v_p and v_1

In the case of a concentrated alcohol solution, a high degree of self-association will exist. Hence the observed chemical shift of the hydroxyl proton will be close to the theoretical maximum value, v_p. Thus:

$$1 - \frac{(v_p - v)}{(v_p - v_1)} \sim 1 \qquad (1.48)$$

Application of this approximation enables equation (1.47) to be rearranged to give:

$$v = v_p - \frac{(v_p - v_1)}{\sqrt{K}} \times \frac{1}{\sqrt{[A]}} \qquad (1.49)$$

It follows, therefore, that a plot of v against $1/\sqrt{[A]}$ should give a straight line of intercept v_p. Furthermore, application of the same graphical technique over a series of temperatures should still yield

the same intercept, since v_p represents the chemical shift of a fully bound alcohol OH, irrespective of temperature.

A series of propan-2-ol solutions was prepared using cyclohexane as solvent. In order to maintain comparability with the variable concentration oxygen-uptake experiments, the same concentration range was applied ie. neat propan-2-ol (13.06 mol dm^{-3}) down to 3.25 mol dm^{-3}, encompassing five solutions in all. The chemical shift (with respect to TMS) for the hydroxyl proton was determined for each solution over the temperature range 283 K to 313 K. The data obtained from these variable temperature experiments are shown in Table 1.11.

Table 1.11: Chemical Shift (in Hz) as a Function of Temperature For Each Alcohol Solution

	CONCENTRATION (mol dm^{-3})				
	3.25	4.55	6.50	9.75	13.06
TEMP. (K)					
283.0	416.26	420.95	427.49	434.45	435.79
288.0	407.14	413.38	421.51	428.34	429.56
292.5	401.12	406.79	415.65	423.22	424.43
298.0	390.40	397.09	406.73	415.41	417.50
303.0	382.60	389.49	400.02	409.30	411.99
309.0	370.88	378.90	390.52	400.94	403.64
313.0	361.82	370.71	382.93	394.41	396.97

Plots of v against $1/\sqrt{[A]}$ are illustrated in Figures 1.22 and 1.23, with the corresponding data, obtained from linear regression analysis of the plots, given in Table 1.12. Clearly, although a range of intercepts is obtained, the tendency of the plots is to converge as the magnitude of $1/\sqrt{[A]}$ decreases. An average of the intercepts yields a value for v_p of 447 Hz. Consideration of the spread of the intercepts leads to an estimate of the uncertainty as being +/- 5%. Given the assumptions made in equations (1.41) and (1.48), this is a very reasonable error bound.

Table 1.12: Linear Regression Analysis of the $(1/\sqrt{[A]}, v)$ Plots From Figures 1.22 and 1.23

TEMP (K)	CORR. COEFF. (r)	INTERCEPT (Hz)
283.0	-0.99	457.1
288.0	-0.99	454.4
292.5	-0.99	450.5
298.0	-0.99	446.9
303.0	-1.00	443.7
308.0	-1.00	440.7
313.0	-1.00	435.3

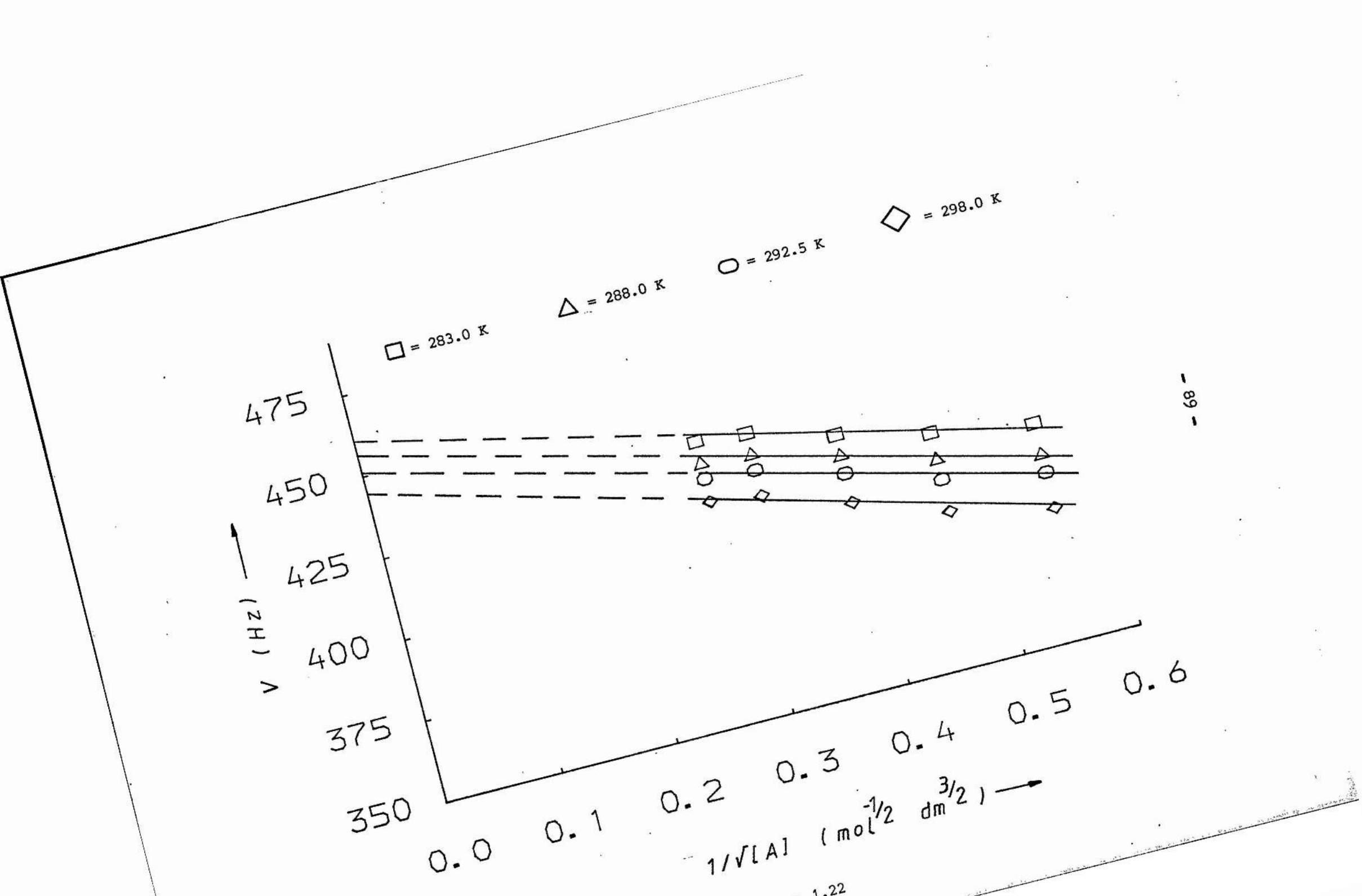
□ = 283.0 K
△ = 288.0 K
○ = 292.5 K
◇ = 298.0 K
475
450
425
400
375
350
ν (Hz)
0.0
0.1
0.2
0.3
0.4
0.5
0.6
1/√[A] (mol^-1/2 dm^3/2)

Figure 1.22

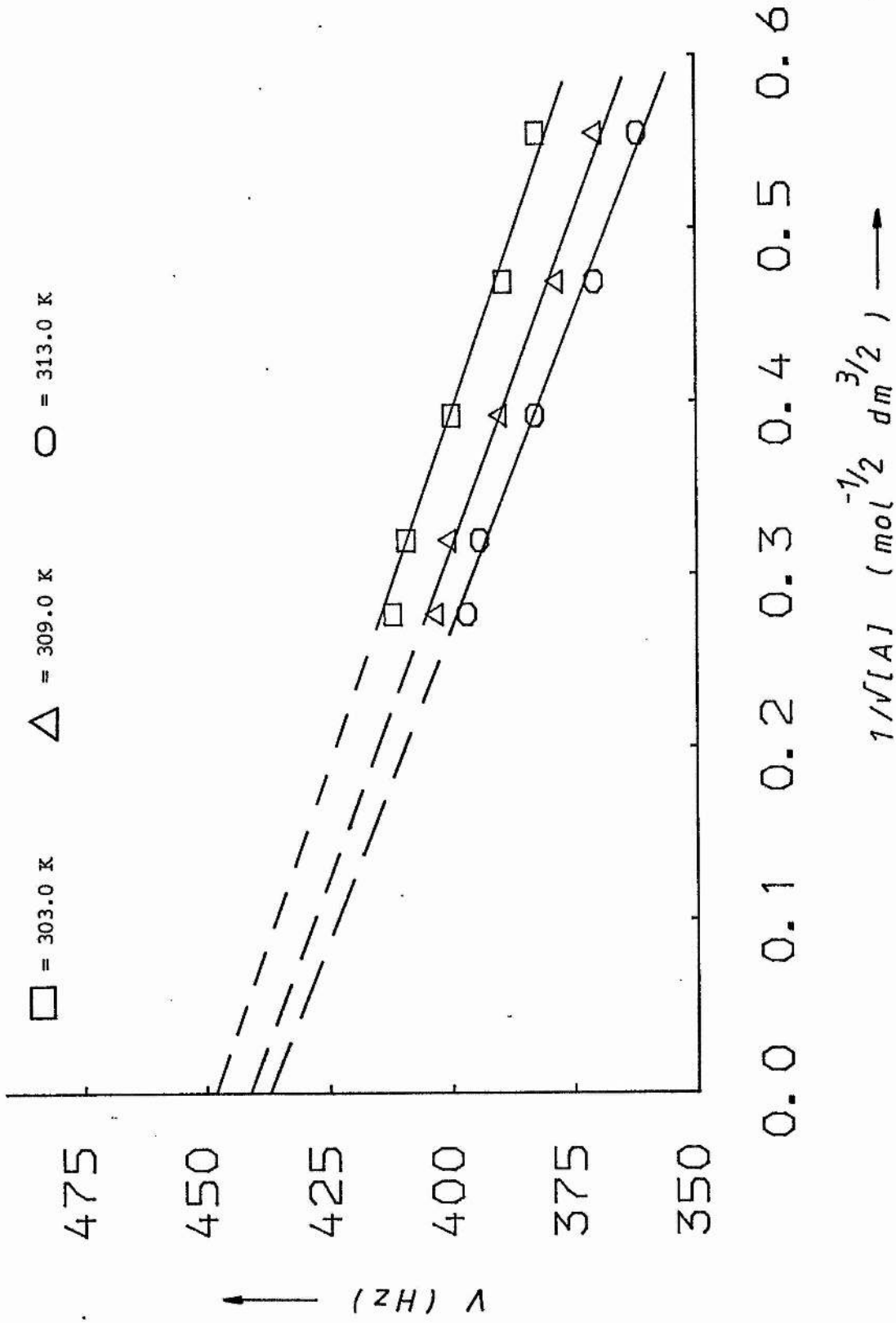
□ = 303.0 K
△ = 309.0 K
○ = 313.0 K
ν (Hz)
475
450
425
400
375
350
0.0
0.1
0.2
0.3
0.4
0.5
0.6
1/√[A] (mol^-1/2 dm^3/2)

Figure 1.23

Several authors report that to a good approximation[61-63]:

$$\nu_1 \sim \nu_p - 4.5 \text{ ppm} \qquad (1.50)$$

Since the field strength of the spectrometer used in the above experiments was 80 MHz, then application of equation (1.50) suggests a value of 88 Hz for ν_1.

From equation (1.49) it is clear that the self-association constant, K, could be calculated from the slopes of the plots given in Figures 1.22 and 1.23. However, because of the additional uncertainty due to the assumption inherent to equation (1.48), values calculated in this way would be less accurate than those obtained from the two alternative routes ie. via equation (1.47) and by combination of equations (1.45) and (1.46).

1.8.3 Evaluation of Self-Association Constant for Propan-2-ol

The graphical method for the evaluation of K - plotting the right hand side of equation (1.47) against [A] and obtaining K at a particular temperature - was applied by A.B. Littlewood and F.W. Willmott for the system 1-dodecanol in squalane[64]. The corresponding plots, using the propan-2-ol/cyclohexane NMR data obtained above, are shown in Figures 1.24 and 1.25 (once again two separate figures are

used to maintain clarity). Clearly, these plots show slight departures from linearity. This important observation suggests that the assumption of purely linear chain association is not fully justified and that the solution behaviour of the alcohol is complicated by other modes of association.

The most obvious alternative associative mechanism open to propan-2-ol would be the formation of cyclic structures[45]. Obviously, values calculated for the self-association constant will not take this into account. Since linear regression analysis of the plots in Figures 1.24 and 1.25 yield poor correlation coefficients, there will be a large uncertainty in any K values obtained from the slopes.

The alternative method of association constant calculation at a particular temperature involves calculation of the free hydroxyl concentration $[A_F]$ from equation (1.46). Substitution of the appropriate $[A_F]$ values into equation (1.45) can then lead to evaluation of K. The variation in $[A_F]$ with bulk alcohol concentration, [A], and temperature is presented in Table 1.13.

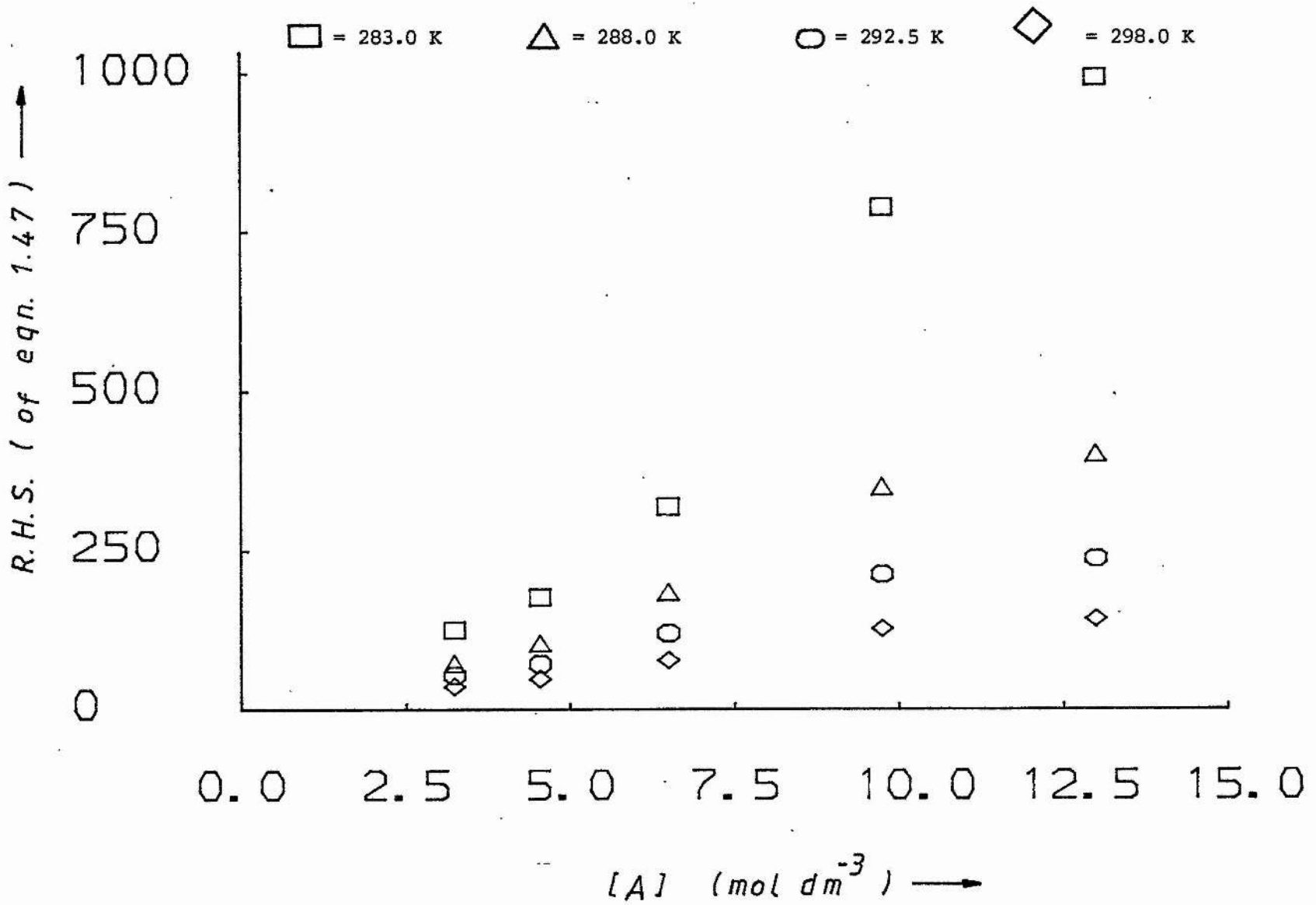
□ = 283.0 K
△ = 288.0 K
○ = 292.5 K
◇ = 298.0 K
R.H.S. (of eqn. 1.47) ⟶
1000
750
500
250
0
0.0
2.5
5.0
7.5
10.0
12.5
15.0
[A] (mol dm^{-3}) ⟶

Figure 1.24

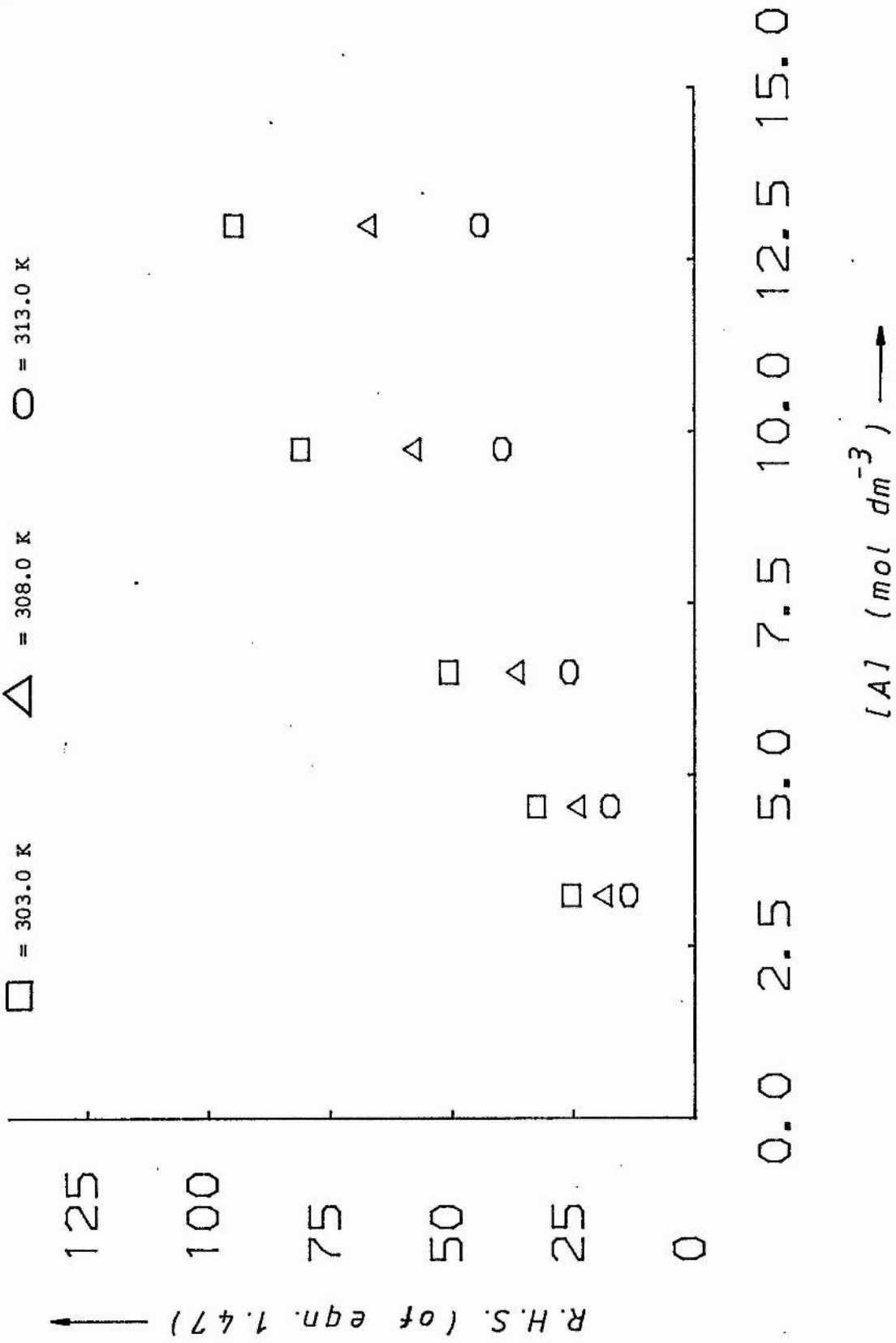
□ = 303.0 K
△ = 308.0 K
○ = 313.0 K
R.H.S. (of eqn. 1.47) ⟶
125
100
75
50
25
0
0.0
2.5
5.0
7.5
10.0
12.5
15.0
[A] (mol dm^{-3}) ⟶

Figure 1.25

Table 1.13: Variation in $[A_F]$ With Bulk Alcohol Concentration, [A] and Temperature.

	BULK PROPAN-2-OL CONCENTRATION, [A] (mol dm^{-3})				
	3.25	4.55	6.50	9.75	13.06
TEMP. (K)					
283.0	0.28	0.33	0.35	0.34	0.41
288.0	0.36	0.43	0.46	0.51	0.63
292.5	0.42	0.51	0.57	0.65	0.82
298.0	0.51	0.63	0.73	0.86	1.07
303.0	0.58	0.73	0.85	1.02	1.27
309.0	0.69	0.86	1.02	1.25	1.57
313.0	0.77	0.97	1.16	1.43	1.81

The data contained in Table 1.13 may be interpreted in a physical sense by considering the temperature effect. An increase in temperature will increase the thermal motion of the propan-2-ol molecules. There will therefore be less opportunity to undergo self-association. Furthermore, any associated structures which are formed will break up much more readily as the temperature is raised. The net effect will therefore be to progressively disfavour self-association on increasing temperature. This tendency is reflected in the increase in $[A_F]$ with temperature.

The calculated $[A_F]$ values may be used in the evaluation of self-association constant data and Table 1.14 shows the effect of temperature and total alcohol concentration on this parameter. The observed influence of temperature is as one would expect; namely a temperature increase inducing a reduced tendency for propan-2-ol molecules to self-associate, leading to a decrease in the K values.

Table 1.14: The Effect of Temperature and [A] on the Association Constant K (mol^{-1} dm^3)

	BULK PROPAN-2-OL CONCENTRATION, [A] (mol dm^{-3})				
	3.25	4.55	6.50	9.75	13.06
TEMP (K)					
283.0	37.9	38.8	50.2	81.4	74.9
288.0	22.3	22.3	28.5	35.5	31.2
292.5	16.5	15.5	18.3	21.5	18.1
298.0	10.5	9.9	10.8	12.0	10.4
303.0	7.9	7.2	7.8	8.4	7.3
309.0	5.4	5.0	5.3	5.4	4.6
313.0	4.2	3.8	4.0	4.1	3.4

The effect of [A] on K is not so readily explicable. If the propan-2-ol/cyclohexane mixture is considered to be ideal and if the linear association mechanism is the only route to propan-2-ol aggregation, then the value of K would depend only on temperature and be unaffected by the total alcohol concentration. For the higher

temperatures, there is indeed only a small variation in K with [A]. In the low temperature cases of Table 1.14, particularly below 292.5 K, a large discrepancy is apparent. Clearly it is at these lower temperatures, where the tendency to undergo self- association will be greatest, that the contribution to association by other mechanisms, possibly involving ring formation, will be most pronounced. It is interesting to note that Littlewood and Willmott, although studying a different alcohol/hydrocarbon self-association system, did not publish results for temperatures below 296.5 K[64].

1.8.4 Determination of the Enthalpy of H-Bonding in Propan-2-ol

Knowledge of the self-association constant values over a range of temperatures may be used to calculate the enthalpy of hydrogen bonding (ΔH^{o}). Such calculations employ the Van't Hoff relationship:

$$\frac{d(\ln K)}{d(1/T)} = -\frac{\Delta H^{o}}{R} \qquad (1.51)$$

where R is the universal gas constant (8.314 J mol^{-1} K^{-1}). A plot of ln K against reciprocal temperature should thus enable ΔH^{o} to be extracted from the value of the slope.

Clearly, the Van't Hoff plot will only be of value if reliable self-association constant data is available. As explained in the previous section, the K values show a marked concentration dependence, particularly below ca. 292.5 K. Thus the data relating to the lowest temperatures were eliminated from the plot. Average values of K were calculated at each temperature and the Van't Hoff plot is shown in Figure 1.26, with the relevant data given in Table 1.15.

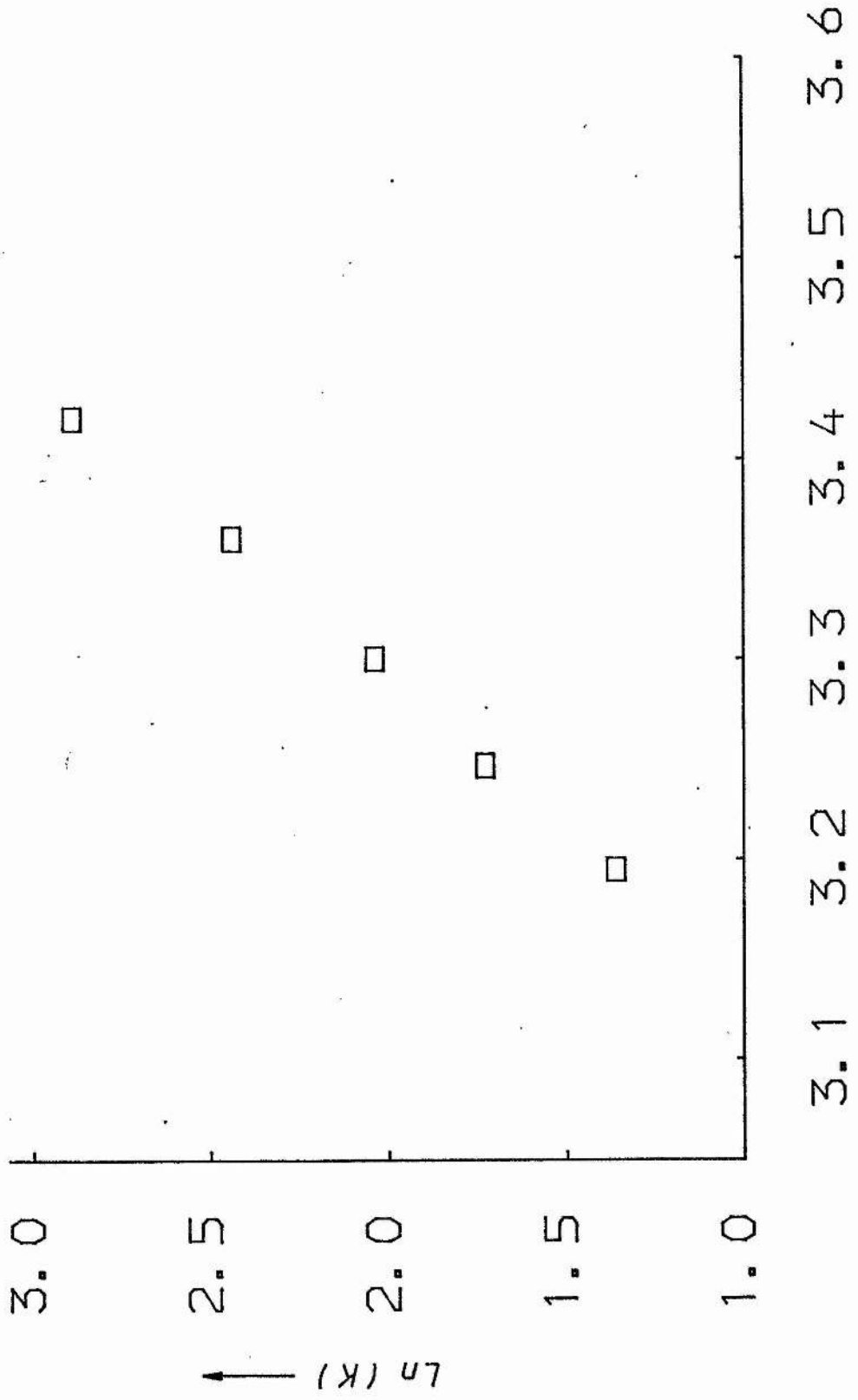

Figure 1.26

Table 1.15: Data Relating to Van't Hoff Plot for Propan-2-ol

AVERAGED LN K	T(K)	1/T ($K^{-1}/10^{-3}$)
2.89	292.5	3.42
2.44	298.0	3.36
2.04	303.0	3.30
1.73	308.0	3.25
1.36	313.0	3.20

As can be seen from Figure 1.26, the Van't Hoff plot reveals a high degree of linearity (correlation coefficient, r = 1.00). From the slope, a value of -53.6 kJ mol^{-1} is obtained for ΔH^{o}. This value may be compared with that of Littlewood and Willmott, who calculated ΔH^{o} to be -42.3 kJ mol^{-1} for 1-dodecanol[64]. However, both of these are considerably greater than the "average" value quoted by G.C. Pimentel and A.L. McClellan[44] of ca. -20 kJ mol^{-1}. One reason for this discrepancy might be that the lower values were obtained using the less sensitive techniques mentioned in a previous section. Furthermore, in many of the low value cases, solvents were often used which themselves participated in hydrogen bonding. Alternatively, our value of -53.6 kJ mol^{-1} for ΔH^{o} may reflect the fact that other associative mechanisms may be contributing; leading to a distorted ΔH^{o} value, despite the highly linear Van't Hoff plot.

1.8.5 Oxygen-Uptake Rate Dependence on Free OH Concentration

At the end of the section on variable concentration oxygen-uptake studies, it was concluded that no clear-cut linear correlation could be established between the uptake rate using anatase, and the bulk propan-2-ol concentration. However, having studied the self-association properties of propan-2-ol solutions, it is clear that the hydroxyl groups can be divided into two classes - bound and free. Furthermore, since the interaction of the alcohol with the TiO_2 surface occurs via the hydroxyl group[24,41,65], then it follows that the rate may be highly dependent on the free OH concentration available to the surface at a given moment in time.

From the NMR studies on propan-2-ol, values for $[A_F]$, the free hydroxyl concentration, were obtained for several bulk concentrations of alcohol/cyclohexane solutions over a range of temperatures. The relevant data was presented previously in Table 1.13. The variable, bulk concentration oxygen-uptake studies were carried out at 298 K and 309 K. Since these were two of the temperatures used in the NMR studies, Figure 1.18 may be re-plotted with the total alcohol concentrations replaced by the relevant $[A_F]$ values. To enable a detailed examination of the features of the $[A_F]$ dependence on uptake rate, a separate figure is shown for the 298 K and 309 K experiments - Figures 1.27 and 1.28 respectively.

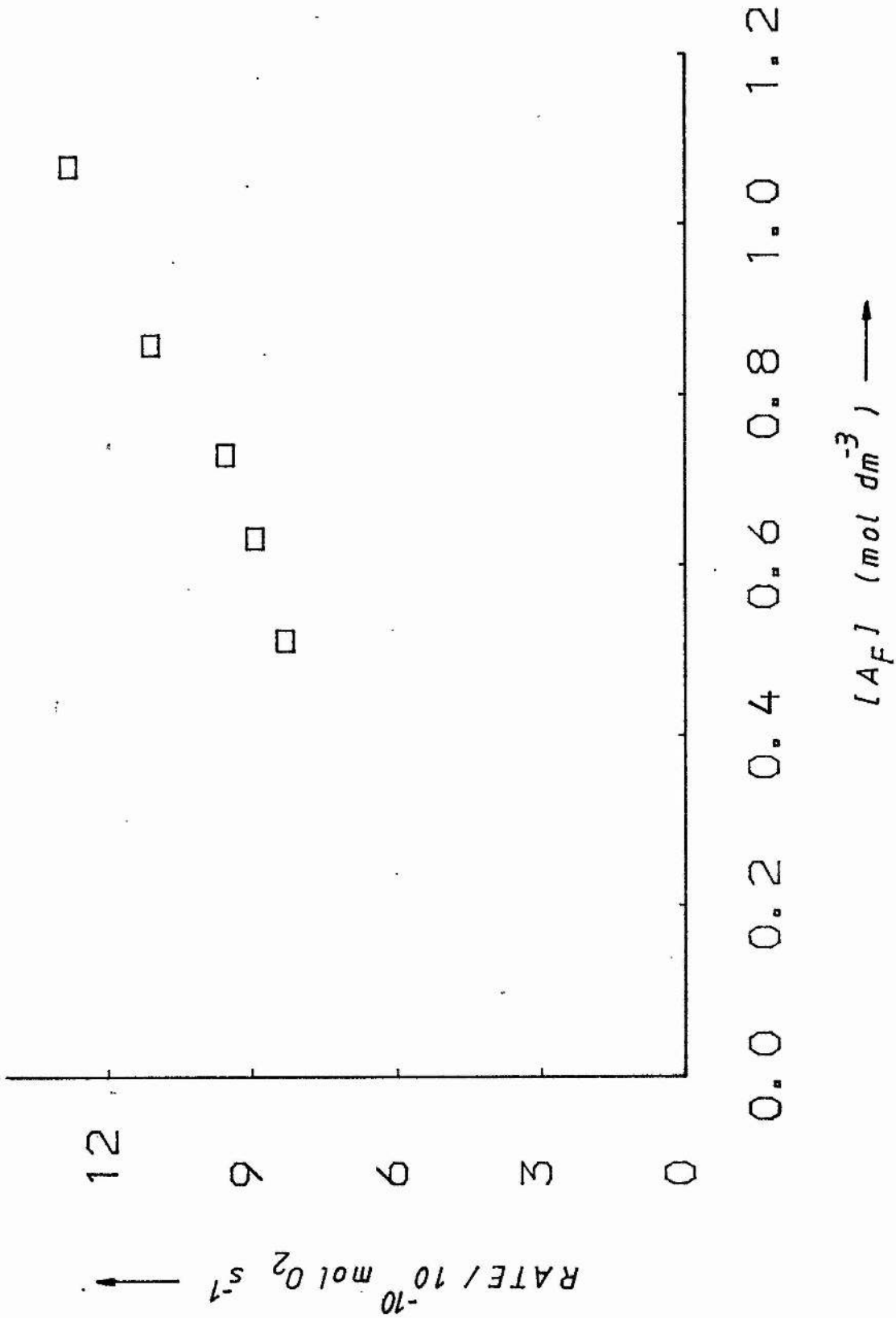

Figure 1.27

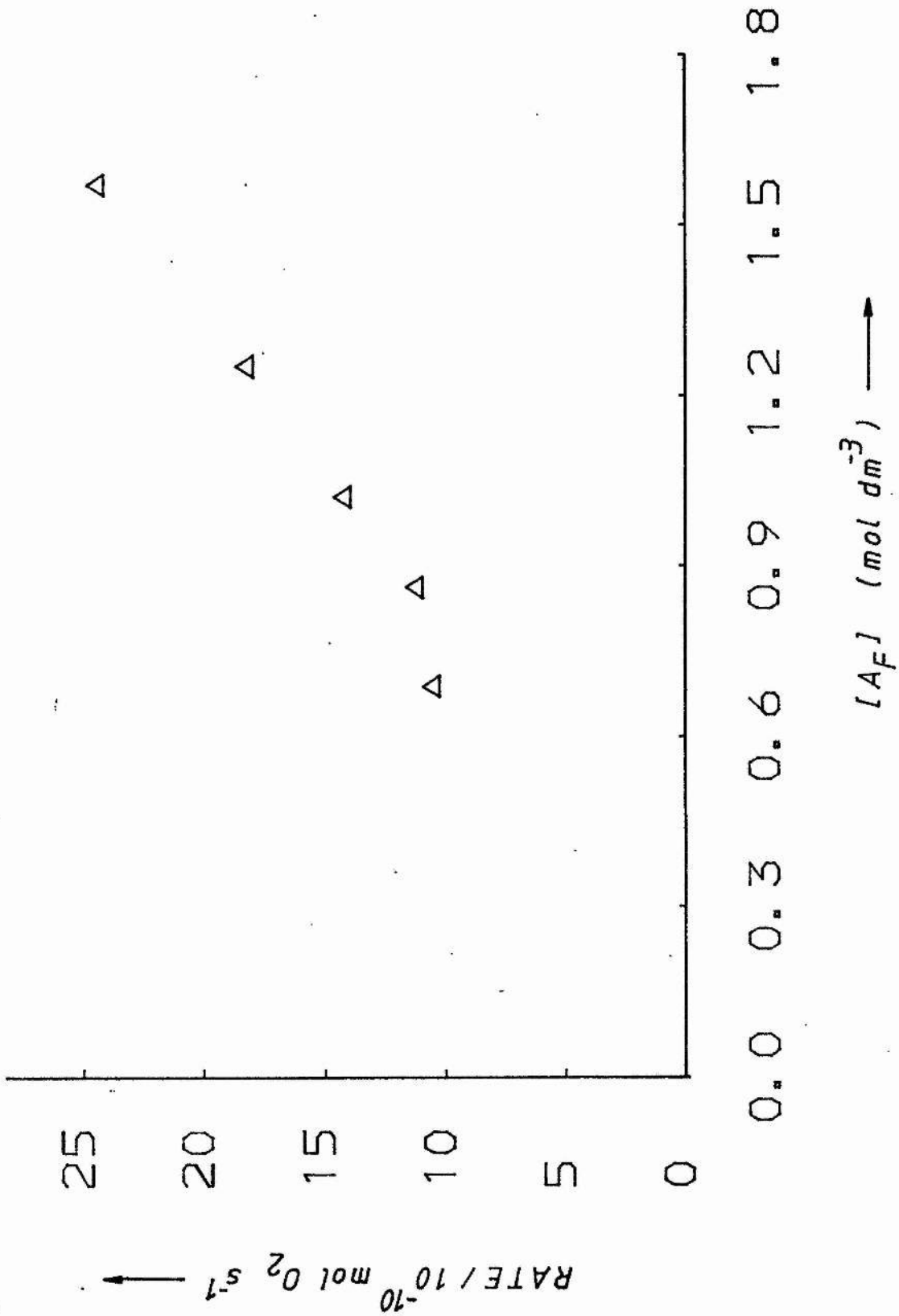

Figure 1.28

In the case of the 309 K data, Figure 1.28, linear regression analysis yields a correlation coefficient, r of 0.99. Hence the actual "degree of linearity" of the plot using $[A_F]$ data is no better than that obtained previously when [A] values were used (Figure 1.18). However, recent evidence suggests that values of r may be insensitive to underlying non-linear trends in experimental data[66]. Thus slight changes in the absolute magnitude of this parameter should not be used as the sole criterion for confirming the existence of a linear relationship. Of greater importance in this case, is the fact that extrapolation of the 309 K plot back to zero $[A_F]$ yields an intercept approximately at the origin. This is in marked contrast to the positive intercept which one would obtain on extrapolation of the rate against [A] plot for this temperature. Hence:

$$\text{Rate} = k_a[A_F] \qquad (1.52)$$

and the slope of the plot in Figure 1.28, assuming that a linear relationship does exist, gives a value of 1.6×10^{-9} mol O_2 s^{-1} mol^{-1} (free OH) dm^3 for k_a.

Figure 1.27 shows the rate against $[A_F]$ relationship at 298 K. Linear regression analysis reveals, once again, a correlation coefficient of 0.99 and the comments made regarding the significance of this result at 309 K are applicable at this temperature also. However, at this lower temperature, a positive intercept is still obtained on extrapolation to zero $[A_F]$, albeit the magnitude of this

is much smaller than the corresponding bulk alcohol plot in Figure 1.18 would suggest.

The physical meaning of a positive intercept is that when no free hydroxyl groups are present - ie. in neat cyclohexane - there is an additional, slow, oxygen consuming process in operation. This is at variance with the previous observation that no oxygen-uptake could be measured when a neat cyclohexane/anatase suspension was employed. However if, during the irradiation of a propan-2-ol/anatase suspension, another species (say "X") was formed, which could itself carry out an oxygen consuming sequence of reactions, then extrapolation of slurry composition to zero free hydroxyl concentration would still leave this species present and could account for the positive intercept.

The properties of X would have to be such that variation of its reaction rate with temperature would be very small. This must be the case since its contribution at 309 K to the total extent of oxygen consumption would be completely out-weighed by that of the free hydroxyls, leading to the observed zero intercept in this case. Hence, once X is formed, a competition for surface site interaction would be set-up between X and the free hydroxyl groups.

An estimation of the magnitude of the effect of X can be obtained by analysing the oxygen-uptake rate against $[A_F]$ plot at 298 K. Let it be assumed that the relative contribution to the total oxygen-uptake rate by X is proportional to the cyclohexane concentration. Provided it is accepted that propan-2-ol is essential

for X formation, this assumption is reasonable, since if there is a high alcohol concentration, X will contribute relatively little to the overall oxygen-uptake rate. Hence:

$$\text{Rate} = k_b[A_F] + k_x[\text{cyclohexane}] \qquad (1.53)$$

From the intercept in Figure 1.27, of 4.2×10^{-10} mol O_2 s^{-1} and knowing that the concentration of neat cyclohexane at 298 K is 9.26 mol dm^{-3}, a value for k_x of 4.6×10^{-11} mol O_2 s^{-1} mol^{-1} (cyclohex.) dm^3 is obtained. A data analysis computational routine was written (see Appendix II) which utilised this estimated k_x value and adjusted it, in an iterative fashion, until the k_x[cyclohexane] contribution could be subtracted, so as to leave the corrected rate against $[A_F]$ intercepting approximately at the origin. This "corrected" plot is given in Figure 1.29 and the associated data used in connection with the computer program are listed in Table 1.16.

Table 1.16: Corrected Uptake Rate Data at 298 K

RATE (MEASURED) (mol O_2 s^{-1}/ 10^{-10})	RATE (CORRECTED) (mol O_2 s^{-1}/ 10^{-10})	$[A_F]$ (mol dm^{-3})	[CYCLOHEXANE] (mol dm^{-3})
8.32	6.12	0.51	6.95
8.94	7.03	0.63	6.02
9.54	8.07	0.73	4.63
11.10	10.40	0.86	2.32
12.80	12.80	1.07	0.00

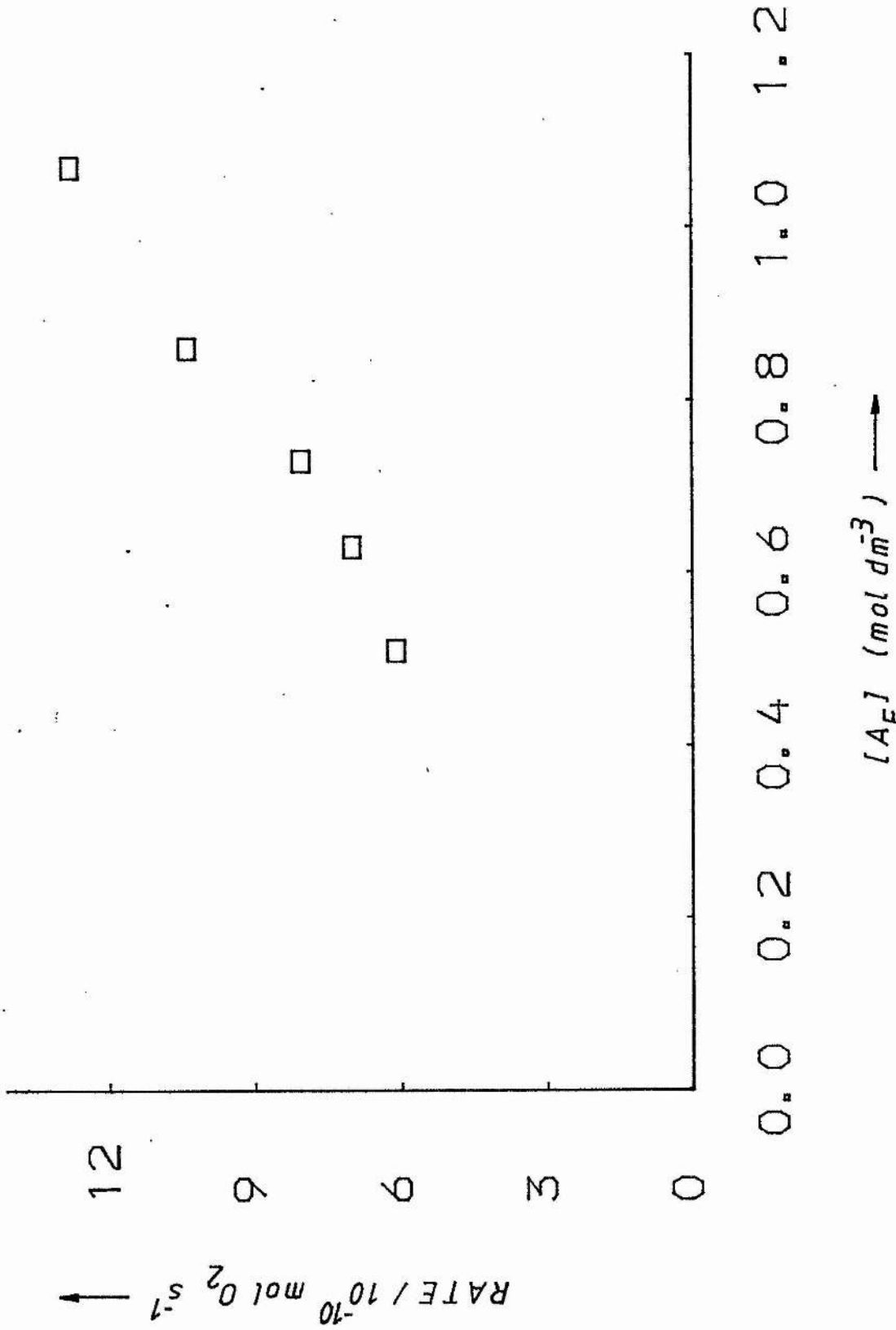

Figure 1.29

As a result of the computer controlled data correction, an optimised value for k_x is 3.2 x 10^{-11} mol O_2 s^{-1} mol^{-1}(cyclohex.)dm^3, while from the slope of the plot in Figure 1.29, a value of 1.25 x 10^{-9} mol O_2 s^{-1} mol^{-1}(free OH)dm^3 may be assigned to k_b. Thus an increase in temperature of 11 K, from 298 K to 309 K yields an approximate increase of 28% in the oxygen-uptake rate constant. This suggests an activation energy of *ca.* 17.5 kJ mol^{-1} (calculated using the two available points).

1.8.6 The Identification of Species X

Several researchers have reported the detection of hydrogen peroxide (H_2O_2) in irradiated propan-2-ol/TiO_2 suspensions[26,27]. However the exact nature of the involvement of this species has not yet been fully established. A line of research was therefore carried out; firstly to confirm the presence of H_2O_2 in our propan-2-ol/anatase system, when irradiated, and secondly to see if deliberate addition of this species could lead to an enhancement in oxygen-uptake rate. Positive results in each of these sets of experiments would then enable the assignment of H_2O_2 as being a probable candidate for species X.

1) The Detection of H_2O_2

A propan-2-ol/anatase (Tioxide) suspension was prepared in the usual way. The slurry was placed in the uptake cell and two samples were withdrawn; one before irradiation (sample A) and one after exposure to the mercury arc lamp for 1 hour (sample B). Both samples were carefully centrifuged and the supernatent liquid separated from the anatase. A few drops of an acidic solution of Ti^{3+} ions were added to each solution. In the case of sample A, no change in colour was observed but with sample B, the characteristic orange/yellow colouration due to complex formation was observed.

The use of Ti^{3+} ions to detect the presence of H_2O_2 constitutes a sensitive and widely used confirmatory test[67-69]. No attempt was made to quantify the H_2O_2 concentration, however this experiment gave clear evidence that this species is produced only upon irradiation of the suspension. Hence, as with propanone formation, the production of H_2O_2 must be dependent on the initial exciton formation in TiO_2.

2) Participation of H_2O_2 in Oxygen-Uptake

A fresh propan-2-ol/anatase suspension was prepared and *ca.* 2 cm^3 of a 30 wt% solution of H_2O_2 added. Full thermal equilibration in the dark was effected and an oxygen-uptake experiment performed at 298 K, in the usual manner. Because of the high energy requirement for absorption by H_2O_2[70], direct photodissociation in the pyrex experimental cell would be improbable in view of the wavelength

cut-off at ca. 310 nm. In addition the anatase, present in great excess relative to H_2O_2, possesses a very high extinction coefficient in the accessible spectral region.

On exposure to the lamp, a fast rate of oxygen consumption was observed, after the usual initial equilibration phase. This rapid uptake behaviour lasted for ca. 32 mins; thereafter the rate decreased gradually to give a new linear rate. This was close to the expected value at 298 K in the absence of any added H_2O_2. The relevant oxygen-uptake isotherm is illustrated in Figure 1.30. Comparison of the linear regions reveals that the initial enhancement was ca. 30% greater than would be expected under identical experimental conditions but without the addition of H_2O_2. The linear rate data obtained from the isotherm in Figure 1.30 is given in Table 1.17.

Table 1.17: Effect of H_2O_2 Addition on Uptake Rate

TIME REGION (mins)	CORR. COEFF. (r)	UPTAKE RATE (mol O_2 $s^{-1}/10^{-9}$)
12 - 32	0.995	1.6
36 - 60	0.988	1.2

We have shown that H_2O_2 is produced during irradiation of a propan-2-ol/anatase suspension and furthermore that once produced, this species can interact with the system in such a way that an enhancement in oxygen-uptake rate is observed. Hence the action of the H_2O_2, produced during the photoprocesses, is consistent with that

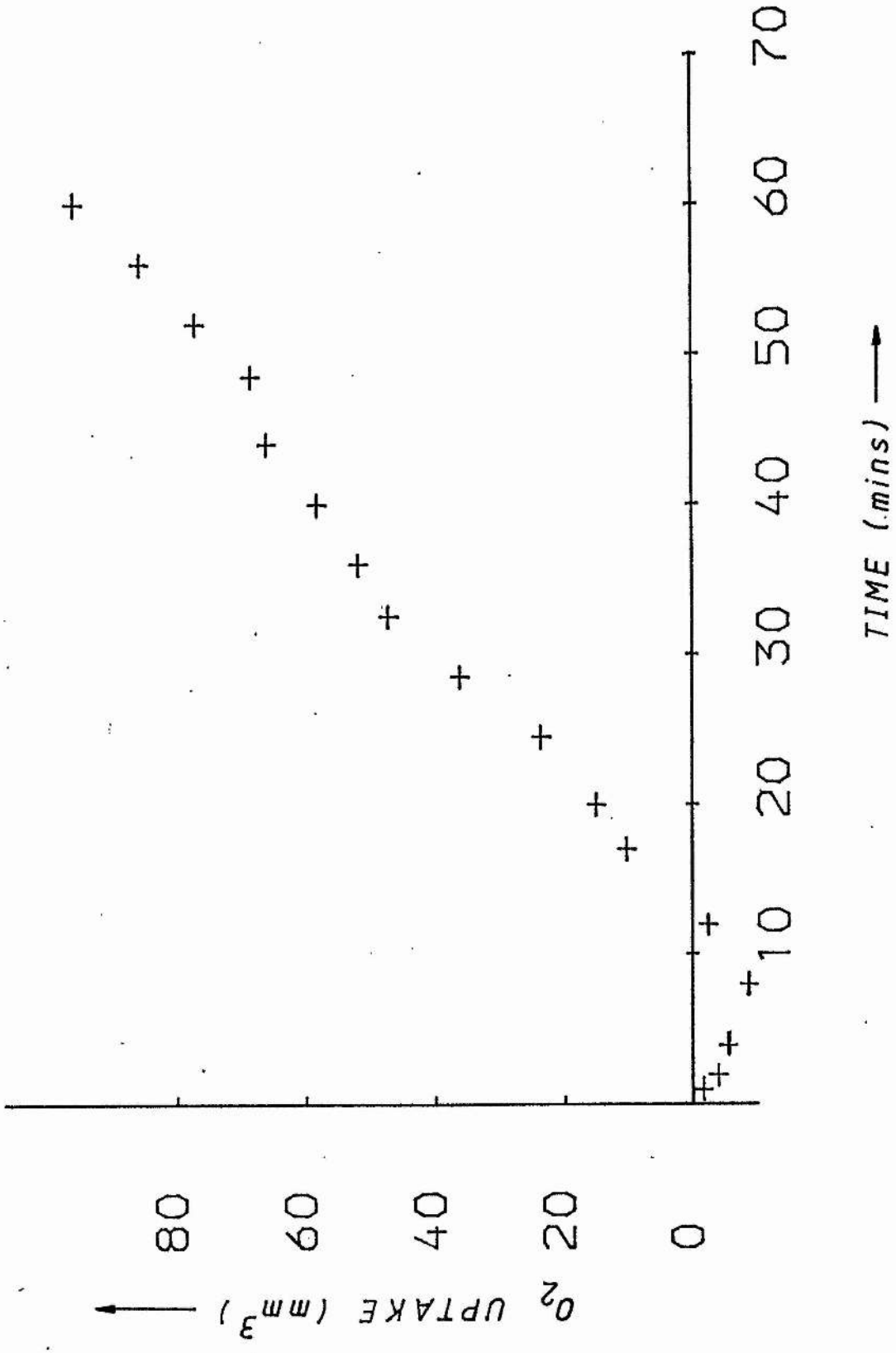

Figure 1.30

of species X since, once formed, it appears to initiate oxygen consumption which may be independent of alcohol concentration. In addition, if the concentration of H_2O_2 produced is low, then its contribution to the total oxygen consumption rate may be small and hence its involvement may be masked at higher temperatures by competitive oxygen-uptake processes.

In the case of the experiment in which H_2O_2 was added to the system, the levelling-off of the uptake rate after a period of time suggests that the H_2O_2 may be consumed until a balance is achieved between H_2O_2 production and consumption. Evidence in support of this assertion comes from studies by P.R. Harvey et al.[27], who added H_2O_2 to a propan-2-ol/rutile suspension which was then irradiated. By monitoring the H_2O_2 concentration, they observed a rapid drop followed by a levelling-off after ca. 30 mins.

1.9 Utility of the Oxygen-Uptake Technique

The important points regarding the effectiveness of this method may be summarised as follows:

1) This technique may be used in a quantitative manner to compare the photoactivity of different TiO_2 pigment grades.

2) Unlike conventional weathering techniques (see before), the oxygen-uptake system produces results over a short period of time.

3) The main advantage of measuring oxygen consumption rather than propanone formation is that the suspension need not be disturbed and hence more data can be obtained.

4) Provided that the position of the excitation source relative to the uptake cell remains fixed for a given series of comparative experiments - in view of the rate dependence on this parameter - good reproducibility of results (ca. 12%) can be obtained.

5) In consideration of the behaviour of a given pigment with varying temperature, care must be exercised in interpreting the results, since these will reflect, at least in part, the associative properties of the propan-2-ol. This is a constraint which has not not at all been appreciated in previous studies of this system.

6) The oxygen-uptake technique could be used effectively in the development and testing of agents which will reduce the photocatalytic activity of TiO_2 pigments.

7) Care must be taken to ensure that any material added to the suspension does not seriously affect the propan-2-ol self-association. In accordance with this important point, NMR studies were carried out on DABCO/propan-2-ol and H_2O_2/propan-2-ol mixtures and it was found that in both cases the self-association of the alcohol was unaffected by either additive, in the concentrations used previously.

Up to this point, this work has confined itself to studies of oxygen-uptake under various experimental conditions. In order to understand more fully the nature of the involvement of H_2O_2 and the role of oxygen molecules with the TiO_2 surface, a new technique was developed and this is the subject of the next Chapter.

CHAPTER 2

2 FIBRE OPTIC SURFACE MONITORING OF TITANIUM DIOXIDE

2.1 Introduction

This section of experimental work was initiated as a result of observations made during the oxygen-uptake studies. When a propan-2-ol/TiO_2 (anatase or rutile) suspension was placed in the uptake cell, a deep vortex was produced on agitation with the magnetic stirrer. On irradiation in the presence of air or oxygen, a yellow/green luminescence (YGL) was observed, originating from the vortex. Oxygen-uptake could be measured under these conditions. If, however, nitrogen gas was slowly bubbled into the suspension, the YGL gradually disappeared, to be replaced by a dull colouration. In addition, if nitrogen was employed as the atmosphere for an uptake experiment, no volume change was observed after the initial equilibration period. Clearly, therefore, the presence of the YGL is associated with an "activated" TiO_2 surface and the dull colouration with a "passivated" state. A novel technique was developed to enable direct measurement of the luminescence emanating from the vortex.

2.2 Description of Apparatus

Throughout this series of experiments, a specially constructed pyrex cell was employed. The cell was of ca. 50 cm^3 capacity and was elongated so that a deep vortex could be created when a suspension was activated by magnetic stirrer. A sketch showing the design features of the cell is given in Figure 2.1.

To enable the spectral distribution of the emission from the vortex to be detected, a fibre optic bundle (of ca. 5 mm diameter) was prepared. Each end was sealed into a brass ring and one end slotted into a holder attached to the top of the cell. The other end of the bundle was surrounded by a section of black cardboard and connected to the entrance window to the emission monochromator of a spectrofluorimeter (Perkin-Elmer model MPF-2A). The description and operational details of this instrument will be given in a later section. For these experiments, only the emission monochromator apparatus was employed, producing a chart recorder output of arbitrary intensity as a function of emission wavelength.

The excitation source used throughout was the medium pressure mercury arc lamp / power supply 2 combination, to maintain comparability with the oxygen-uptake experiments. The cell was masked with black tape over its entire surface, with the exception of a small, circular area centred approximately three quarters of the way down. A tube was used to connect this unmasked region to the mercury lamp. These precautions were carried out in order to minimise the

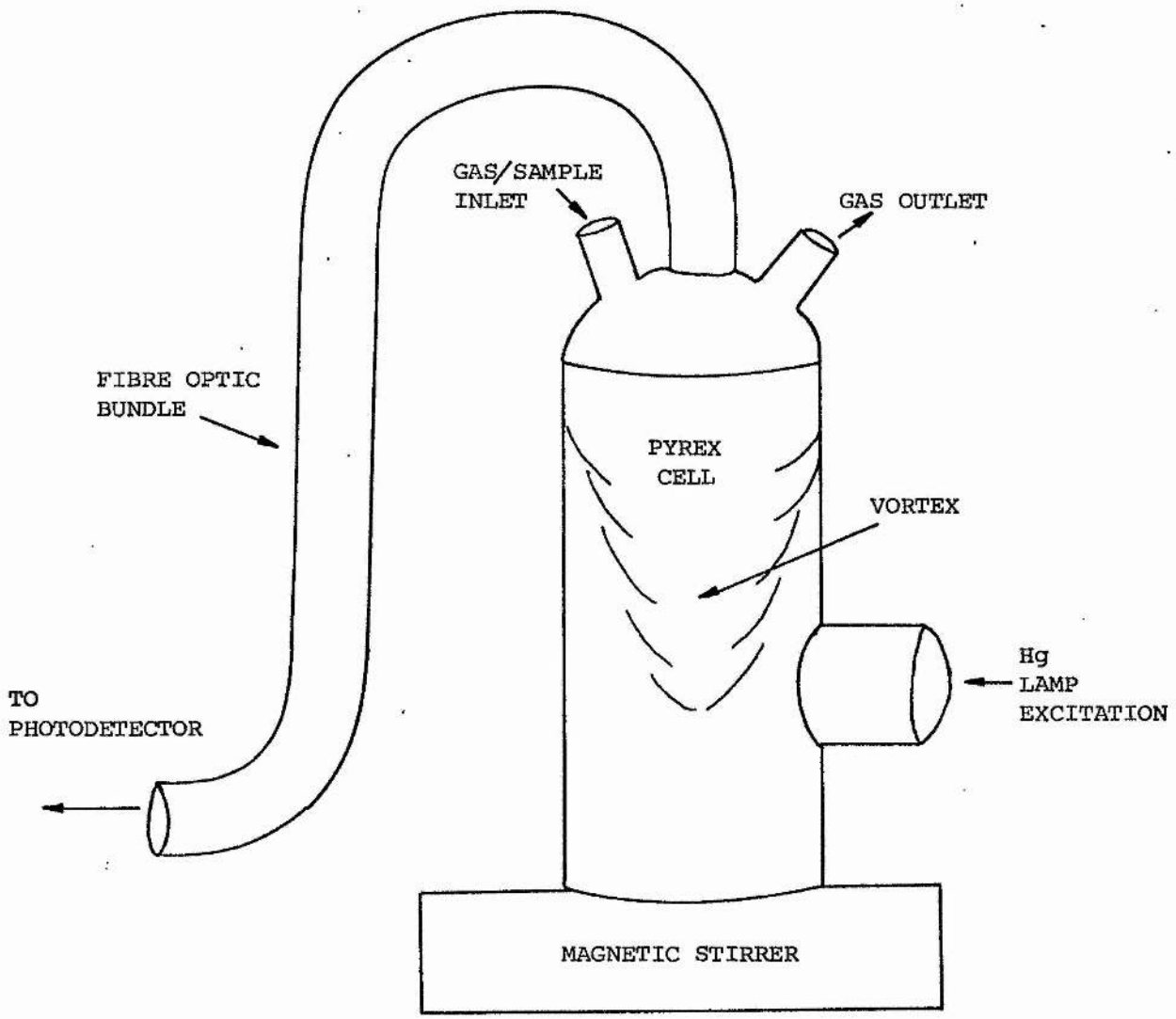

Figure 2.1 Fibre Optic Vortex Luminescence Apparatus

risk of the exciting radiation passing directly into the vortex, without first penetrating the suspension.

In order to keep the distance between cell and emission monochromator as short as possible, the cell and magnetic stirrer (Chemlab Instruments ltd.) were placed inside the sample compartment of the spectrofluorimeter. A special heat sink had to be provided for the stirrer to prevent it from overheating. Another advantage of incorporating the apparatus into the sample compartment was that the cover could be closed, thus isolating the cell from all light, other than from the mercury lamp, hence further reducing interference from extraneous sources of light.

Two sockets (B10 Quickfit) were incorporated into the top of the cell. One of these was used for bubbling either oxygen or nitrogen into the suspension, while the other was connected to a glass bubbler unit. Thus the flow rate could be maintained - albeit in a qualitative fashion. The composition of the suspension was 0.5 g of the appropriate TiO_2 grade in 50 cm^3 of propan-2-ol (Analytical Grade (Fisons). Hence the same pigment:volume ratio was used as in the oxygen-uptake experiments. The H_2O_2 used in a few of the experiments consisted of a 30 wt % solution.

2.3 Results and Discussion

The transmission characteristics of the fibre optic bundle were assessed by exposing one end directly to the mercury lamp. Figure 2.2 shows that the bundle is capable of transmitting light down to the near UV region. In particular, the 366 nm line is readily detectable.

2.3.1 Vortex Spectrum of Propan-2-ol/Anatase in Air

Initial studies were carried out using a propan-2-ol/anatase (Tioxide) suspension in air. The characteristic YGL was observed and the associated "vortex spectrum" was detected by the emission monochromator via the fibre optic bundle. The vortex spectrum, obtained from the chart recorder output, is shown in Figure 2.3. Several points are worthy of note regarding this spectrum:

1) The mercury line at 366 nm is completely absent from the vortex luminescence. This is excellent confirmation that no direct radiation from the lamp was able to reach the vortex. Thus anatase, with its high extinction coefficient at 366 nm, readily removed this line leaving only the output lines in the visible region of the mercury lamp to pass through the suspension and reach the vortex.

2) The vortex spectrum obtained was of high intensity. Hence the detection system required to be operated only in a low sensitivity mode. The lines appear to show slight broadening, relative to the fibre optic response spectrum of Figure 2.2. This is to be expected since a certain amount of light scattering would occur on passing through the suspension. However, in the case of the response spectrum, narrower monochromator slit widths were used (1.75 nm as opposed to the 3.5 nm used in Figure 2.3) and this would account for a large part of the broadening.

3) A further consequence of the high intensity (and hence good signal to noise ratio) of the vortex spectrum was that a high degree of reproducibility could be obtained. Several runs of the same sample and under the same experimental conditions yielded lines, the relative intensities of which varied by only ca. 3%.

4) The four mercury lines constituting the vortex spectrum in Figure 2.3 may be divided into two categories: the yellow/green (YG) lines at 579 nm and 546 nm and the blue lines (B) at 405 nm and 436 nm. Since the yellow/green lines appear relatively more intense

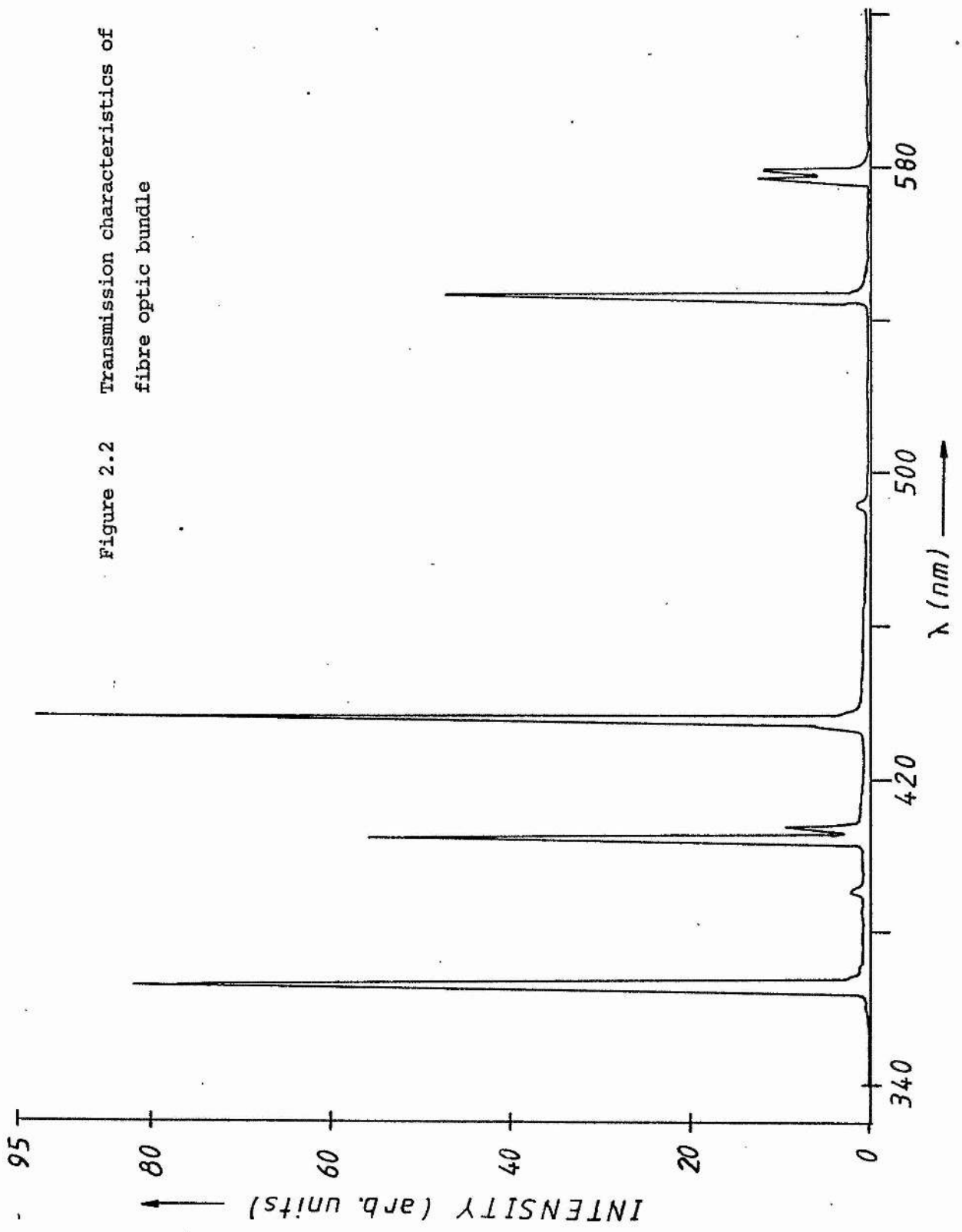

Figure 2.2 Transmission characteristics of fibre optic bundle

Figure 2.3 Vortex Spectrum of propan-2-ol/anatase in air

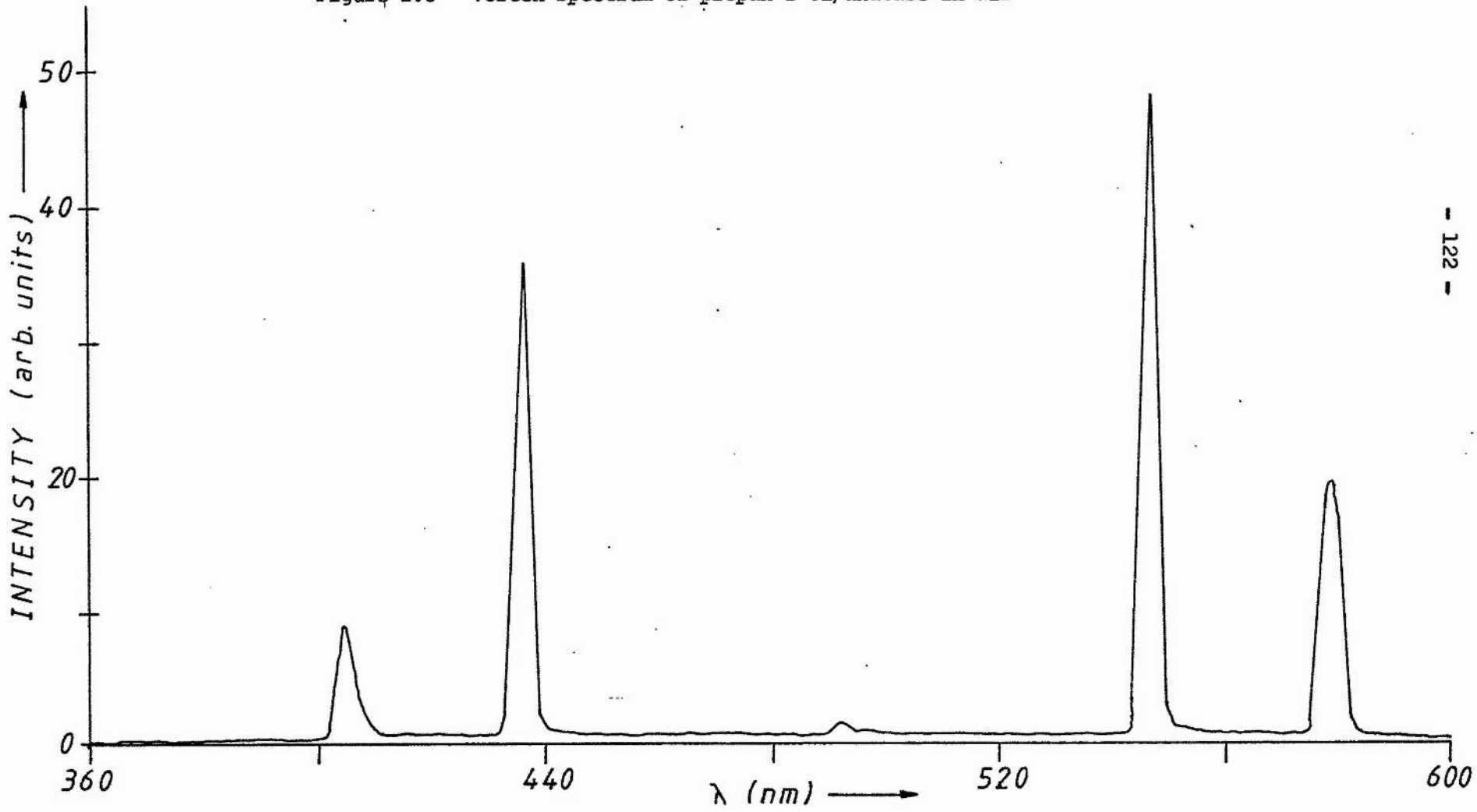

than those at the blue end of the spectrum, this explains why the vortex spectrum appears to the observer to be yellow/green under these particular experimental conditions.

2.3.2 Vortex Spectrum of Propan-2-ol/Rutile in air

A fresh suspension of propan-2-ol/rutile (Tioxide) was placed in the cell and a vortex spectrum obtained in air. This is illustrated in Figure 2.4. The major obvious difference between this spectrum and the corresponding one for anatase (Figure 2.3) is the almost complete absence of the 405 nm blue line. This important observation constitutes excellent experimental evidence for the lower band gap energy of rutile. Since photons at this longer wavelength will be absorbed on passing through the suspension, they will thus be absent once the vortex is reached.

In view of the above observation, this vortex spectral technique could be applied, specifically, to a determination of the bandgap energies of modified TiO_2 samples. Such determinations would, however, require a continuous excitation source. An example of this is the xenon lamp, which forms the light source for the spectrofluorimeter instrument itself. However, the output of this particular lamp (150W) proved to be too low to be of any value.

Figure 2.4 Vortex Spectrum of propan-2-ol/rutile in air

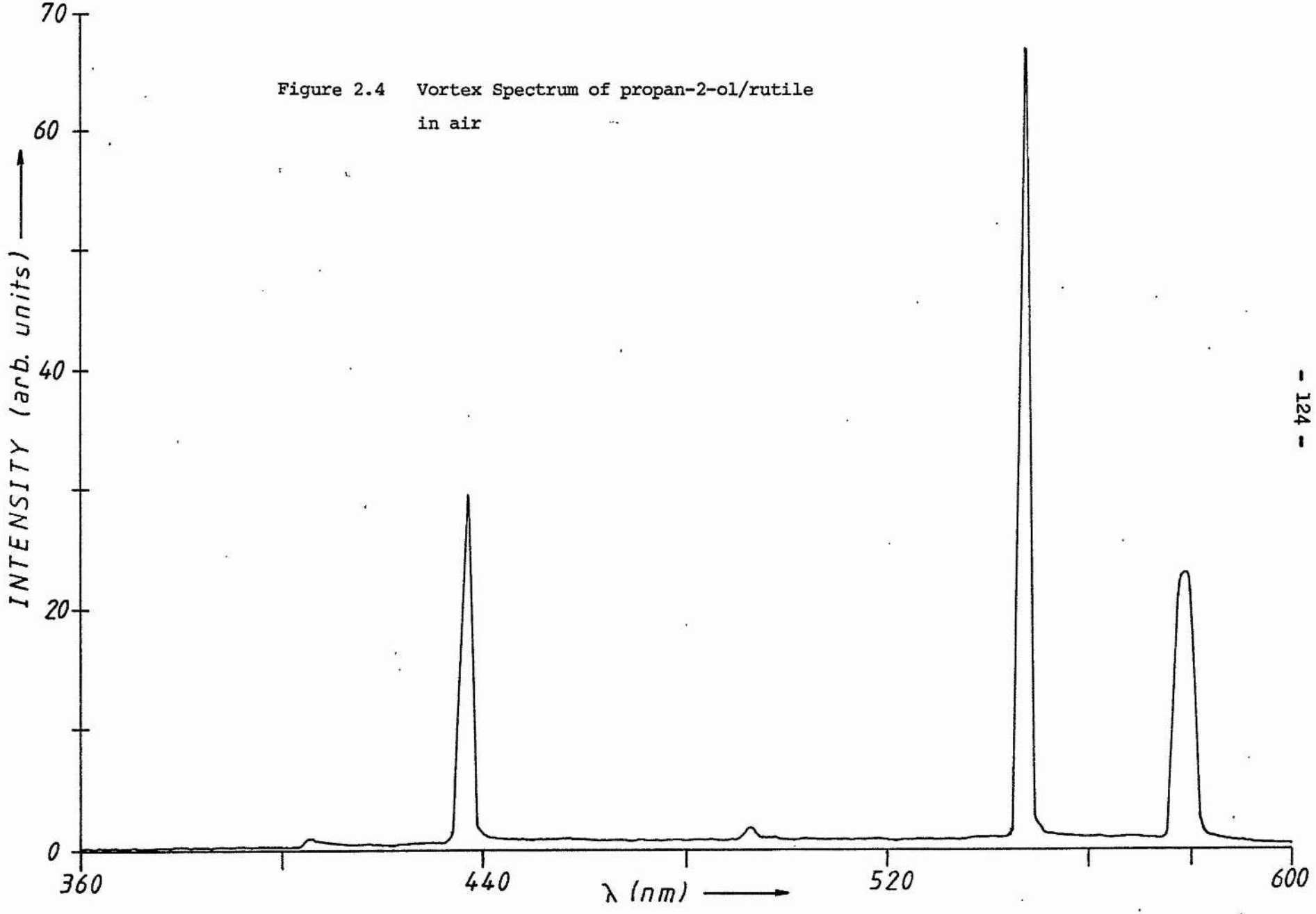

It should be noted when drawing a comparison between the anatase and rutile vortex spectra of Figures 2.3 and 2.4, that the cell had to be removed between each experiment to allow sample changing etc. Since the replacement of the cell in the exact same position could not be guaranteed, the absolute intensities of the spectral lines cannot be compared directly. However, the ratios of line heights should be comparable and to this end, one can define a YG:B ratio. This parameter may be calculated from the following equation:

$$\text{YG:B} = \frac{\text{Height of 546 nm Vortex Line}}{\text{Height of 436 nm Vortex Line}} \qquad (2.1)$$

These particular lines were chosen as they are the more intense YG and B lines - and in the case of rutile, the 436 nm line represents the only possible one. Hence where possible, YG:B ratios will be quoted when drawing comparisons between samples under different experimental conditions.

2.3.3 Effect of O_2/N_2 on Vortex Spectra for Propan-2-ol/Anatase

On irradiation of a fresh suspension of propan-2-ol/anatase in air, the YG:B ratio was observed to increase from an initial value of ~1.3 up to ~2.3 - consequently the vortex emission appeared more intense on visual examination. This optimum value in air of ca 2.3

could not be improved upon (using constant experimental conditions).

If oxygen was gradually bubbled through the suspension during irradiation, the YG:B ratio increased slowly until a maximum value of ca. 4.0 was attained after approximately 20 mins. Alternatively, if at this stage nitrogen gas was substituted for oxygen and this was passed through the suspension at approximately the same rate, a gradual reduction in YG:B ratio was observed. A minimum value was reached (after ca. 40 mins continuous bubbling with N_2) of ~0.8. The onset of the dull colouration in the vortex coincided with the point at which the relative intensity of the blue lines exceeded that in the yellow/green region ie. when YG:B became < 1.0).

Up until this point, only relative intensity changes have been mentioned; due to the problems of maintaining the same optical alignment, discussed above. However, in order to gain an idea of the absolute change in line intensities making up the vortex spectrum, a carefully controlled experiment was performed in which the optical alignment was maintained constant and the same sample used throughout. The experimental conditions employed were such that a spectrum was obtained, in the usual way, for a propan-2-ol/anatase suspension in which N_2 had been bubbling very slowly for ca. 30 mins. Over the following 30 mins, the onset of the dull colouration was observed and a final spectrum obtained at the end of this period.

The vortex spectra corresponding to the controlled alignment experiment are shown in Figure 2.5. As can be seen, the magnitudes of the blue lines remained very nearly the same in each case. This was in marked contrast to the behaviour of the lines in the yellow/green region, which decreased by a factor of two between 30 mins and 60 mins purging with N_2. Hence the differences in the YG:B ratios may be accounted for entirely by changes in the absolute intensities of the yellow/green lines.

2.3.4 Effect of H_2O_2 on Vortex Spectra for Propan-2-ol/Anatase

In a previous section, it was established that the presence of H_2O_2 in a propan-2-ol/anatase slurry had a profound effect on the oxygen-uptake rate of the system. In order to test the effect of H_2O_2 on the vortex spectrum, an experiment was carried out in which a fresh propan-2-ol/anatase suspension was prepared and carefully purged with N_2 during irradiation. Once the minimum YG:B ratio had been reached (~0.8), 2 drops of a solution of 30 wt % H_2O_2 were added and an instantaneous reappearance of the yellow vortex luminescence was observed. Another vortex spectrum was recorded immediately and a YG:B ratio of 1.2 obtained. Figures 2.6 and 2.7 show the vortex spectra before and immediately after the addition of H_2O_2 respectively.

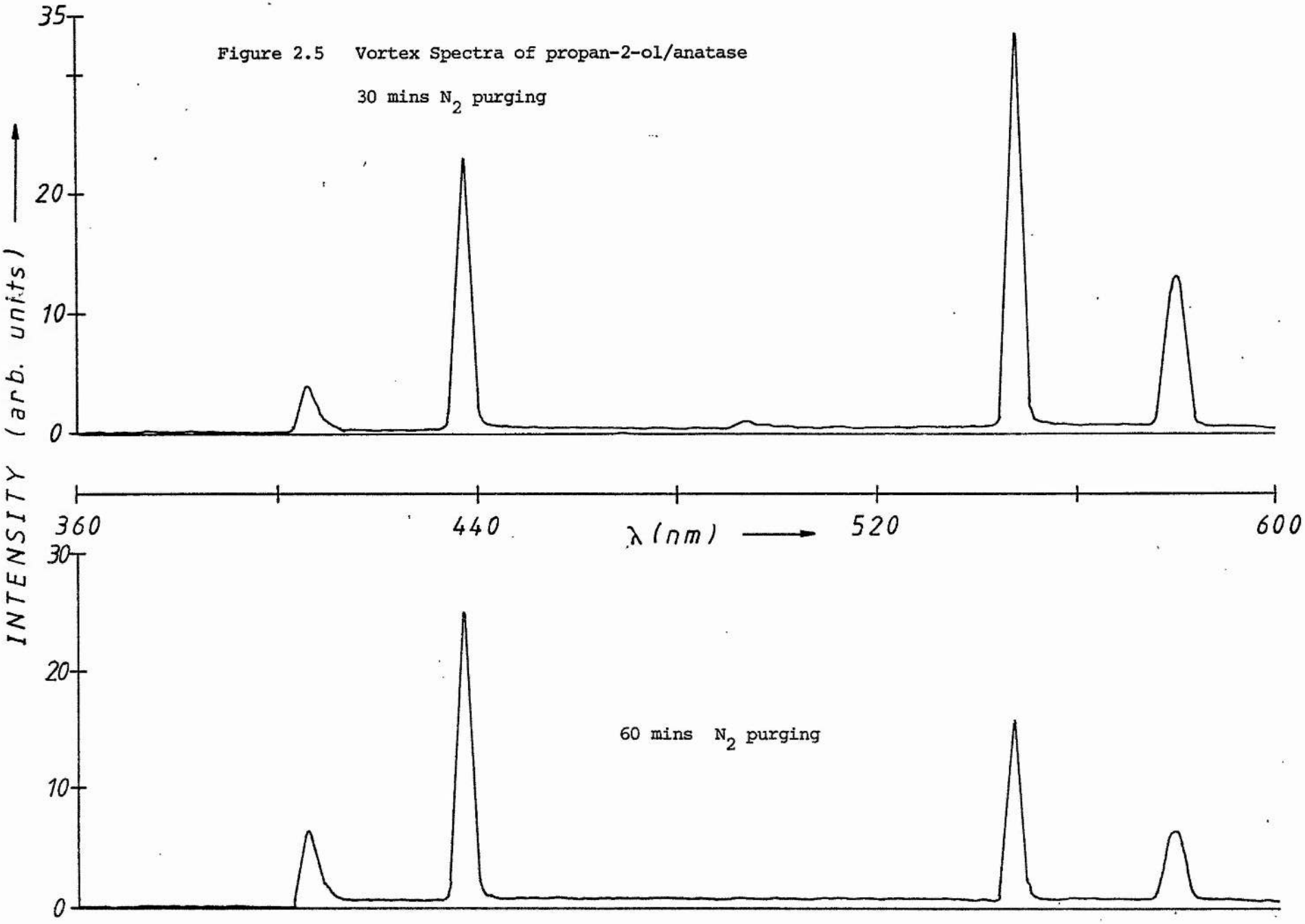

Figure 2.5 Vortex Spectra of propan-2-ol/anatase

30 mins N_2 purging

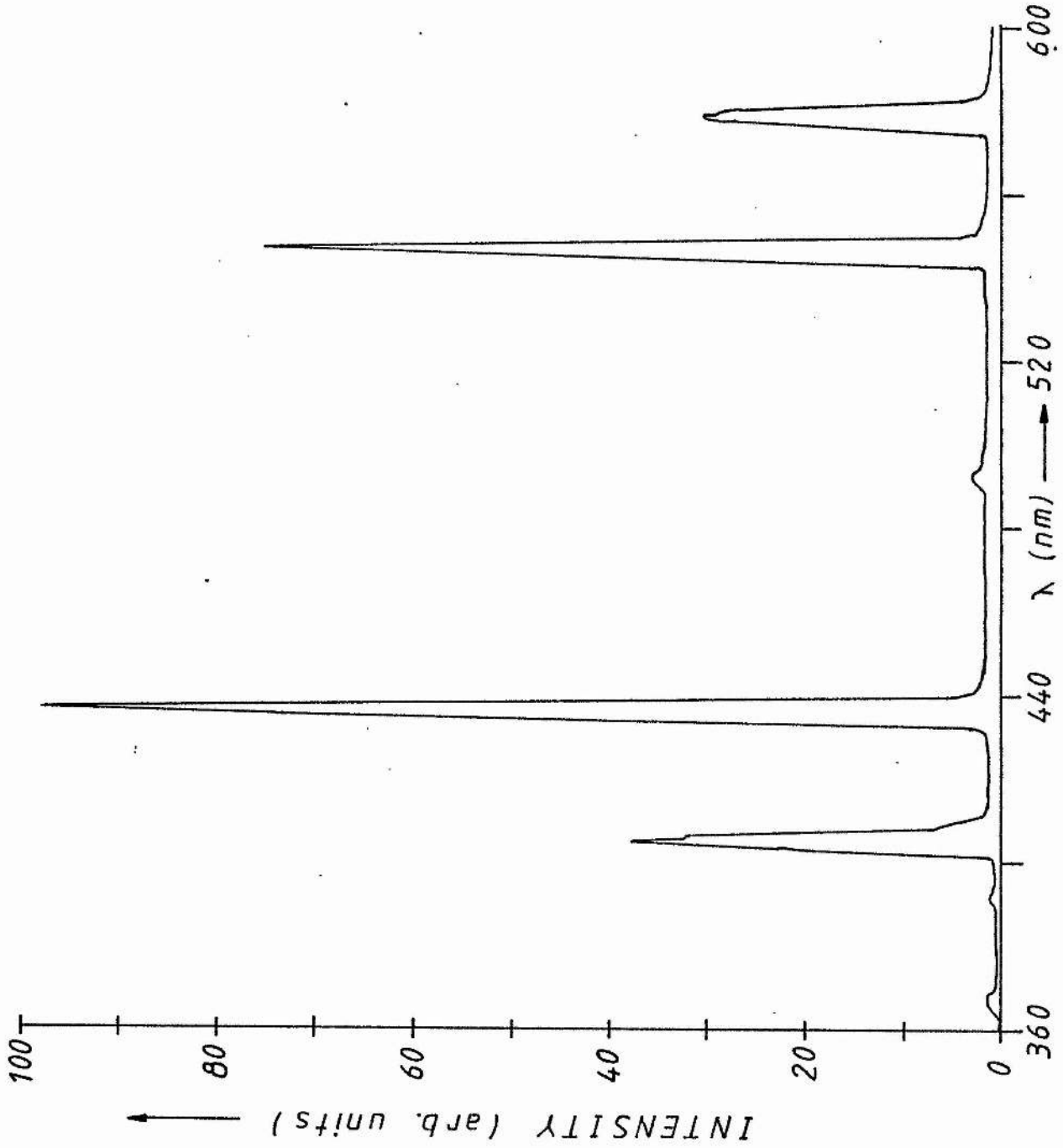

Figure 2.6

Vortex Spectrum of propan-2-ol/anatase purged with N_2

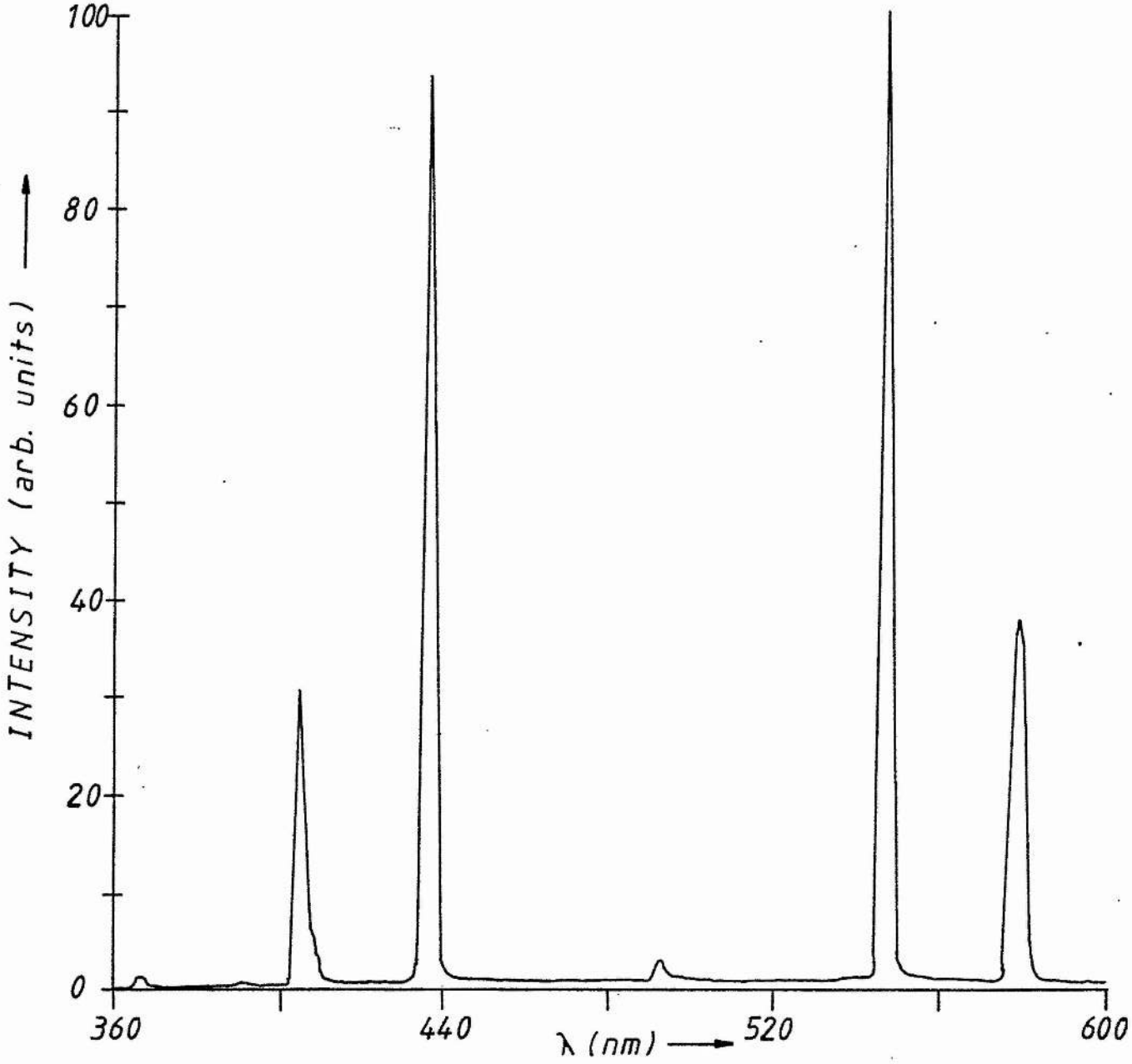

Figure 2.7

Vortex Spectrum (as for figure 2.6 plus H_2O_2)

Clearly the effect of H_2O_2 on the vortex spectrum is the same as that of O_2. The faster action of H_2O_2 may be due either to the greater solubility of this species in the suspension, or that the surface affinity for H_2O_2 is greater than that for O_2. It is obvious, however, that the readiness of H_2O_2 to induce ygl must be linked to the rate enhancement for oxygen-uptake and consideration must now be given to the nature of the surface interaction of H_2O_2 and O_2 in the light of all the vortex data obtained.

2.3.5 Rationalisation of the Yellow/Green Vortex Luminescence

From the experiment in which the optical and sample alignment remained fixed, it was concluded that the appearance of the YGL depended on the intensity of the mercury lines at 579 nm and 546 nm penetrating through to the vortex. Thus in the dull (passive) state, the suspension must be able to selectively absorb the visible radiation above 500 nm, leaving the blue lines at 405 nm and 436 nm to pass through unimpeded.

The selective absorption phenomenon, which gives rise to the dull colouration may be explained by the production of surface Ti^{3+} sites. Figure 2.8 shows the visible absorption spectrum of $[Ti(H_2O)_6]^{3+}$. Clearly the maximum absorption occurs in the 500 - 600 nm region. Absorption in this spectral area is due to the t_{2g} ---> e_g electronic

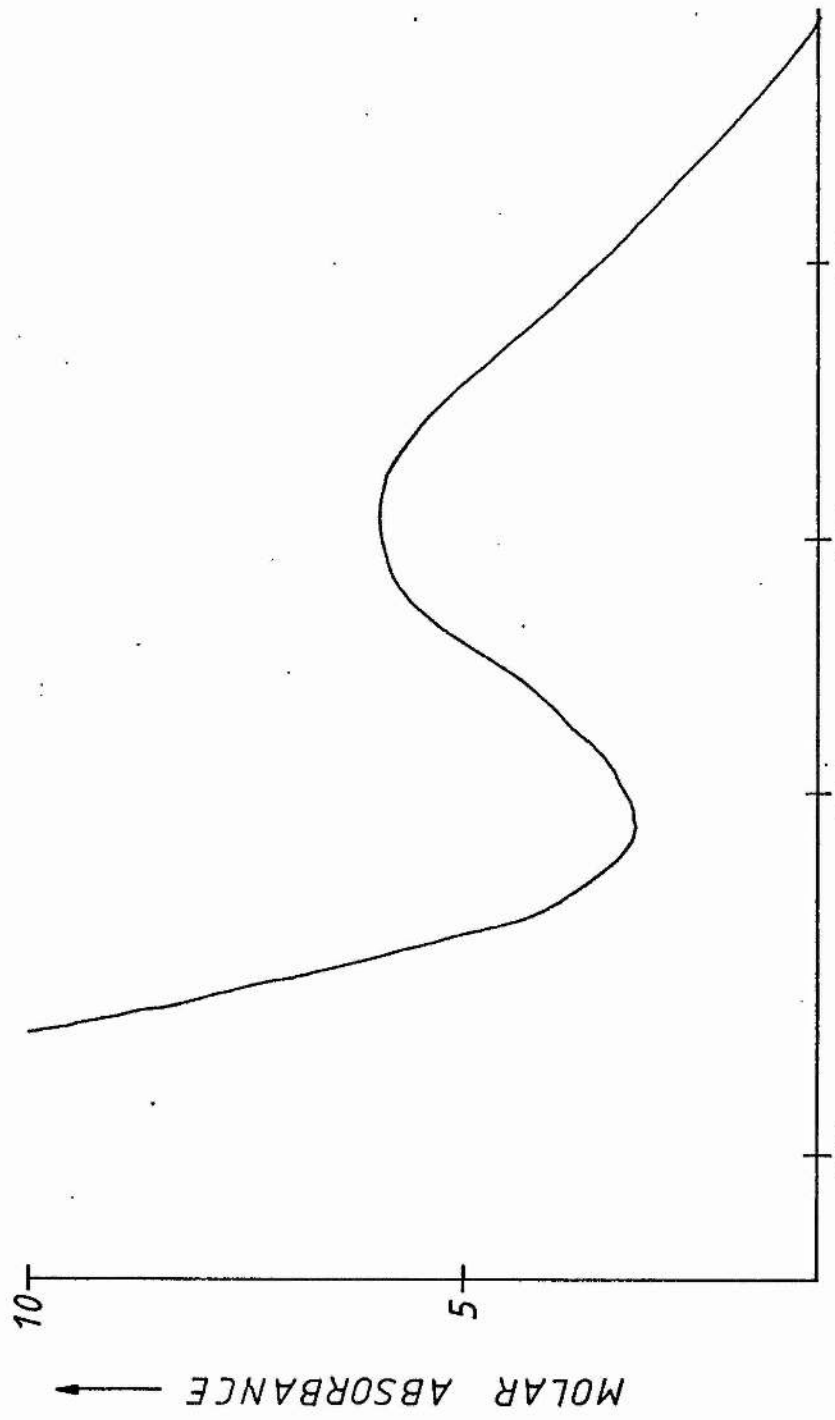

Figure 2.8 Absorption Spectrum of $[Ti(H_2O)_6]^{3+}$

transition of the single d electron associated with the Ti^{3+} ion[71]. By contrast, the Ti^{4+} ion, since it possesses no d electrons, cannot undergo a comparable transition in the visible region.

Although Figure 2.8 relates to absorption by a Ti^{3+} complex in solution, there is good experimental evidence in the literature to suggest that the energy required for the analogous electronic transition in the solid state is of comparable magnitude[29,72-74]. Thus the passive state of TiO_2, resulting from irradiation in the absence of oxygen or externally added H_2O_2, must be associated with a build-up of Ti^{3+} surface sites. In the presence of either O_2 or H_2O_2, the active state is formed in which the surface sites are converted to Ti^{4+} centres. Support for these assertions comes from esr studies in which a signal characteristic of Ti^{3+} ions was detected for an irradiated TiO_2 sample with no O_2 present. On subsequent admission of O_2, the signal gradually disappeared[75].

On the basis of the above arguments, it is reasonable to assume that both O_2 and H_2O_2 molecules are capable of converting Ti^{3+} sites to Ti^{4+}. The Ti^{3+} sites could be formed initially by trapping of excitons and evidence in support of this being an important process on anatase was obtained previously in the study of oxygen-uptake rate dependence on intensity of radiation (section 1.6). Thus:

$$TiO_2 + h\nu \longrightarrow e + h \qquad (2.2)$$

followed by migration of excitonic species to surface traps:

$$h + [Ti^{4+}\ {}^{-}OH]_s \longrightarrow [Ti^{4+}\ {}^{\cdot}OH]_s \qquad (2.3)$$

$$e + [Ti^{4+}\ {}^{\cdot}OH]_s \longrightarrow [Ti^{3+}\ {}^{\cdot}OH]_s \qquad (2.4)$$

where $[\ ]_s$ represents a site at the TiO_2 surface (bonds to adjacent O^{2-} ions are not shown). These surface sites will most likely occur at defect regions of the TiO_2 particles[76].

Clearly, in the absence of any additional agent, the build-up of Ti^{3+} surface ions will be maintained. In the presence of oxygen, however, the most likely step leading to conversion to Ti^{4+} involves the production of the super-oxy-radical anion[77-79]:

$$[Ti^{3+}\ {}^{\cdot}OH]_s + O_{2\ (ads)} \longrightarrow [Ti^{4+}\ {}^{\cdot}OH\ O_2^-]_s \qquad (2.5)$$

where the adsorption of O_2 onto the TiO_2 surface is shown as a prerequisite to reaction. Good evidence in support of oxy-radicals remaining adsorbed at transition metal centres comes from the work of A. Tkac[80].

The data from the vortex experiments highlights the need to find an additional Ti^{3+} ---> Ti^{4+} reconversion step, mediated by H_2O_2. Two different possibilities must be considered:

1) That H_2O_2 decomposes at the TiO_2 surface with the production of oxygen, thus:

$$2\ H_2O_2 \longrightarrow 2\ H_2O + O_2 \qquad (2.6)$$

The oxygen molecule would then be able to initiate the conversion of Ti^{3+} ions via equation (2.5). However this possibility may be discounted, since the oxygen-uptake experiment in which H_2O_2 was added to the suspension did not result in any observed increase in gas pressure in the cell (see section 1.8.6).

2) The direct conversion of Ti^{3+} to Ti^{4+} by H_2O_2 via a Fenton type reaction:

$$[Ti^{3+}]_s + H_2O_2 \longrightarrow [Ti^{4+}\ {}^{\bullet}OH\ {}^{-}OH]_s \qquad (2.7)$$

Once again, the results of A. Tkac suggest that the hydroxyl radical will remain adsorbed at the surface[80]. This is a much more probable step since it is energetically favourable (with E^{o} = +1.57 V) as compared with only E^{o} = +0.25V for the well established Fe^{2+}/Fe^{3+} process[81]:

$$Fe^{2+} + H_2O_2 \longrightarrow Fe^{3+} + {}^{\bullet}OH + {}^{-}OH \qquad (2.8)$$

The vortex monitoring equipment has been used to explain the origins of the characteristic dull colouration in the absence of O_2 or added H_2O_2. Further applications of the technique could involve the effect of other agents, added to the suspension, on the vortex spectrum thereby enabling the deduction of their influence on the balance of oxidation states at the TiO_2 surface. As an example, it was found that when a small quantity of DABCO (see section 1.7) was added, no change in the YG:B ratio was observed. Hence the blocking

action of this material, established previously, cannot be preventing reaction (2.5) from occurring. It is thus likely that chelation of DABCO at surface sites acts in such a way as to inhibit further reactions, by stabilising the complex formed in this reaction. Evidence in support of chelation complexes of this sort achieving stabilisation may be readily found in the literature[68,69].

2.4 Mechanism of Propan-2-ol Photodehydrogenation to Propanone

In the light of the observations and experimental results obtained from both the oxygen-uptake and the fibre optic surface monitoring techniques, it is relevant, in this concluding section, to consider the mechanism of photocatalytic conversion of propan-2-ol to propanone by TiO_2.

From the oxygen-uptake studies, it is clear that the adsorption of the free OH group in a chain of propan-2-ol molecules will be a necessary prerequisite for conversion to take place, thus:

$$H\left(\begin{matrix}R\\O\end{matrix}---H-\begin{matrix}R\\O\end{matrix}---H\right)_x\begin{matrix}R\\O\end{matrix} + [Ti^{4+}]_s \longrightarrow H\left(\begin{matrix}R\\O\end{matrix}---H-\begin{matrix}R\\O\end{matrix}---H\right)_x\begin{matrix}R\\O\end{matrix}----[Ti^{4+}]_s \qquad (2.9)$$

(where x = 0 to max. chain length).

After exciton trapping, the vortex luminescence studies showed that either oxygen or H_2O_2 could be used to reconvert the surface Ti^{3+} ions to Ti^{4+} (via equations (2.5) or (2.7) respectively). Confirmation has been obtained, showing that in the presence of O_2, the super-oxy-radical anion is detectable[82]. In addition, experimental evidence has revealed the production of hydroxyl radicals - presumably as a consequence of hole trapping by adsorbed

hydroxide anions (as shown previously in equation (2.3))[29].

P.R. Harvey et al.[27], have suggested that the $O^-_{2(ads)}$ species will readily react with an adsorbed H_2O molecule via the following:

$$O^-_{2(ads)} + H_2O_{(ads)} \longrightarrow HO^{\bullet}_{2(ads)} + HO^-_{(ads)} \qquad (2.10)$$

The esr technique has been applied to detect the presence of the per-hydroxyl radical at the photoactivated TiO_2 surface[83]. Infrared studies have shown that only by thorough and prolonged outgassing can all traces of adsorbed water be removed from the TiO_2 surface[84]. Hence in all practical photocatalytic experiments, this species will be present to an appreciable extent. The hydroxide ion formed in reaction (2.10) can be viewed as replacing that which was lost in the hole trapping step.

Thus far in the mechanistic discussion, the net effect of the photoactivation of TiO_2 has been to convert one molecule each of O_2 and H_2O into $HO^{\bullet}_2$ and $HO^{\bullet}$ species, if one considers only the oxygen and not the H_2O_2 involvement. Once formed, these reactive free radical species will readily undergo hydrogen abstraction reactions with the adsorbed propan-2-ol molecule. The generally accepted sequence is:

$$(Me)_2CHOH_{(ads)} + HO^{\bullet}_{2(ads)} \longrightarrow (Me)_2\dot{C}\text{-}OH_{(ads)} + H_2O_2 \qquad (2.11)$$

$$(Me)_2\dot{C}\text{-}OH_{(ads)} + HO^{\bullet}_{(ads)} \longrightarrow (Me)_2C{=}O_{(ads)} + H_2O_{(ads)} \qquad (2.12)$$

with the H_2O molecule produced in reaction (2.12), replacing that

which was consumed in reaction (2.10). It is clear that equation (2.11) can provide a route to H_2O_2 formation. That H_2O_2 is formed during irradiation of the suspension was established in section 1.8.6. Once formed, a balance must be maintained between H_2O_2 molecules in the liquid phase and adsorbed on the TiO_2 surface. Evidence in support of this equilibrium comes from the fact that the H_2O_2 was detected in the liquid phase, ie. after removal of TiO_2, while P.R. Harvey et al. have suggested that H_2O_2 will readily adsorb onto the TiO_2 surface[27].

The H_2O_2 molecules which are adsorbed on the surface will have the opportunity to oxidise other $[Ti^{3+}]_s$ sites to $[Ti^{4+}]_s$ via equation (2.7). Hence two separate pathways may be envisaged. One of these would involve oxygen as the oxidising agent and in the course of its sequence of reactions, H_2O_2 can be produced by reaction (2.11). This alternative oxidising agent can then be consumed in competition with O_2. An analogous sequence of free radical processes may be depicted for the H_2O_2 pathway; culminating in the conversion of propan-2-ol to propanone. In both cases, once the propanone is formed, adsorption studies have shown that it will be readily displaced by a fresh propan-2-ol molecule[25]. The propan-2-ol dehydrogenation pathways involving oxygen and H_2O_2 are shown in Figures 2.9 and 2.10 respectively.

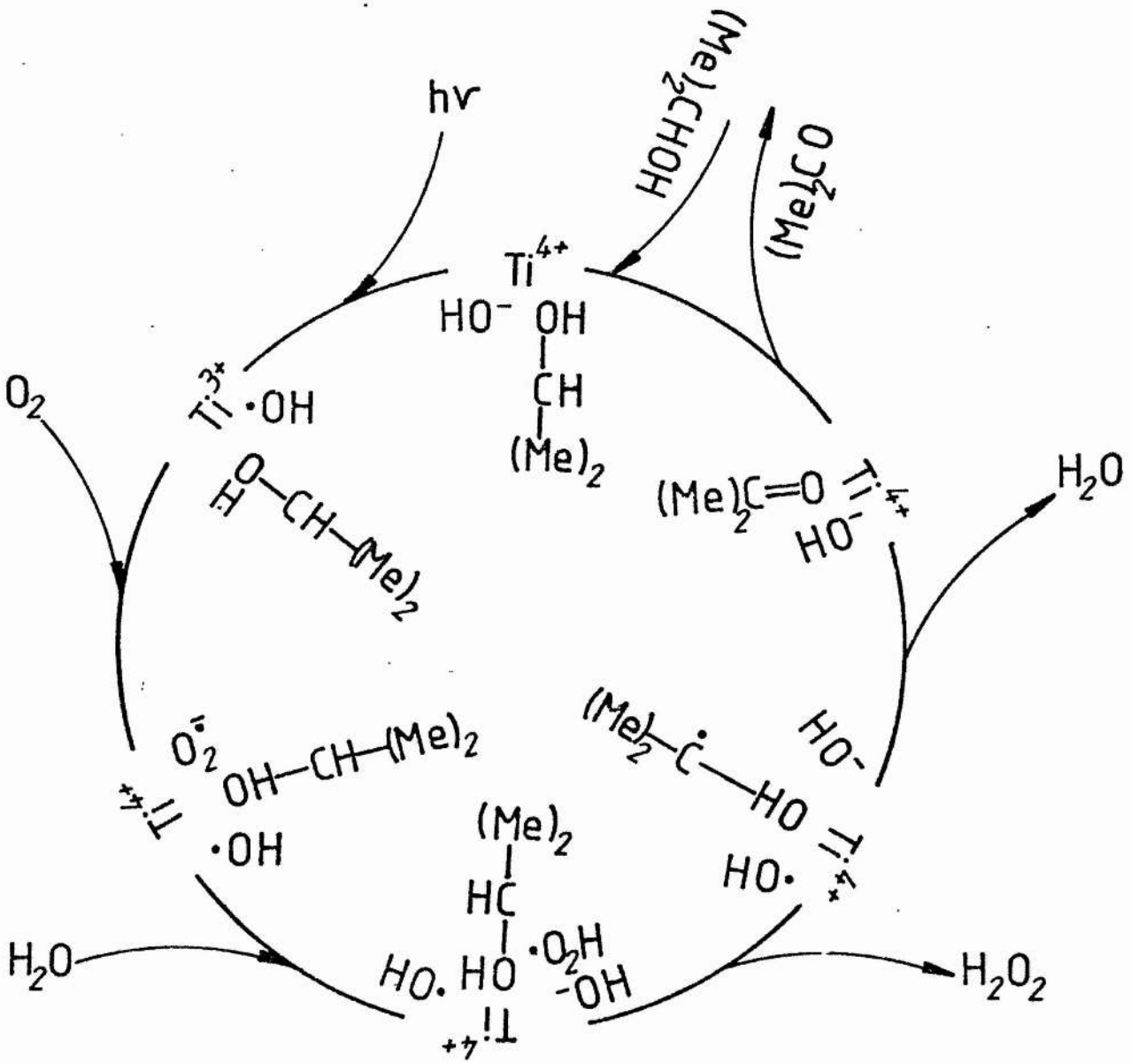

OXYGEN PATHWAY

Figure 2.9

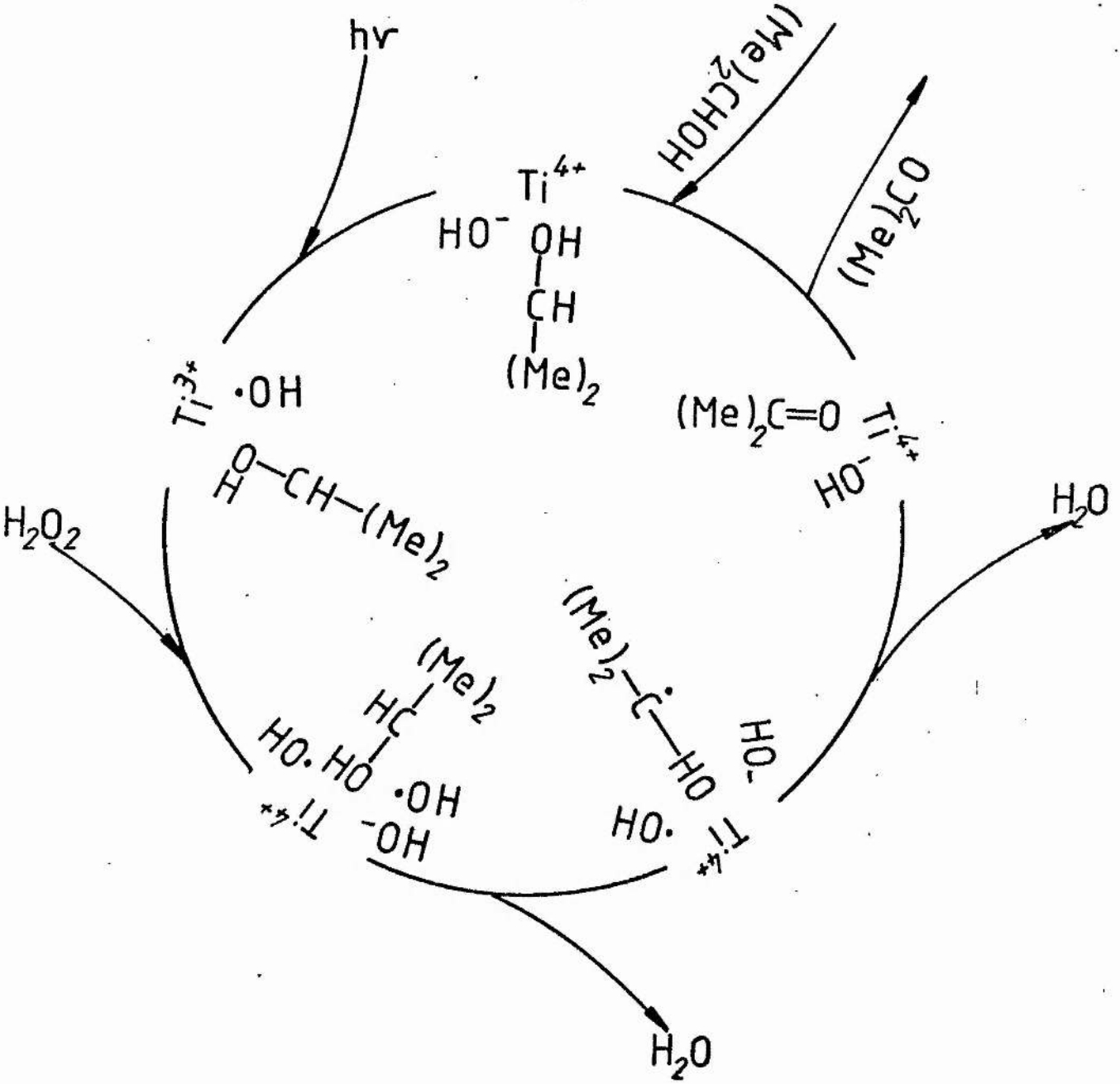

H_2O_2 PATHWAY

Figure 2.10

2.5 Conclusion

Both the oxygen-uptake and fibre optic monitoring systems are new techniques in the context of their application to TiO_2 catalysed photoprocesses. The former technique is of use both in establishing a mechanism for propan-2-ol dehydrogenation and for providing a fast, reliable test as to the extent of the photoactivity of a given pigment. The latter has revealed the first spectroscopic evidence of the involvement of H_2O_2 at the TiO_2 surface.

The results obtained from the studies on the propan-2-ol/propanone dehydrogenation system are in agreement, to a large extent, with those of other workers. The one major area which has, however, been highlighted for the first time in this work is the system dependence on propan-2-ol self-association. Clearly, therefore, this effect must be taken into account when comparing results obtained from different alcohol/TiO_2 suspensions as has been attempted recently[28].

CHAPTER 3

3 LASER INDUCED PHOTOLUMINESCENCE FROM TITANIUM DIOXIDE

3.1 Introduction

Much attention has been paid in previous sections of this work and in the literature, to the requirement for electromagnetic radiation, above a certain energy threshold, as a prerequisite to photoactivity of TiO_2[85]. This energy barrier, resulting from the semiconductor nature of TiO_2, is associated with promotion of an electron from the valence band to the conduction band in the crystal (see Figure 1.2) yielding a hole in the former and an excited electron in the latter. The electrostatic force of attraction between these species enables them to move together in a concerted fashion. This electron/hole pair is known as an exciton.

The fate of an exciton is determined, predominantly, by two competing processes: electron/hole recombination and exciton trapping. This statement is generally applicable to all semiconductor materials.

1) In the case of electron/hole recombination, the excited electron returns to the valence band, to the energy level occupied by the hole. The energy released by this process is dissipated as heat throughout the crystal. This is illustrated in Figure 3.1.

2) The exciton trapping mechanism depends on the ability of the exciton to migrate rapidly through the crystal. Movement of excitation energy in this fashion has been studied by R.D. Wieting et al.[86] and by D.D. Dlott et al.[87]. These workers modelled the migration of excitons on the basis of a statistical hopping mechanism, carried out in one dimension. The crystal may contain impurity levels, often occurring below the conduction band and associated with the presence of trace impurities or defect sites. If the exciton has a reasonable probability of migrating to a site before undergoing electron/hole recombination, then it may be trapped as indicated in Figure 3.2.

A trapped electron can release its energy and return to the valence band by thermal deactivation, as in the case of electron/hole recombination. However, an alternative route is for the energy to be released as electromagnetic radiation[36]. The wavelength of the emitted radiation is dependent on the energy gap between the valence band and the impurity level (shown as "E" in Figure 3.2). The actual wavelength is calculable from the Einstein relationship:

$$E = \frac{hc}{\lambda} \qquad (3.1)$$

in which: h = Planck's Constant (= 6.63×10^{-34} J s molecule $^{-1}$)

c = velocity of light in a vacuum (= 3×10^{8} m s^{-1})

λ = wavelength of emitted radiation (m)

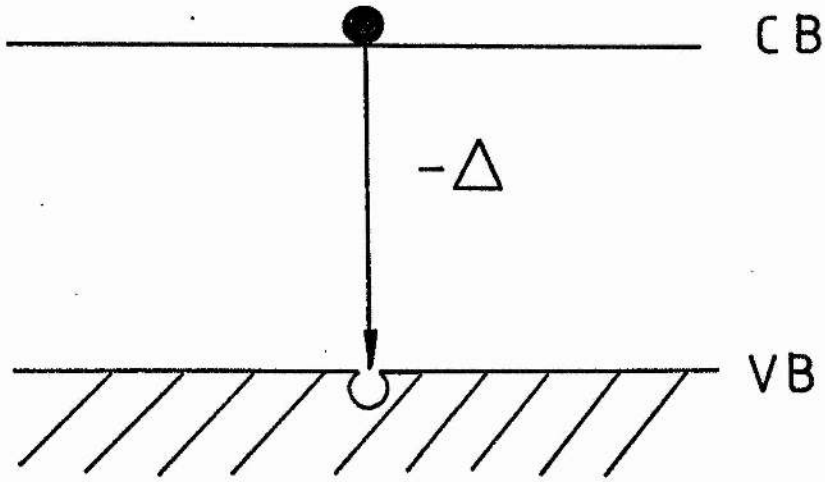

Figure 3.1 Electron/hole recombination

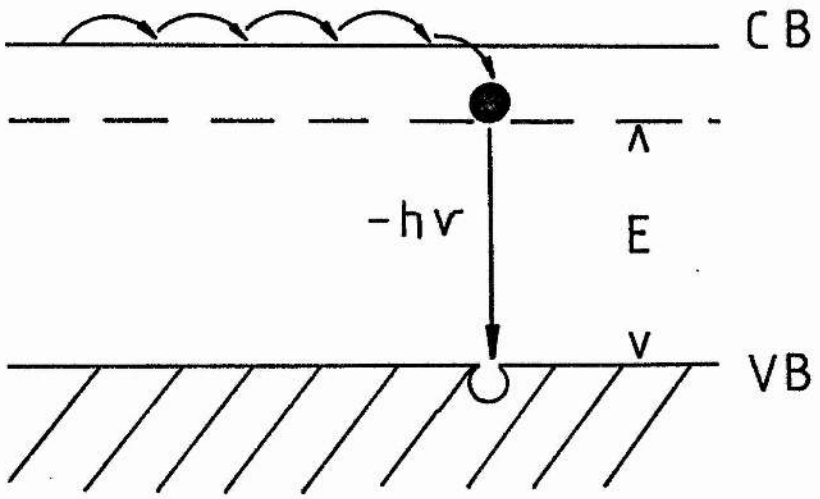

Figure 3.2 Migration and trapping of excited electron

It should be noted that the above discussion of exciton migration and trapping constitutes a simplification of what is, in fact, a highly complex process. In addition, the analogous mechanism involving hole trapping has not been mentioned. With these limitations in mind, however, it is clear that the possibility should exist for observing radiative decay from the exciton trapping sites, presumed to exist at the surface of the anatase and rutile particles. A series of experiments was therefore undertaken with a view to observing any photoluminescence emitted from dry, powdered samples of anatase and rutile. Radiative emission from surface sites has recently been observed from strontium oxide powder by S. Coluccia and A.J. Tench[88].

3.2 Experimental

For the purposes of these experiments, a custom built laser spectrophosphorimetry apparatus was employed[89,90]. A diagram of the equipment involved is shown in Figure 3.3. The various sections of the apparatus will be described individually.

1) Excitation Source

The source of exciting radiation used throughout this series of experiments was a pulsed nitrogen laser (Lambda Physik type K600). The radiation produced by a N_2 laser occurs at 337.1 nm and is therefore absorbed by both anatase and rutile forms of TiO_2.

Laser radiation was selected as the excitation source for two main reasons. Firstly, the fact that only a single spectral line (of high intensity) is produced, meant that the radiation emitted from a sample (at a different wavelength) would be readily detected. This is in direct contrast to a continuous radiation source (eg xenon lamp) which would produce radiation in the same region of the spectrum as the sample emission. Hence filtering techniques would have to be applied. The second reason was that the very short duration of the laser pulses (ca. 4 ns) meant that the decay characteristics of any

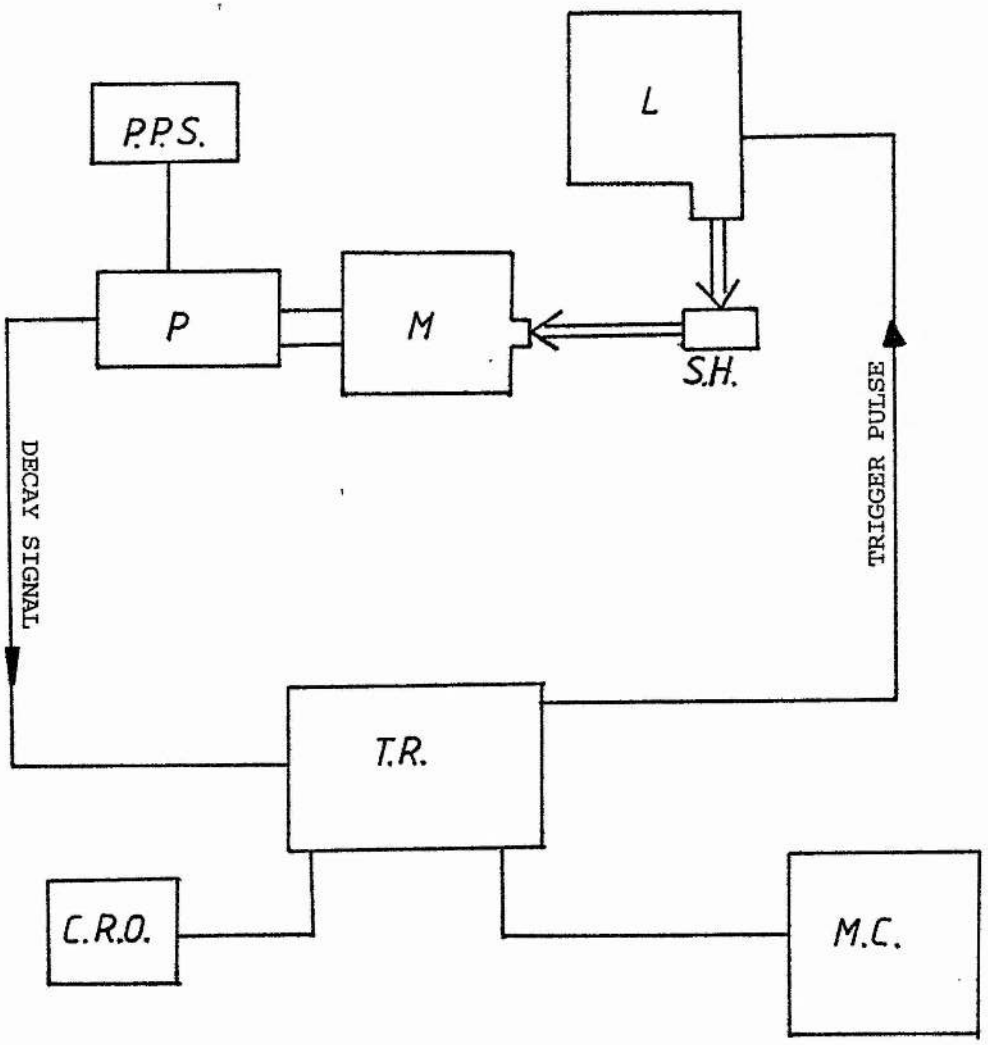

KEY:

L	=	PULSED N_2 LASER
S.H.	=	SAMPLE HOLDER
M	=	MONOCHROMATOR
P	=	PHOTOMULTIPLIER
P.P.S.	=	PHOTOMULTIPLIER POWER SUPPLY
T.R.	=	TRANSIENT RECORDER
C.R.O.	=	CATHODE RAY OSCILLOSCOPE
M.C.	=	"APPLE II" MICRO

Figure 3.3 Schematic of Spectrophosphorimetry Apparatus

photoluminescence produced could be determined (provided the decay did not occur any faster than the microsecond time domain).

2) Sample Holder

TiO_2 powder samples were placed in a 1 mm path length absorption cell which was of high quality quartz (Thermal Syndicate Ltd.). The top of the cell was fused onto a glass tube equipped with a tap, such that samples could be evacuated prior to the experiment. The cell was held inside a pyrex dewar vessel and positioned in such a way that the sample excitation and any resulting emission utilised the same face - a technique known as "front viewing". A platinum resistance temperature sensor was positioned alongside the sample holder. This was connected to a digital device which displayed the sample temperature. Temperature adjustment was achieved by dispensing a controlled quantity of liquid N_2 into the dewar.

As a safety precaution, the entire sample assembly was located inside an aluminium box, fitted with excitation and emission ports, with the laser cavity coupled securely to the former. In this way there was no possibility of the operator coming into contact with any hazardous laser radiation[91].

3) Emission Detection

Positioned at the emission port of the sample box and at right angles to the laser excitation was a monochromator which could be adjusted to select the desired emission wavelength. Radiation passing through the monochromator was detected by a photomultiplier tube (EMI bialkali serial no. 9798 QB), controlled by a high voltage power supply (EMI type PM 28 B). Typical voltages employed were ca. 900 V.

A custom built electrical circuit, utilising a high gain operational amplifier, was used to optimise emission detection sensitivity. This high gain circuit, however, introduced a time delay which restricted the decay studies to no better than millisecond lifetimes.

4) Data Acquisition

Storage of the decay trace, produced from the photomultiplier detection system, was carried out by a transient recorder (Datalab model DL920). This was linked to an oscilloscope (Telequipment type D1010) which displayed the decay. Sweep times were controlled by the transient recorder - the range being 2×10^{-4} s. up to 8 s.

A parallel interface connected the transient recorder with a microcomputer (Apple II) which operated a controlling program (stored on floppy disc). This program (written by Gate Microsystems Ltd.) supervised the transient recorder functions and hence the entire experiment, with the exception of the laser controls, was operated under computer control.

The digitised emission decay trace was transferred from the transient recorder to the computer via the interface. The controlling program divided the signal into ca. 900 time channels. Hence operating in this multichannel analyser mode, many decay traces of the same sample could be recorded and an average of the intensities in each time channel calculated. In this way, the signal to noise ratio could be improved. Typically, 32 or 64 decays were obtained for a given sample emission. This corresponds to enhancements in signal to noise ratio of 5.7 and 8.0 respectively - since X scans result in a S:N improvement factor of $X^{0.5}$. Hard copy output of a selection of the averaged time channels was obtained on a dot matrix printer (Anadex model DP 9001).

The Apple II microcomputer was also used to generate programs for analysis of the decay data. The application of these programs will be discussed in Appendix I. The experimental decay, along with the model decay data generated by a curve fitting program, were displayed on a visual display unit (VDU) (BMC model no. BM-12EA) and hard copy output obtained from a graph plotter (Tektronix model T4662).

3.2.1 Sample Materials

Two grades of TiO_2 were used during the course of these studies. These were the uncoated anatase and rutile grades supplied by Tioxide International Ltd. (code nos. CLD 1729/F and CLD 1729/A respectively).

3.3 Results and Discussion

3.3.1 Anatase Photoluminescence

An anatase powder sample was placed in the sample cell. In practice, it proved difficult to evacuate the samples and hence the experiments were carried out in air. Early experiments were undertaken with an amplification circuit which produced a very high gain but also introduced a time constant of 60 microseconds. Hence, operating in the 0.2 millisecond sweep mode, a decay trace entirely due to the system electronics was observed. Excitation of the anatase sample, at room temperature, produced no alteration in the decay trace. On reduction of the sample temperature (by the method described in the Experimental Section) below ca. 150 K, however, a marked increase in the "apparent time constant" was observed at ca. 450 nm. Since the true time constant depended only on the electronic components in the amplification circuit and was completely unaffected by the sample temperature, it was clear that a genuine emission from the anatase sample was being detected.

The next stage in gaining further information on the anatase emission was to modify the time constant characteristics of the amplification circuit. To this end, the feedback circuit connecting the operational amplifier was adjusted, such that the time constant was in the same time domain as the laser pulse itself. The advantage of improved time resolution had, however, to be set against the inevitable decrease in signal to noise ratio which accompanied this adjustment.

Excitation of the anatase powder sample was repeated using the modified amplification apparatus. At room temperature, no decay trace was observed. However, as expected, on reducing the temperature below ca. 150 K a decay trace was observed on the oscilloscope. The monochromator was carefully adjusted and it was established that the maximum emission intensity occurred at 447 nm. Similarly, reducing the temperature to 77 K - ie. totally immersing the sample in liquid N_2 - produced an increase in emission intensity, although no change in the profile of the decay was observed.

3.3.2 Rutile Photoluminescence

Analogous experiments to those employing anatase were carried out for powdered rutile samples. On using the high sensitivity / long time constant amplifier configuration, however, no change in the "apparent time constant" was observed - even at 77 K. Nevertheless it was decided, for completeness, to repeat the laser excitation with the modified short time constant amplifier. A decay was indeed observed to "grow-in" below ca. 150 K, which became steadily more intense as the temperature was reduced to 77 K.

Three features were apparent regarding the luminescence profile, which distinguished it from that of anatase. Firstly, the emission maximum for rutile was red shifted to 460 nm. Secondly, the initial intensity , I_o, of the rutile decay was much less than that of anatase. Finally, the decay of rutile luminescence was much more rapid than in the case of anatase. Presumably a combination of the second and third reasons were responsible for the lack of effect in the preliminary studies using the unmodified amplification apparatus.

3.4 Analysis of Photoluminescence Decays

Because of the much lower gain obtainable from the modified amplification circuit, this meant that the signal:noise ratio of the observed decays was low, particularly in the case of rutile. To a certain extent, this was compensated by taking the average of 64 decay scans for each sample (as outlined in the Experimental section). This decreased the level of scatter to the extent that the decays could be analysed. For simplicity, consideration is only given to two possible photoluminescence conditions:

3.4.1 One Type of Luminescent Site

In this situation, the TiO_2 crystal can absorb radiation of bandgap energy or greater, leading to promotion to the conduction band (see previously). Exciton migration and trapping is then assumed to occur, by a single type of trapping site (say type R) which is capable of decaying with the production of photoluminescence. Obviously this mechanism does not preclude thermal electron/hole recombination as an additional deactivation pathway.

Let the concentration of excitons trapped at site R be [Y]. In addition, let it be assumed that the migration and trapping of the excitons occurs fast enough such that the kinetically controlling step is concerned only with emission from the traps. Thus the rate of emissive decay from these sites may be given by:

$$\frac{-d[Y]}{dt} = k_R'[Y] \qquad (3.2)$$

where k_R' is the rate constant for the unimolecular decay process. This expression can be integrated to give:

$$[Y]_t = [Y]_o \exp(-k_R' t) \qquad (3.3)$$

where $[Y]_o$ and $[Y]_t$ represent the concentrations of trapped excitons at time t = 0 and t = t seconds respectively.

Since the intensity of photoluminescence is proportional to the concentration of trapped species:

$$[Y] \propto [I] \qquad (3.4)$$

then equation (3.3) may be re-written in terms of intensity thus:

$$[I]_t = [I]_o \exp(-k_R t) \qquad (3.5)$$

where k_R incorporates the constant of proportionality, inherent to

equation (3.4). Rearrangement of equation (3.5) leads to the following:

$$\ln([I]_t/[I]_o) = -k_R t \qquad (3.6)$$

and hence, since $[I]_o$ is a constant, a plot of $\ln([I]_t)$ against t should give a straight line, with the decay constant, k_R, obtainable from the negative gradient.

The experimental decays for anatase and rutile photoluminescence are annotated by the "+" symbols in Figure 3.4 and 3.5 respectively (where $[I]_o$ has been normalised to 10,000 in each case). Clearly, neither decay profile follows a straight line. Hence an alternative photoluminescence model must be considered.

3.4.2 Two Types of Luminescent Sites

Assume that two separate types of trapping site exist at the TiO_2 surface (say types P and Q). Thus excitonic species may be trapped at either of these sites, which may each decay with the production of photoluminescence, as in the single luminescent site case. The analogous differential rate equation for the two component decay process is as follows:

$$\frac{-d[Y]}{dt} = k_P'[Y] + k_Q'[Y] \qquad (3.7)$$

where [Y], as before, represents the total concentration of trapped excitons and k_P' and k_Q' are the rate constants for decay from sites P and Q respectively. Once again, rapid migration and trapping are assumed. Integration of equation (3.7), along with the substitution of [I] for [Y] given in equation (3.4), yields:

$$[I]_t = [I]_{o(P)}\exp(-k_P t) + [I]_{o(Q)}\exp(-k_Q t) \qquad (3.8)$$

where $[I]_{o(P)}$ and $[I]_{o(Q)}$ are the emission intensities at t = 0 (ie. before any decay) for sites P and Q respectively, such that:

$$[I]_o = [I]_{o(P)} + [I]_{o(Q)} \qquad (3.9)$$

Clearly, for this function, a plot of $\ln([I]_t)$ against time would be non-linear.

In order to test whether or not the biexponential decay, given in equation (3.8), is an effective model for the photoluminescence profiles, a study of curve fitting techniques was undertaken. As a result of this, a computer program was written which was capable of fitting a theoretical expression to experimental decay data. The details of the curve fitting study, together with the listing of the computer program used, are given in Appendix I.

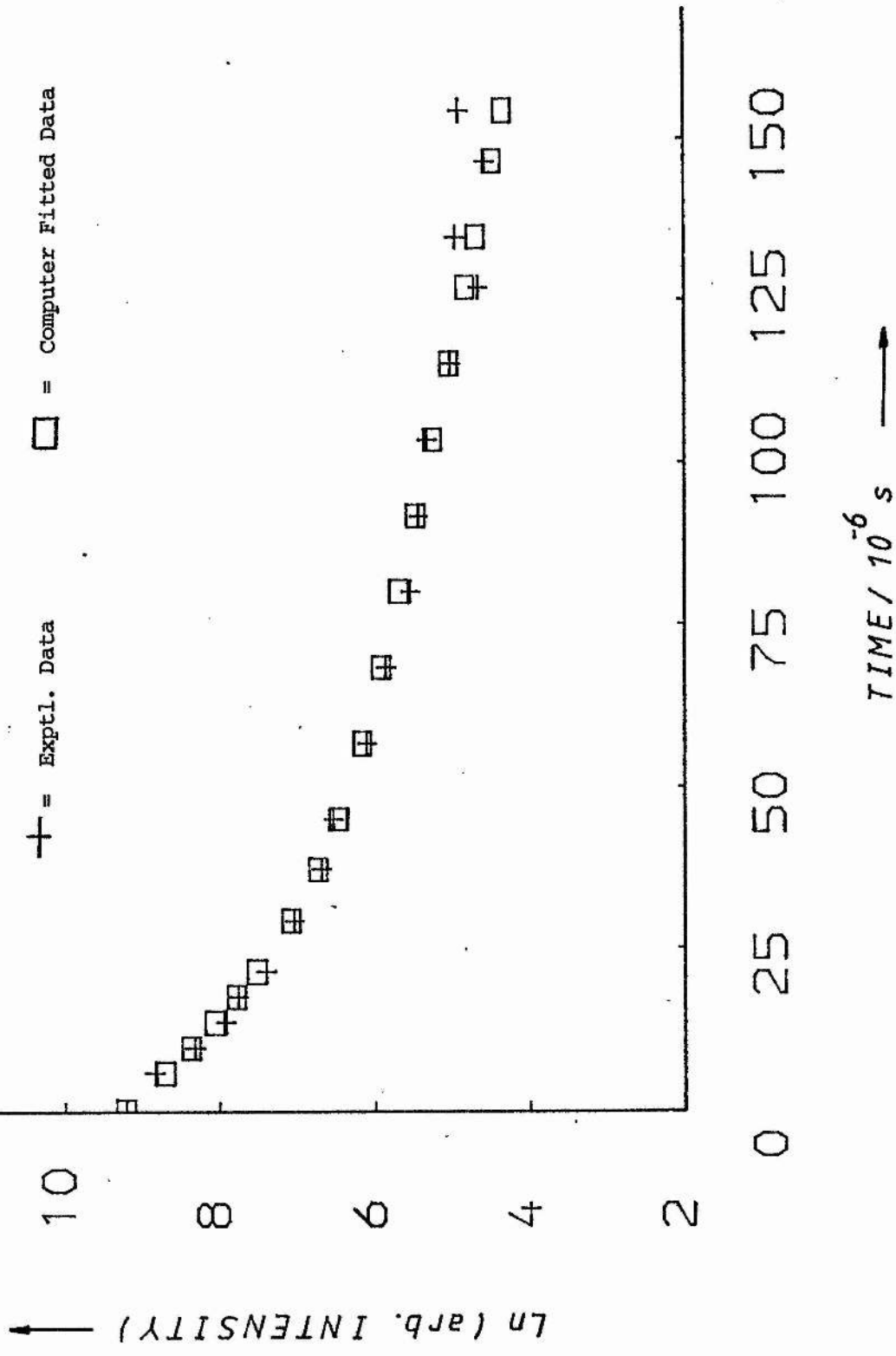
+ = Expt1. Data
□ = Computer Fitted Data
ln (arb. INTENSITY)
10
8
6
4
2
0
25
50
75
100
125
150
TIME / 10^-6 s

Figure 3.4

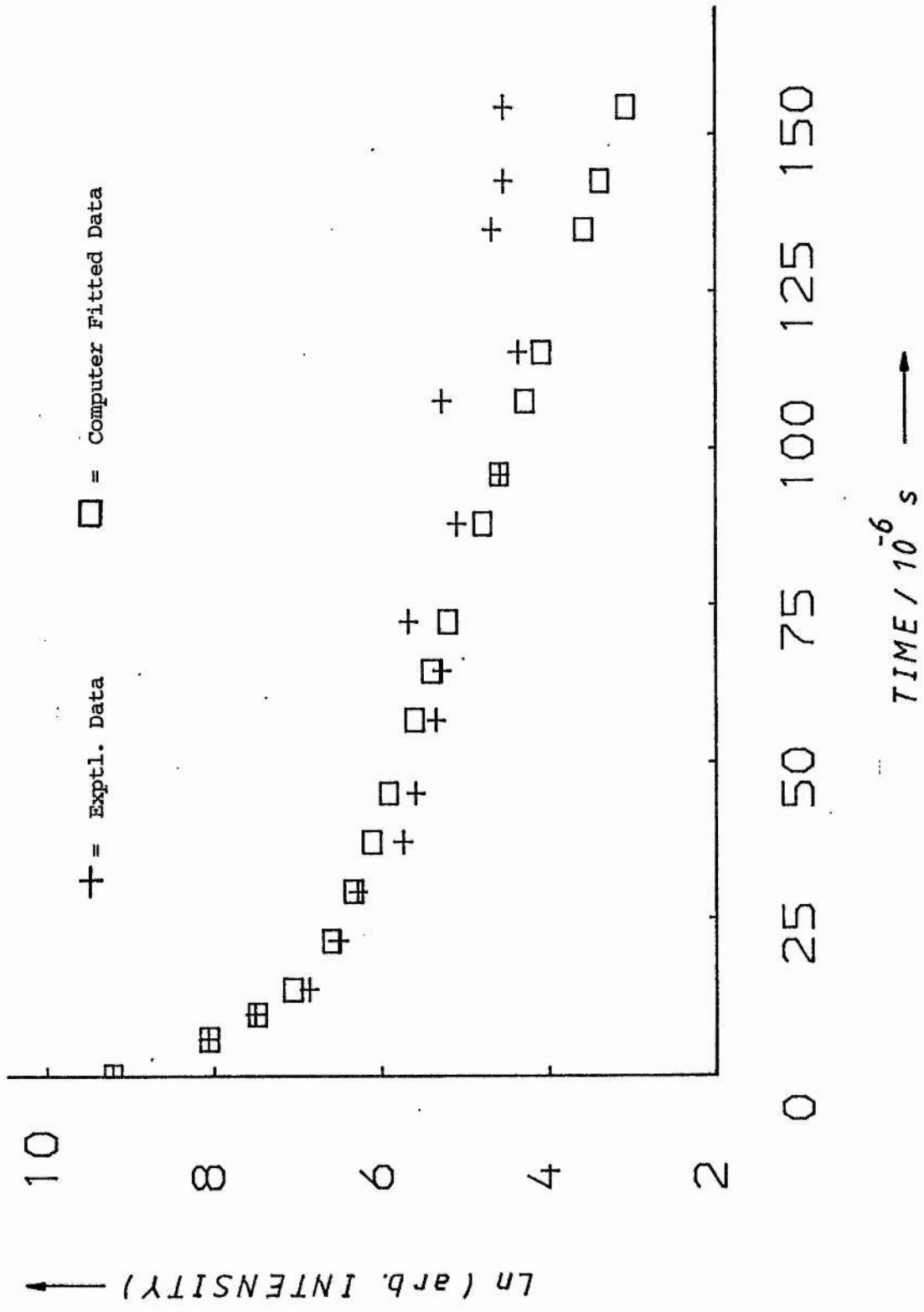
+ = Expt1. Data
□ = Computer Fitted Data
ln (arb. INTENSITY)
10
8
6
4
2
0
25
50
75
100
125
150
TIME / 10^-6 s

Figure 3.5

Upon application of the computer program (on the Apple II microcomputer) it was found that the biexponential decay could fit the experimental photoluminescence decays very effectively. The computer simulated decays are depicted by the "□" symbols in Figures 3.4 and 3.5. By observation, the quality of the fit is better for the anatase decay. The most probable reason for this is that the greater signal:noise ratio of the anatase data meant that there was less distortion of the statistical weighting factors which determined the goodness of the fit. (Further discussion of the criteria defining the quality of a fit will also be given in Appendix I).

The optimised parameters, corresponding to the four unknowns in equation (3.8), obtained from the fitting routine for both the anatase and rutile photoluminescence decays at 77 K are listed in Table 3.1. Since the experimental decays had been normalised to $[I]_o$ = 10,000, this value was also applied to the program, which then optimised the separate $[I]_{o(P)}$ and $[I]_{o(Q)}$ values. Also shown in Table 3.1 are the decay times (τ) which may be calculated from the corresponding decay constants by the following relationship:

$$\tau = 1/k \qquad (3.10)$$

Table 3.1: Computer Optimised Biexponential Decay Data

SAMPLE	$[I]_{o(P)}$	k_P $(s^{-1})/10^4$	Υ_P $(s)/10^{-6}$	$[I]_{o(Q)}$	k_Q $(s^{-1})/10^4$	Υ_Q $(s)/10^{-6}$
anatase	1245	1.8	56.9	8755	10.0	9.6
rutile	1195	2.6	38.5	8805	24.0	4.2

From the results above, it is clear that the experimental decay data for anatase and rutile may each be accurately modelled by a system consisting of two distinct sets of exciton trapping sites which are capable of decaying emissively, with different rate constants. In addition, it is interesting to compare the bandgap energies of both forms of TiO_2 with their corresponding photoluminescence wavelength maxima. The bandgap energy of anatase is ca. 385 nm, while the emission maximum occurred at ca 447 nm (a red shift of ~62 nm). Similarly for rutile, with bandgap of ca. 415 nm, the maximum intensity of emission appeared at 460 nm, a red shift of ~45 nm. By applying the Einstein relationship between energy and wavelength (equation (3.1)), it can be calculated that the trap sites in anatase and rutile lie approximately 43 and 28 kJ mol^{-1} below their respective conduction bands.

Another interesting feature of the photoluminescence results is that no emission was detected until the temperature was lowered. This may be explained by considering the effect of temperature on exciton migration. At room temperature, an excited electron, after being

trapped, may be thrown back into the conduction band by the action of thermal vibrations, before it has time to decay radiatively. This is the reason for the relatively long decay lifetimes (microseconds for the anatase and rutile decays). Once back in the conduction band, non-radiative decay can occur via electron/hole recombination. Thus, at room temperature, an excited electron may be trapped and re-promoted to the conduction band many times before it remains trapped for a sufficiently long period to decay radiatively[92]. Clearly, on decreasing the temperature, the electron will, on average, remain trapped for a longer period and hence the probability of radiative decay will increase at the expense of electron/hole recombination. This qualitative explanation is consistent with the fact that no photoluminescence is observed from anatase or rutile until the temperature is reduced to ca. 150 K in each case.

3.5 Conclusion

This section of experimental work has provided clear evidence for the production of photoluminescence from anatase and rutile powder samples at low temperatures. The luminescence decays for each sample may be successfully modelled in terms of two sets of trapping sites, giving rise to a biexponential decay profile.

CHAPTER 4

4 PHOTOPHYSICAL BEHAVIOUR OF BENZOPHENONE IN PMMA

4.1 Introduction

Previous chapters have highlighted the fact that irradiation of TiO_2 in the presence of oxygen and a trace of water, can lead to the production of free radical species - notably hydroxyl and per-hydroxyl radicals ($HO^{\bullet}$ and $HO_2^{\bullet}$ respectively). The mechanism discussed previously, considered the participation of these species in hydrogen abstraction reactions involving propan-2-ol.

In a practical situation, where the TiO_2 pigment is dispersed in a polymeric medium, the $HO^{\bullet}$ and $HO_2^{\bullet}$ radicals are produced as before and these can then react with the polymer chain - also via hydrogen abstraction. This similarity in mechanism between the propan-2-ol and polymeric systems is the main reason for the effectiveness of the propan-2-ol/TiO_2 suspension system in monitoring pigment performance in a polymeric binder[23].

As a consequence of hydrogen abstraction from a polymer molecule, a polymer radical ($P^{\bullet}$) will be formed thus[93]:

$$P\text{-}H + X^{\bullet} \longrightarrow P^{\bullet} + HX \qquad (4.1)$$

where X = $HO^{\bullet}$ or $HO_2^{\bullet}$.

Rapid reaction of the polymer radical with oxygen from the atmosphere has been shown to occur[94,95]:

$$P^{\bullet} + O_2 \longrightarrow PO_2^{\bullet} \qquad (4.2)$$

Further abstraction from an adjacent polymeric chain segment can lead to the formation of hydroperoxides:

$$PO_2^{\bullet} + P\text{-}H \longrightarrow POOH + P^{\bullet} \qquad (4.3)$$

which can decompose efficiently to give alkoxy and hydroxy radicals[96,97]:

$$POOH \longrightarrow PO^{\bullet} + HO^{\bullet} \qquad (4.4)$$

Once formed, the alkoxy radicals can be converted to carbonyl groups via several possible reaction pathways[98,99], one of which is disproportionation by two polymer alkoxy radicals:

$$PCH\text{-}O^{\bullet} + PCH\text{-}O^{\bullet} \longrightarrow PC{=}O + PCH\text{-}OH \qquad (4.5)$$

It must be emphasised at this stage that this sequence of reactions represents only one of several reaction pathways open to the $P^{\bullet}$ radical. For example, an alternative would involve direct attack on an adjacent polymer molecule to give crosslinking[100]. Furthermore, the participation of an oxygen molecule in equation (4.2) must be

viewed in the context of competing oxygen-uptake catalysed by the TiO_2 particles themselves. Hence the true picture of polymer photo-oxidation is of a complex interplay between competing reaction pathways. Nevertheless, the build-up of carbonyl groups, which is photocatalysed by TiO_2 in polymers, is an important phenomenon. The purpose of the experimental work comprising this chapter was to examine the photophysical behaviour of carbonyl groups deliberately added to a polymer. More specifically, the source of carbonyl groups was the aromatic ketone benzophenone, dispersed in poly(methylmethacrylate) (PMMA). The behaviour of benzophenone in the liquid state has been extensively studied by others[101,102], hence this work confined itself to studies in the solid state.

4.2 Experimental

The following two light sources were used to excite the benzophenone:

4.2.1 Pulsed Nitrogen Laser Source

The description of the laser spectrophosphorimetry apparatus was given in a previous chapter. Samples, in the form of polymer films, were also placed in the same sample holder as before.

4.2.2 Continuous Excitation Source

This experimental apparatus made use of a spectrofluorimeter (Perkin-Elmer model MPF-2A). The excitation in this instrument was derived from a xenon lamp (150 W), the emission from which is continuous and extends from the UV region up to IR (specifically from

wavelengths of 250 nm up to 800 nm). The xenon lamp spectral distribution is shown in Figure 4.1.

The spectrofluorimeter incorporated an excitation monochromator, which made it possible to select a particular wavelength of the lamp output for sample excitation. Similarly, an emission monochromator, positioned at right angles to the path of excitation, could be scanned over a wide wavelength range in order to detect any sample emission. The slit widths of both monochromators were adjustable while that of the emission monochromator controlled the resolution of the emission spectrum: the narrower the slit width, the sharper the spectrum.

The emission was detected by a photomultiplier (Hamamatsu R106), placed at the exit of the emission monochromator. Further signal enhancement was obtained from an amplification circuit. Finally, the converted sample emission was output to an X-Y chart recorder, which plotted intensity as a function of emission wavelength.

Sample holder design was similar to that used in the laser apparatus, in that it consisted of a 1mm pathlength quartz cell (Thermal Syndicate Ltd.) fused to a glass tube which, in turn, was fused to a short length of glass tubing. After loading the film sample, the holder was connected to a vacuum line and evacuated prior to and throughout an experiment. A pyrex dewar, equipped with quartz excitation and emission windows, surrounded the sample holder during an experiment. An attachment was built onto the outside of the instrument so that liquid nitrogen could be poured into the dewar, thereby lowering the sample temperature, without requiring the sample

compartment to be opened. Sample temperature was monitored using an identical method to that adopted for the laser apparatus. The sample holder was positioned vertically, with respect to the path of excitation, and at an angle of 45 degrees across the beam. Emission was therefore detected from the rear of the cell - an arrangement known as "rear viewing".

4.2.3 Sample Preparation

The necessity of adopting pure materials for use in spectroscopic experiments has been emphasised by many researchers[103,104]. Thus the PMMA (BDH Chemicals Ltd.) was dissolved in dichloromethane (CH_2Cl_2) and precipitated from a large excess of methanol. This was then filtered and pumped dry in a vacuum oven for ca. 48 hrs at room temperature. Benzophenone (Fisons) was recrystallised twice from distilled ethanol.

Polymer samples were prepared by dissolving PMMA together with the required amount of benzophenone in distilled CH_2Cl_2. Cast films were then prepared by dispensing a portion of the mixture onto a quartz disc. Solvent evaporation was allowed to proceed slowly and films of ca. 100 microns thickness were obtained. The films were pumped under vacuum for ca. 48 hrs to encourage removal of any remaining CH_2Cl_2 solvent, after which the circular film was cut into strips of ca. 1 cm width. The range of benzophenone concentrations

employed in the films was from 1×10^{-3} to 2×10^{-2} mol dm^{-3}. TiO_2 was not incorporated into any of the samples.

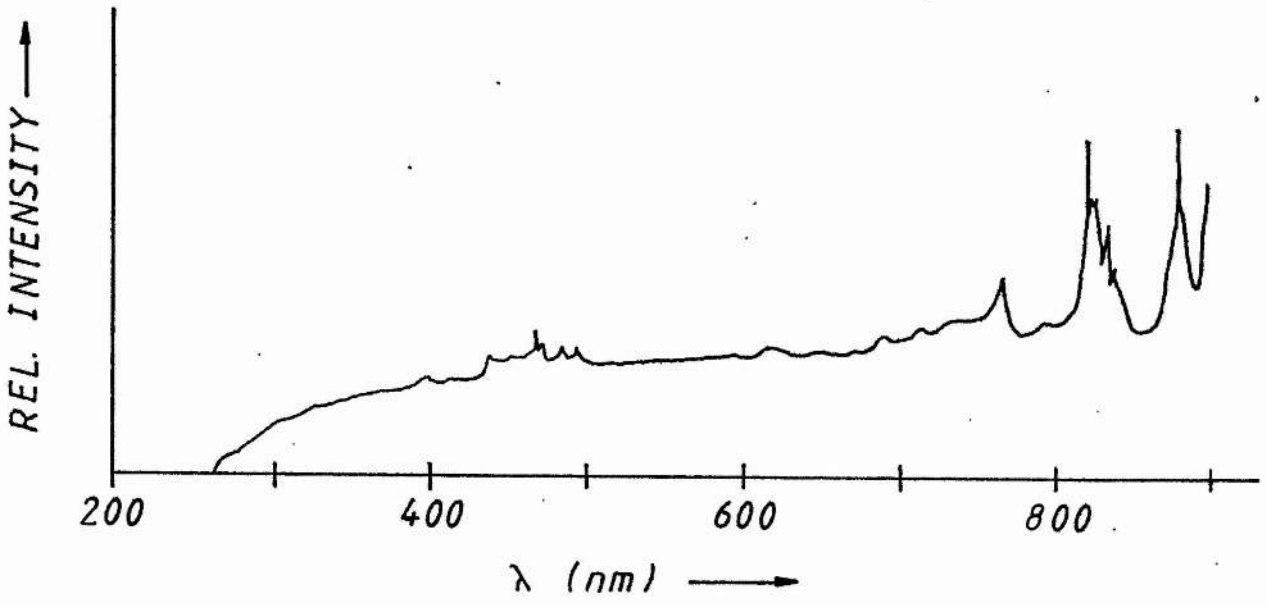

Figure 4.1 Xenon Lamp Emission Spectrum

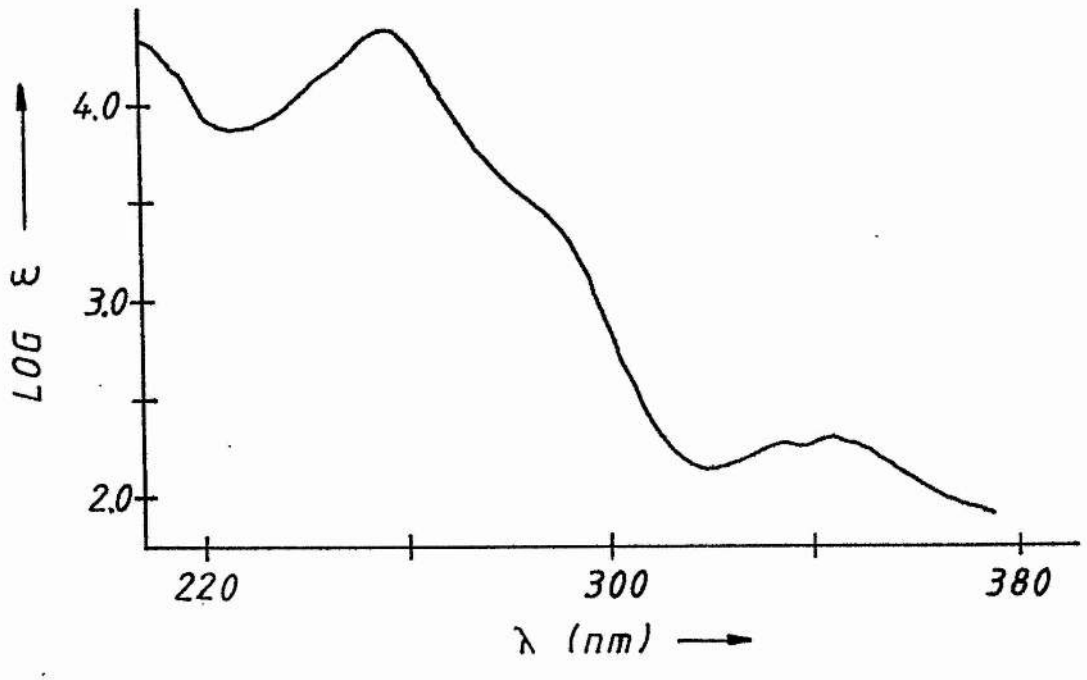

Figure 4.2 Absorption Spectrum of Benzophenone

4.3 Benzophenone Photophysics

Benzophenone has been shown to play an important role in sensitising the photodegradation of polymers[105]. The absorption spectrum for this molecule is shown in Figure 4.2. Using the notation of C.A. Parker[106], the kinetic scheme governing benzophenone photophysics is as follows:

PROCESS	RATE	COMMENTS
(1) $S_o + h\nu \longrightarrow S_1^n$	I_a	Where I_a is the rate of light absorption.
(2) $S_1^n \longrightarrow S_1 + \triangle$	$k_y[S_1^n]$	Singlet internal conversion, where n indicates an excited vibrational state.
(3) $S_1 \longrightarrow S_o + h\nu$	$k_f[S_1]$	Fluorescence emission.
(4) $S_1 \longrightarrow S_o + \triangle$	$k_z[S_1]$	Thermal deactivation.
(5) $S_1 + Q \longrightarrow S_o + Q$	$k_Q[Q]$	Quenching by impurity, Q.
(6) $S_1 \longrightarrow T_1^{n'}$	$k_g[S_1]$	Intersystem crossing.
(7) $T_1^{n'} \longrightarrow T_1 + \triangle$	$k_{n'}[T_1^{n'}]$	Triplet internal conversion.
(8) $T_1 + \triangle \longrightarrow S_1$	$k_e[T_1]$	Thermal activation.
(9) $T_1 \longrightarrow S_o + h\nu'$	$k_p[T_1]$	Phosphorescence emission.
(10) $T_1 \longrightarrow S_o + \triangle$	$k_m[T_1]$	Thermal triplet deactivation.
(11) $T_1 + q \longrightarrow S_o + q$	$k_q[T_1][q]$	Quenching by impurity, q.

This simplified kinetic scheme only considers transitions involving the first excited singlet and triplet states (S_1 and T_1 respectively). In photophysical studies of benzophenone, the T_1 state is the most important as it is well established that this state plays a leading part in polymer photodegradation sensitised by ketones[107].

On steady-state excitation, the triplet formation efficiency, ϕ_t, may be defined as follows:

$$\phi_t = k_g/(k_f + k_n + k_g + k_Q[Q]) \qquad (4.6)$$

(where $k_n = k_y + k_z$)

Thus the rate of formation of triplet state molecules is:

$$\text{Rate} = I_a\phi_t \qquad (4.7)$$

In the case of benzophenone, the rate of triplet formation is high, due, it is believed, to a large k_g value (of ca. 1×10^{10} s^{-1}). The explanation for the rapidity of the intersystem crossing is not fully understood but it has been suggested that the second triplet state (T_2) may play a part[108].

Of particular importance in studying the radiative properties of benzophenone is the detection of phosphorescence. As before, and using the kinetic definitions given above, the phosphorescence efficiency, $\varnothing_p$, may be expressed thus:

$$\varnothing_p = k_p \varnothing_t / (k_p + k_m + k_q[q] + k_e) \qquad (4.8)$$

and the actual triplet lifetime, τ, is derived from:

$$\tau = 1/(k_p + k_m + k_q[q] + k_e) \qquad (4.9)$$

4.4 Results and Discussion

4.4.1 Benzophenone Phosphorescence Decays

The laser spectrophosphorimetry apparatus was used in the observation of the phosphorescence decays from benzophenone in PMMA. When excitation of the sample was carried out at 77 K, an emission was detected with maximum intensity at 423 nm, corresponding, approximately, to the (0,0) $T_1 \rightarrow S_o$ transition energy[108].

A plot of the logarithm of the normalised emission intensity as a function of time is given by the "+" symbols in Figure 4.3. As can be seen, this decay is exponential, since:

$$I = I_o \exp(-kt) \qquad (4.10)$$

hence: $$\ln\left(\frac{I}{I_o}\right) = -kt \qquad (4.11)$$

(by applying a similar argument to that used previously in chapter 3).

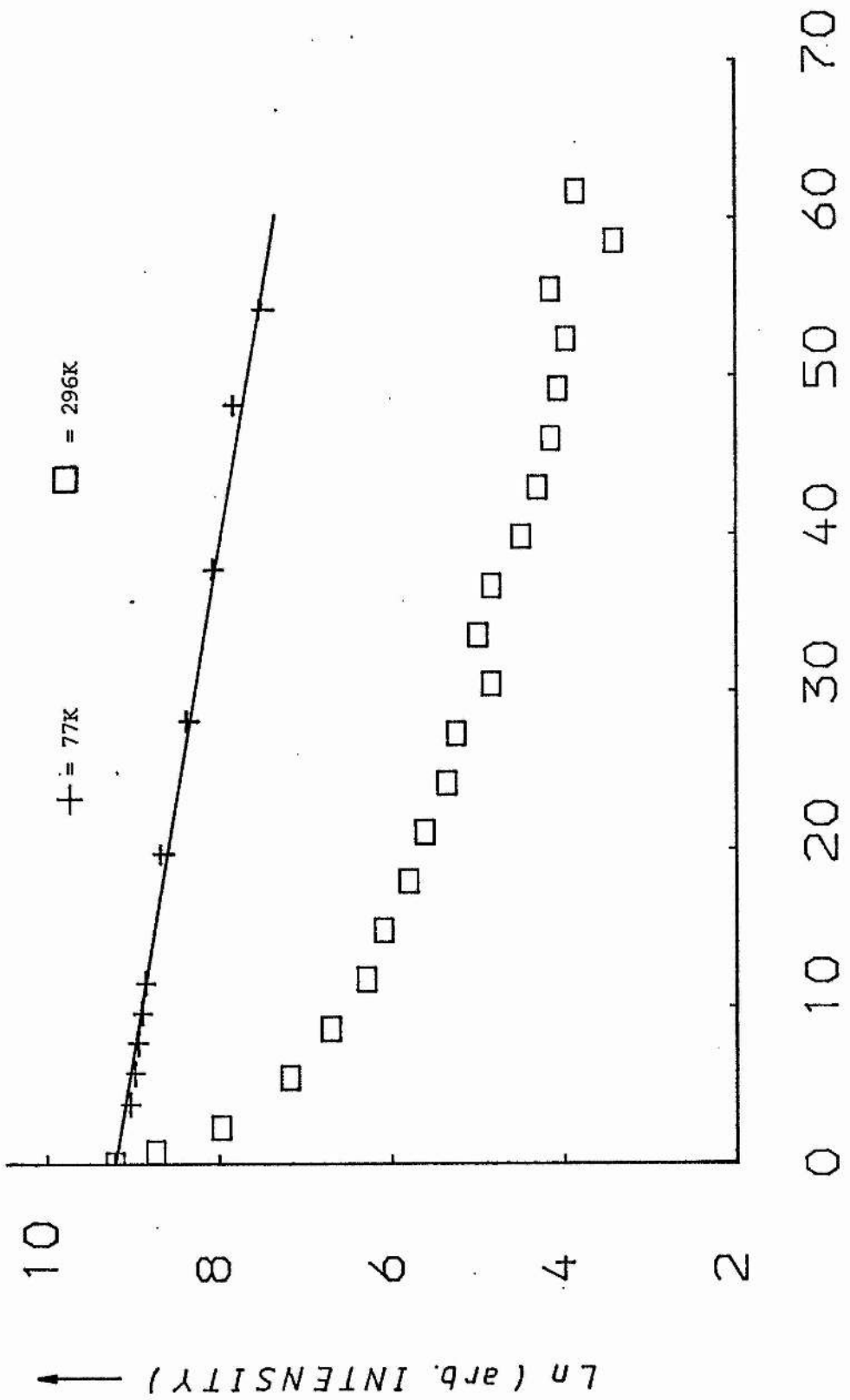
□ = 296K
+ = 77K
Ln (arb. INTENSITY)
TIME / 10^-4 s
10
8
6
4
2
0
10
20
30
40
50
60
70

Figure 4.3

Analysis of the decay gives: slope = k = 230 s^{-1}; correlation coefficient = -1.00. Hence the triplet lifetime, τ = 4.4 x 10^{-3} s. This value for the decay lifetime is in good agreement with that obtained by other workers for benzophenone in various media[90,109]. Thus at this temperature, the benzophenone decay is independent of the surrounding medium.

On carrying out the spectrophosphorimetry experiments at room temperature (296 K) the phosphorescence decay profile of benzophenone altered dramatically, as shown by the "□" symbols in Figure 4.3. The decay is clearly non-exponential and thus the concept of the individual benzophenone molecules deactivating via the normal phosphorescence mechanism (of equation (4.10)) is no longer sufficient to describe the experimental data at this temperature. It should be pointed out that control experiments were carried out using PMMA films with no added benzophenone. In these cases no emission was observed, either at 77 K or room temperature.

The transition from exponential to non-exponential phosphorescence decays has been observed by several other workers. K.T. Moran observed the transition temperature for the onset of non-exponentiality of benzophenone phosphorescence in PMMA films to be ca. 196 K[90].

4.4.2 Rationalisation of the Non-Exponential Decay

Several deactivation mechanisms for the triplet state have been proposed in the past, which can compete with the phosphorescence step. These include the dipole-dipole[110] and exchange[111,112] energy transfer mechanisms. Recently, however, a mechanism involving so-called triplet-triplet annihilation has been proposed for the non-exponential decay of benzophenone in PMMA[90,113,114]. In this scheme, the following photophysical processes can occur, in addition to that of process (9) described previously.

$$T_1 + T_1 \longrightarrow S_o + S_1 \qquad (4.12)$$

and/or $$T_1 + T_1 \longrightarrow 2S_o \qquad (4.13)$$

The differential rate expression governing triplet state depletion is thus:

$$\frac{-d[T_1]}{dt} = k_p[T_1] + k_v[T_1]^2 \qquad (4.14)$$

where k_v is the second order rate constant associated with processes (4.12) and (4.13). (Equation (4.14) makes the assumption that triplet state repopulation arising from process (4.12) is negligible).

Integration of equation (4.14), making use of the fact that the observed decay intensity is proportional to the triplet concentration, gives:

$$[I]_t = \frac{[I]_o \exp(-k_p' t)}{1 + (k_v'/k_p')[I]_o(1 - \exp(-k_p' t)} \qquad (4.15)$$

where $[I]_t$ and $[I]_o$ are the emission intensities at time t = t and t = 0 seconds respectively. In addition, k_p' and k_v' correspond to the respective rate constants given in equation (4.14) but with the incorporation of the constant of proportionality, incurred during the substitution of [I] for [T]. Since k_p is a first order rate constant, its magnitude is unaffected by this substitution and hence $k_p' = k_p$.

In order to test whether or not our room temperature decay for benzophenone could be described by the triplet-triplet annihilation mechanism, a rapid curve fitting program (written in FORTRAN and implemented on the Apple II microcomputer) was employed. The program was based on the method of differential coefficients[115] and a listing is provided in Appendix III.

Computer fitting of the experimental emission decay at 296 K revealed that a close match could be obtained with the theoretical decay in equation (4.15). The optimised values for k_p' and k_v' were 400 s^{-1} and 900 (arbitrary units) respectively. The computer fit, superimposed on experimental decay data is shown in Figure 4.4.

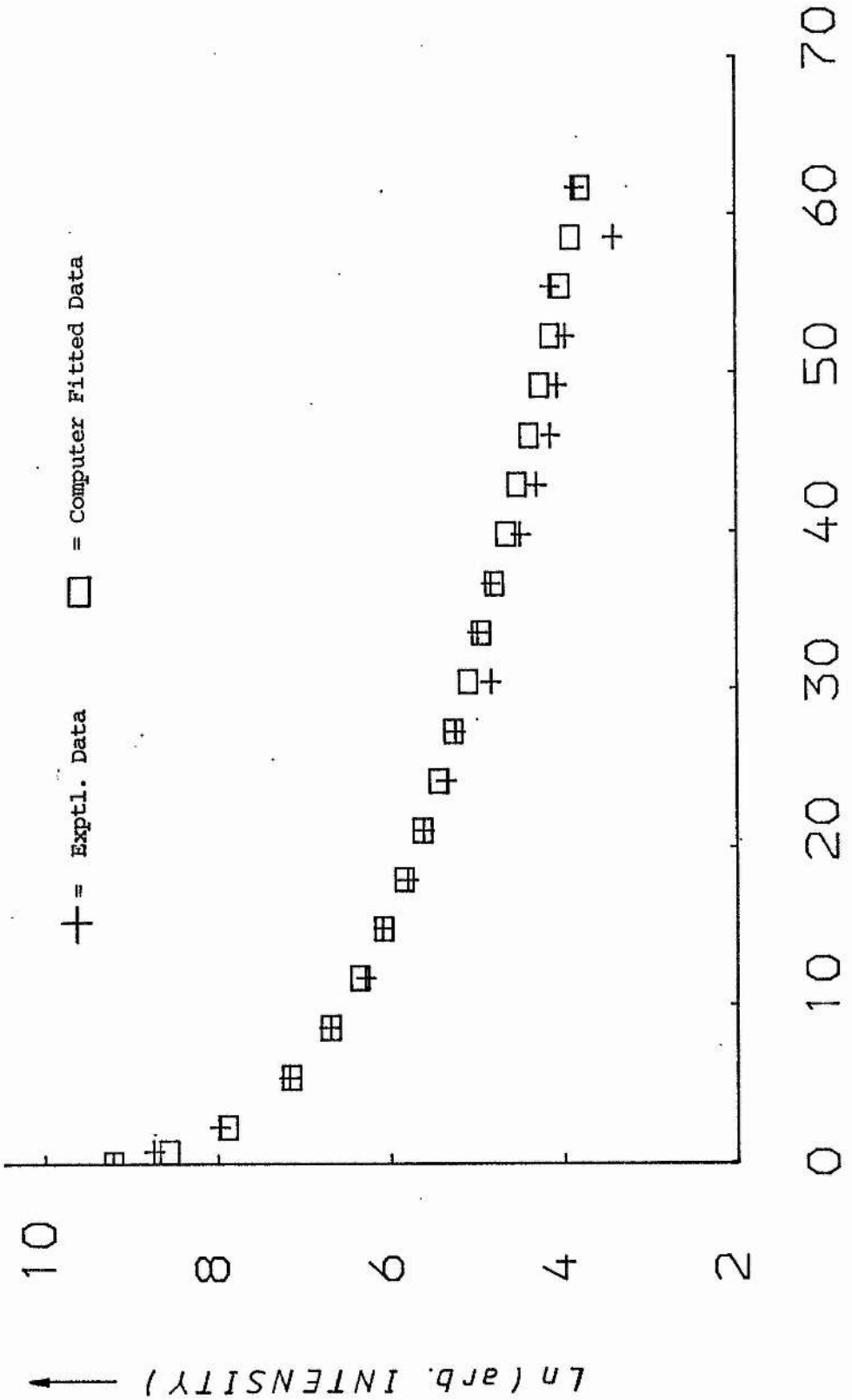
+ = Expt1. Data
□ = Computer Fitted Data
ln (arb. INTENSITY)
10
8
6
4
2
0
10
20
30
40
50
60
70
TIME / 10^-4 s

Figure 4.4

It is clear at this stage, that the triplet-triplet annihilation mechanism fits closely to the experimental decay data. However, this evidence alone is insufficient to identify this as being the only possible origin of the non-exponential decay. For this reason, it was decided to carry out experiments, using the spectrofluorimeter, to determine whether or not any emission from the S_1 state, arising from the triplet-triplet annihilation mechanism (specifically from process (4.12)), could be detected.

4.4.3 Prompt and Delayed Fluorescence

Fluorescence is the term given to radiative deactivation of an excited singlet state - usually S_1. However, it is clear that three different photophysical mechanisms can lead to S_1 formation and thus stimulate the production of fluorescence.

1) Absorption of light of suitable wavelength to populate the S_1 level, followed by $S_1 \longrightarrow S_o$ emission (via processes (1) to (3)).

2) Population of S_1 by thermal activation (process (8)) from the T_1 level.

3) Triplet-triplet annihilation, leading to formation of a molecule in the excited S_1 state.

The first mechanism discussed above involves only the singlet states and hence the transitions involved are all allowed (in the quantum mechanical sense). Thus fluorescence via mechanism (1) is rapid ($\tau \sim 10^{-8}$ to 10^{-9} s) and this is known as prompt fluorescence. Mechanisms (2) and (3), on the other hand, involve population of the T_1 level as a precursor to fluorescence. The $T_1 \longrightarrow S_o$ transition is forbidden and hence the lifetime of the T_1 state is long ($\tau \sim 10^{-3}$ s

for ketones and of the order of 10^1 s in the case of aromatic hydrocarbons). Because of this, population of the S_1 level via mechanisms (2) and (3) proceeds slowly, and for this reason the resulting emission is known as delayed fluorescence. Specifically, fluorescence arising from mechanisms (2) and (3) are known as "E-type" and "P-type" delayed fluorescence respectively. These names derive from the molecules from which the emission mechanisms were first observed - Eosin in the case of E-type[116] and pyrene for P-type[117].

Fluorescence emission, arising from all three mechanisms, has been observed by M.W. Wolf et al.[102] for benzophenone in fluid solution. However, as a result of the very efficient intersystem crossing (process (6)) for ketones in general and benzophenone in particular, prompt fluorescence emission is a very inefficient process[108].

4.4.4 Delayed Fluorescence Measurements

The total emission spectrum, obtained from the spectrofluorimeter, of a benzophenone/PMMA film at 77 K, excited at 337 nm is shown in Figure 4.5(b). This may be identified as the phosphorescence emission spectrum for benzophenone, which has been well established in the literature[118]. Thus at this lower temperature, no fluorescence of any kind was observed. When the emission spectrum was obtained at room temperature, however, a tail

Figure 4.5(a) Room Temperature Benzophenone Emission Spectrum

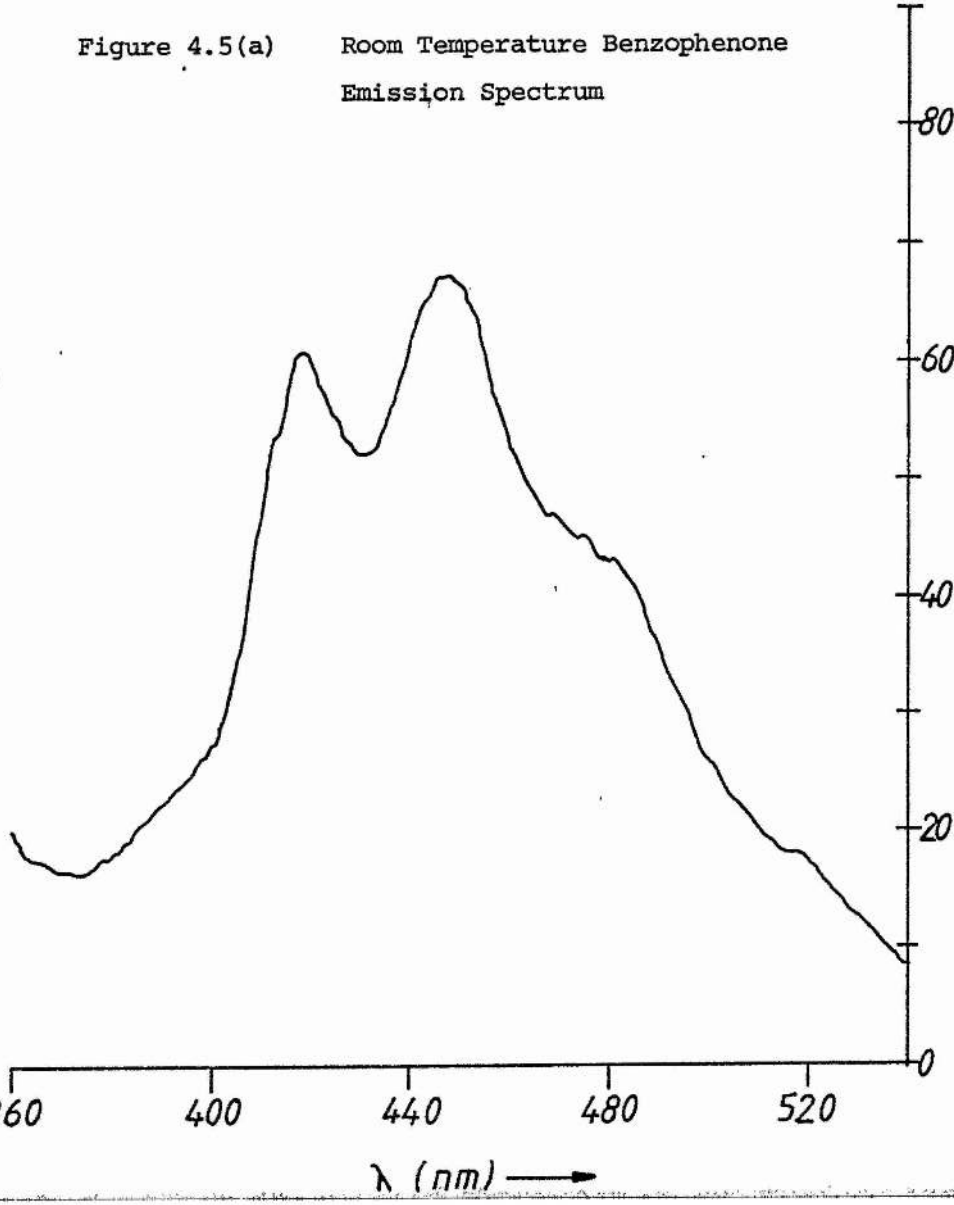

Figure 4.5(b) Benzophenone Emission Spectrum at 77K

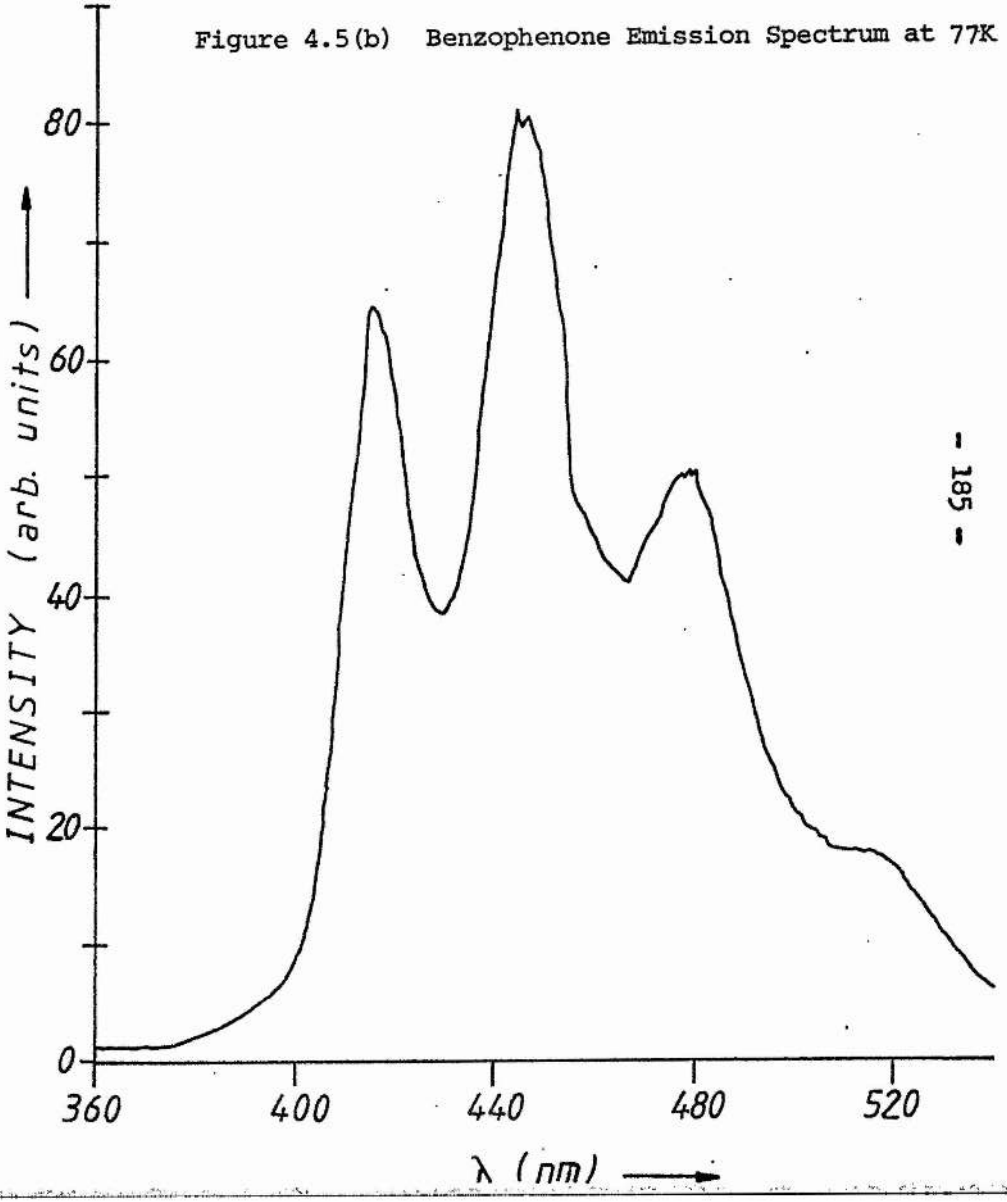

was observed at the high energy edge (ca. 390 nm, as shown in Figure 4.5(a)). The position of this feature coincides, precisely, with the position of the fluorescence band observed by M.W. Wolf et al.[102]. Clearly, this must correspond to delayed fluorescence, as if it were prompt, there would be no reason why it should not be observed at 77 K. In order to test whether the delayed fluorescence was of E-type, a series of experiments was carried out to examine the effect of varying temperature on the intensity of delayed emission.

An expression was derived previously (equation 4.8) for the phosphorescence efficiency, $\emptyset_p$. In a similar way, the efficiency of E-type delayed fluorescence, $\emptyset_e$, may be given as:

$$\emptyset_e = k_e \emptyset_t \emptyset_f / (k_p + k_m + k_q[q] + k_e) \qquad (4.16)$$

where $\emptyset_f$ is the prompt fluorescence efficiency, all other symbols as defined previously. Thus:

$$\emptyset_e / \emptyset_p = k_e \emptyset_f / k_p \qquad (4.17)$$

Since k_e represents thermal activation from T_1 to $T_1^{n'}$ (the latter state being assumed to be of equal energy to S_1) it may be represented by an Arrhenius relationship:

$$k_e = A \exp(-\Delta E/RT) \qquad (4.18)$$

with A being the pre-exponential factor and ΔE the necessary thermal energy barrier. An energy level diagram for benzophenone,

illustrating the thermally induced repopulation of the S_1 level is shown in Figure 4.6. Substitution of equation (4.18) in equation (4.17) leads to:

$$\Phi_e/\Phi_p = (\Phi_f/k_p)\ A\ \exp(-\Delta E/RT) \qquad (4.19)$$

Hence, a plot of $\ln(\Phi_e/\Phi_p)$ against 1/T should yield a straight line of slope = $-\Delta E$.

Equation (4.19) has been used previously by other workers, even for molecules which do possess appreciable prompt fluorescence efficiencies[119]. Such experiments require a "chopper" apparatus to record the emission spectrum, after the prompt fluorescence component has decayed. However, this chopping technique is best applied to molecules which have long phosphorescence lifetimes (of the order of seconds). Because of this, allied to the very efficient intersystem crossing step for benzophenone[108], the assumption was made that all fluorescence observed was of the delayed type and hence the chopper technique was not employed. Furthermore, it was assumed that the efficiencies of delayed fluorescence and phosphorescence were proportional to their respective emission intensities, I_e and I_p, thereby following the procedure of C.A. Parker and C.G. Hatchard[119]. Hence:

$$\Phi_e/\Phi_p = I_e/I_p \qquad (4.20)$$

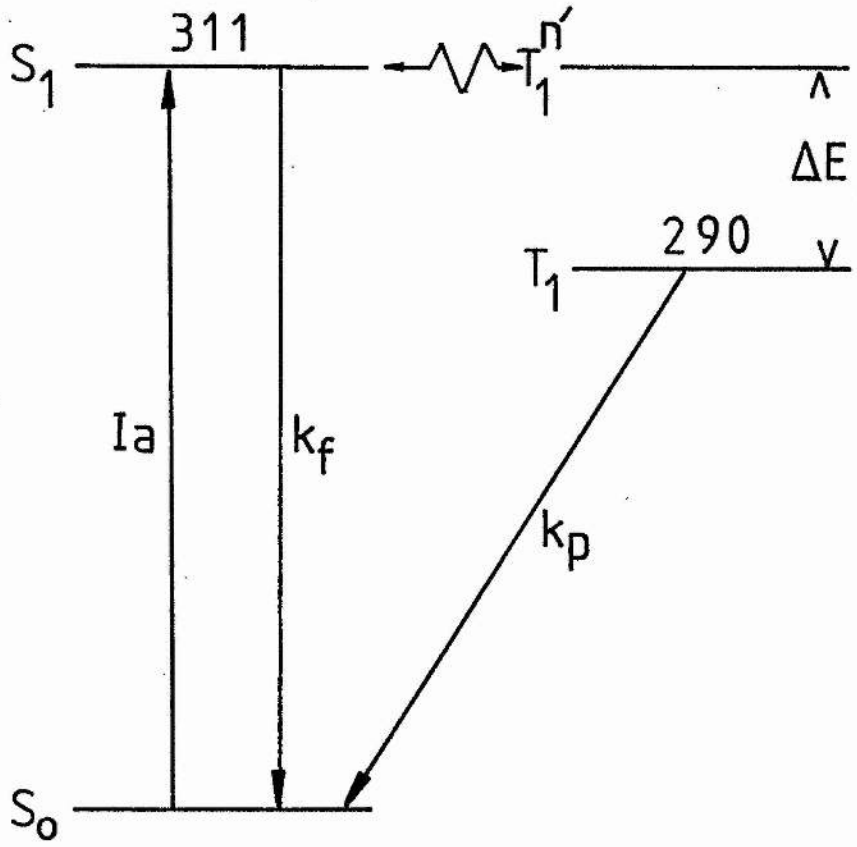

Figure 4.6 Energy level diagram for benzophenone (units are kJ mol^{-1})

On the basis of the arguments given above, the delayed fluorescence and phosphorescence emission intensities were monitored for a benzophenone/PMMA film (containing ca. 1×10^{-2} mol dm^{-3} benzophenone) from 77 K up to room temperature, using the experimental method outlined in the Experimental section. Three emission wavelengths were specifically studied: 390 nm, 446 nm and 480 nm; the first of these being associated with delayed fluorescence and the second and third with phosphorescence band maxima. The reason for monitoring two phosphorescence emission intensities at a given temperature was that it yielded two sets of experimental data, thus providing a consistency check. The resulting plots of $\ln(I_e/I_p)$ vs $1/T$ are shown in Figure 4.7 (for I_p = intensity at 446 nm) and Figure 4.8 (for I_p = intensity at 480 nm).

It is clear from Figures 4.7 and 4.8 that on increasing the temperature to ca. 200 K a transition region is reached. Increasing the temperature beyond this point leads to a rapid and linear variation in $\ln(I_e/I_p)$ with $1/T$. Linear regression analysis over this steep region enables a value for ΔE to be calculated. The results of this treatment, for each plot, are tabulated in Table 4.1.

Table 4.1: Analysis of Linear Regions in Delayed Fluorescence Data

I_p EMISSION (nm)	CORR. COEFF. (r)	INTERCEPT	CALCULATED ΔE (kJ mol^{-1})
446	-0.99	7.9	20.7
480	-1.00	8.6	18.8

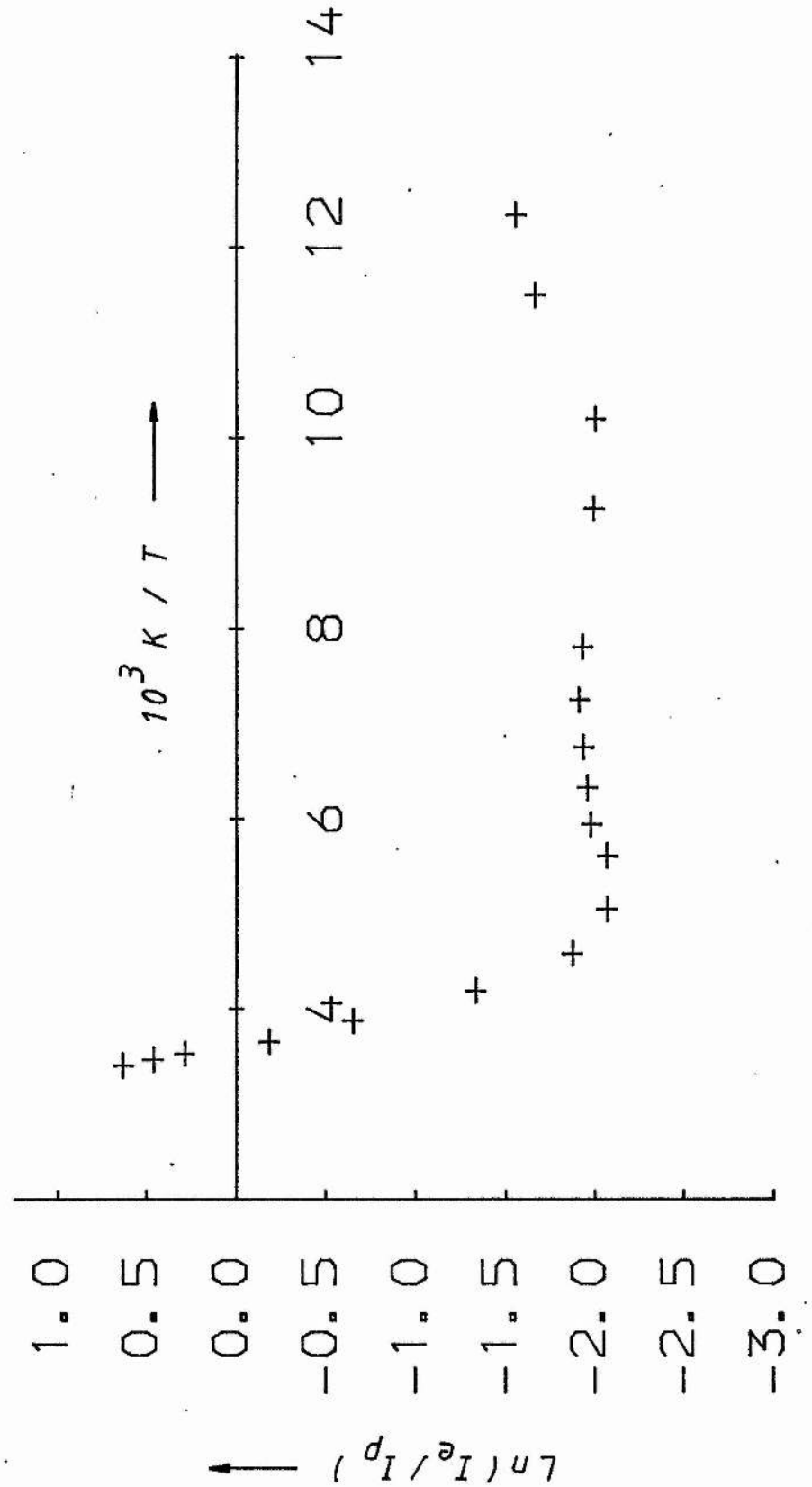

Figure 4.7

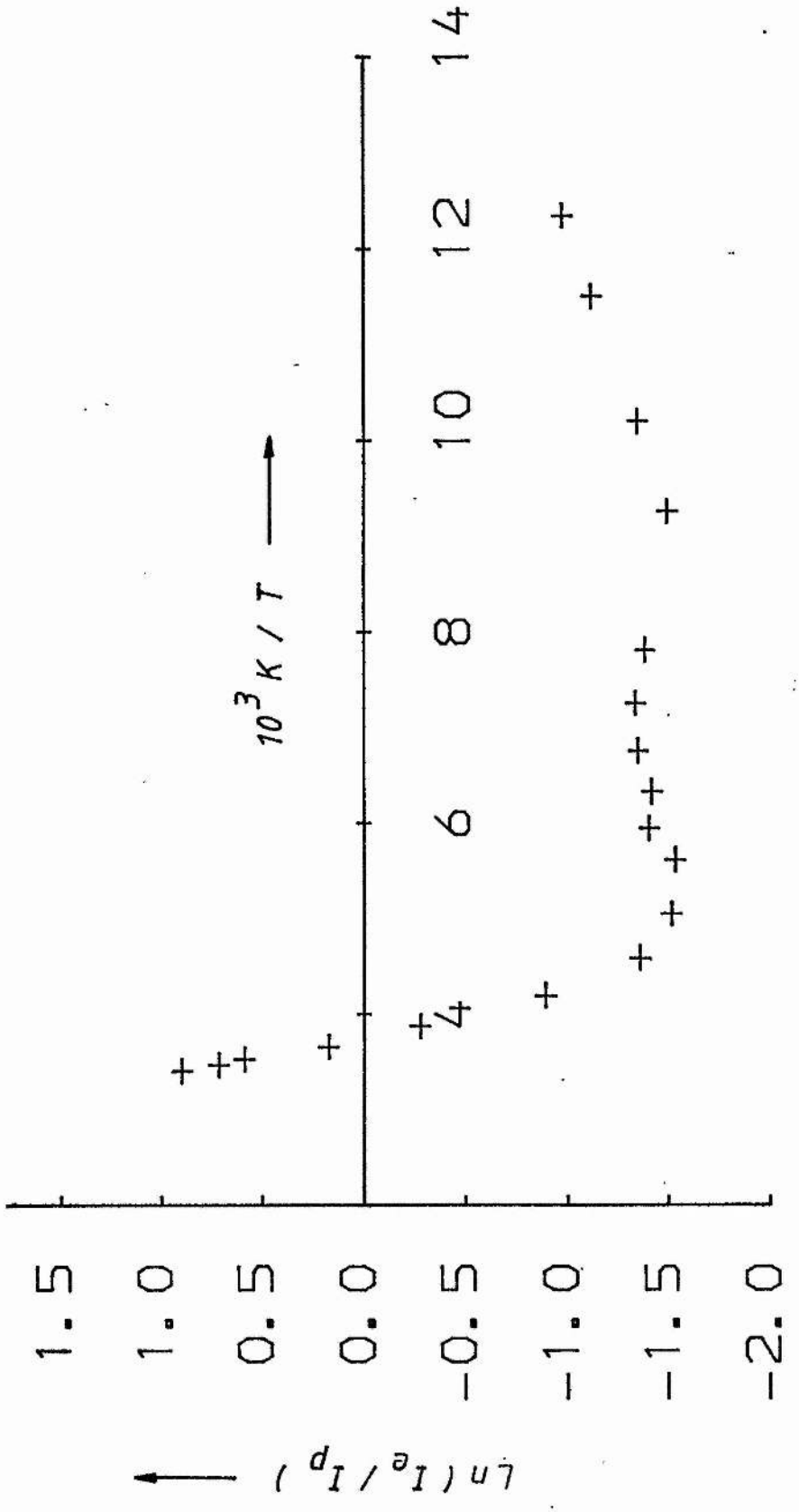

Figure 4.8

The values for ΔE shown in Table 4.1 are in excellent agreement with the value of 20.5 kJ mol^{-1} for the $S_1 - T_1$ energy gap calculated by M.W. Wolf et al.[102] for benzophenone in benzene solution. In addition, the agreement between the plots employing the two different phosphorescence bands is good (uncertainty of ca. 10%).

The results above suggest that the delayed fluorescence, observed from benzophenone, is derived from thermal activation and hence E-type. However, as J.B. Birks points out[120], the production of E-type delayed fluorescence does not introduce non-exponentiality into the triplet decay. It is interesting to compare the transition region for the E-type delayed fluorescence, beginning at ca. 200 K with that observed by K.T. Moran for the onset of the non-exponential decay of benzophenone phosphorescence in PMMA at ca. 196 K[90]. This close similarity suggests that similar levels of activation must be attained before both sets of phenomena can be observed.

The experimental observations of non-exponential phosphorescence decay (which may be modelled by a triplet-triplet annihilation mechanism) and E-type delayed fluorescence may be reconciled if a triplet level of PMMA itself is involved. It has been suggested that such a state may be situated close, in terms of energy, to the S_1 level of benzophenone. Thus on thermal activation of the photoexcited benzophenone/PMMA system, two possible paths would be open to the benzophenone triplet state molecules. The first possibility would involve transfer to the S_1 level of benzophenone with subsequent emission of the E-type delayed fluorescence. The alternative pathway

would require energy transfer to the PMMA T_1 state. Migration of this energy could then occur[121], being eventually trapped by another benzophenone triplet. Phosphorescence emission from this second path would be non-exponential and would follow the triplet-triplet annihilation decay profile. This proposed dual pathway deactivation scheme for the triplet state benzophenone in PMMA is shown in Figure 4.9.

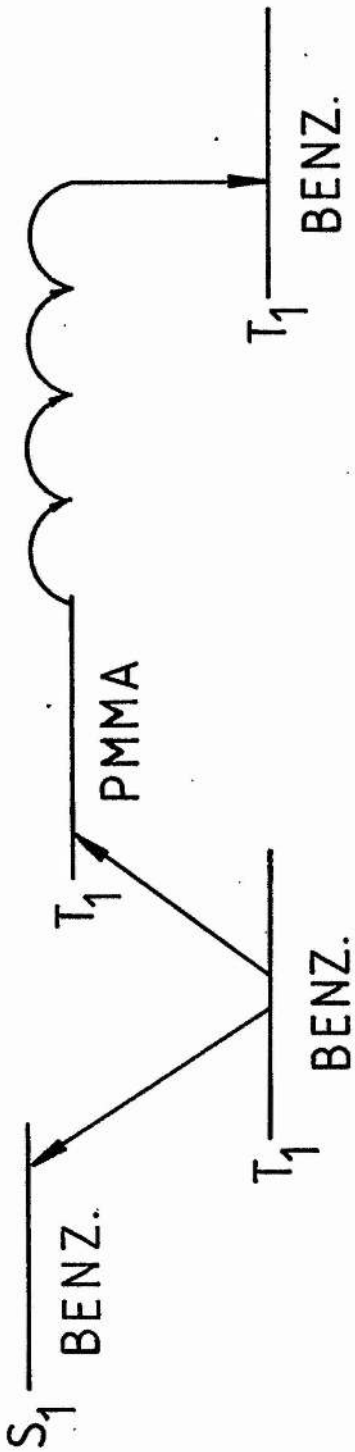

Figure 4.9 Dual deactivation pathway for benzophenone

4.5 Conclusion

Delayed fluorescence has been observed from benzophenone in PMMA films and the experimental evidence is consistent with this being E-type. In addition, the non-exponential phosphorescence decay profile of benzophenone has been adequately modelled by a triplet-triplet annihilation mechanism which may involve the mediation of the first triplet level of PMMA. However, the possibility that some alternative non-exponential decay mechanism could describe this decay profile cannot be ruled out.

It is clear that the photophysical behaviour of benzophenone (and by inference ketones in general) is complicated. The results suggest that once the ketone is formed - due to the participation of TiO_2 or some other initiating agent - a certain amount of energy migration, possibly involving the polymer, is involved. Since photoexcited ketones can promote polymer chain scission, this migration will be an important step in determining the life of a polymer in a practical environment.

APPENDICES

APPENDIX I

Curve Fitting

Introduction

At various stages throughout this work, use has been made of techniques of a statistical nature, in order to fit data either to a straight line or to some other non-linear function. The purpose of this section is to outline the methodology behind the fitting techniques which have been employed and to indicate the limitations of such procedures.

Least Squares Fit to a Linear Function

Consider a series of experimentally observed values, y_1, y_2, ---- y_i, as a function of the corresponding independent variables, x_1, x_2, ---- x_i. An example of this situation would be a series of intensity (y_i) measurements at several known time periods (x_i). If the experimental data are to be fitted to a straight line, this implies that the following relationship exists:

$$y_i = a + bx_i \qquad (A.1)$$

where a and b are constants.

In the ideal case, where the (x_i, y_i) data represent a perfect straight line; the numerical difference between the left and right hand sides of equation (A.1) should be zero. In a more realistic situation however, there will exist a discrepancy between each observed y_i value and that calculated from the right hand side of equation (A.1). These discrepancies (denoted by Δy_i) may be defined as follows:

$$\Delta y_i = y_i - a - bx_i \qquad (A.2)$$

A more useful parameter, which is used to quantify the difference between theoretical and experimental data is "Chi-Squared" (symbol χ^2). This is calculated from:

$$\chi^2 = \sum\left(\frac{\Delta y_i}{\sigma_i}\right)^2 = \sum\left(\frac{1}{\sigma_i^2}\,(y_i - a - bx_i)^2\right) \qquad (A.3)$$

where σ_i is the standard deviation associated with each experimental observation. (The power of 2 which appears in equation (A.3) overcomes the problems of the sign associated with a particular Δy_i value and ensures that the absolute magnitude of the various errors are taken into account).

Clearly, the minimisation of χ^2 ("least squares") can be employed as a means of obtaining a fit to experimental data. This minimisation procedure can be carried out by obtaining the partial derivatives of χ^2 with respect to coefficients a and b in equation

(A.3). The two resulting sets of simultaneous equations may be readily solved via matrix algebra to yield optimised values for each coefficient. These are:

$$a = \frac{\sum x_i^2 \sum y_i - \sum x_i \sum x_i y_i}{N \sum x_i^2 - (\sum x_i)^2} \qquad (A.4)$$

$$b = \frac{N \sum x_i y_i - \sum x_i y_i}{N \sum x_i^2 - (\sum x_i)^2} \qquad (A.5)$$

where N is the total number of (x_i, y_i) data points. These solutions do, however, assume that all standard deviation values are equal.

In addition to the a and b values described above, a third parameter is widely employed, as it provides a measure of how closely the experimental data can be fitted to a straight line. This parameter is known as the correlation coefficient, r, and is calculated via the following equation:

$$r = \frac{N \sum x_i y_i - \sum x_i \sum y_i}{\{N \sum x_i^2 - (\sum x_i)^2\}^{0.5} \{N \sum y_i^2 - (\sum y_i)^2\}^{0.5}} \qquad (A.6)$$

For experimental data lying on a perfect straight line, r has a value of unity. If no correlation exists between the x_i and y_i variables, then the value of r is zero. Furthermore, the sign of r is + or - for the case of an increasing or decreasing gradient respectively.

Because of the limitations on the applicability of the correlation coefficient, which have been highlighted recently[66], the value obtained should be considered along with the plot of the actual experimental data. The main reason for this is that genuine non-linear trends in experimental data, which are gradual, tend to possess r values very close to unity, whereas visual interpretation of the graph would clearly show the non-linear characteristics.

Least Squares Fit to an Arbitrary Function

The expression for χ^2, shown in equation (A.3), may be applied to any function, be it linear, parabolic, exponential or a complex mixture of non-linear terms. This is the case since χ^2 is merely a representation of the discrepancy between experimentally obtained values and those calculated from the chosen function.

The method involving matrix algebra to solve for the optimised parameters, a and b in equation (A.1), can also be applied to higher degree polynomials. However, as the degree of the polynomial increases so complexity of the calculations also increases dramatically. In general, a polynomial of degree "n" will require the solution of a $(n + 1) \times (n + 1)$ matrix. In addition, this matrix method cannot be utilised for cases in which functions contain exponential or trigonometric terms. Thus an alternative method of optimising unknown parameters must be used.

Several methods have been developed for fitting experimental data to an arbitrary function. These are all based on iterative optimisation techniques and as such are ideally suited for implementation using a computer. Various criteria were applied in selection of the most appropriate statistical fitting method. These were that the method had to be general - ie that it could be applied to various fitting functions. In addition, a balance had to be achieved between the efficiency (and hence complexity) of the method adopted and the time required to prepare and implement the computer program. The method which was finally adopted was a modification of the so-called "Grid-Search" technique utilised by P.R. Bevington[122].

Grid-Search Fitting Technique

As an example of the application of this fitting method, consider the specific case of fitting experimental data to a biexponential function of the following form:

$$y_i = a \exp(-b\, x_i) + c \exp(-d\, x_i) \qquad (A.7)$$

where a, b, c and d are the unknown parameters which are to be optimised to fit the experimental data.

On carrying out the fitting routine, the experimental (x_i, y_i) data must first be input to the computer, together with initial estimates for the unknown parameters. A value of χ^2 for these initial conditions is then obtained. The estimate of the first

parameter ("a" above) is then incremented by a preset amount ("DA") and the χ^2 value obtained once more. If the new value of χ^2 is less than that obtained initially, then the correct direction of adjustment for the first parameter has been found. If, however, the new χ^2 value is greater than the original, the sign of DA is reversed and the first parameter is decremented by this amount.

Once the sign of DA has been established, the parameter is successively altered by this amount until χ^2 is observed to increase - indicating that the minimum in the χ^2 value has been passed. Parabolic interpolation is then used to locate the actual minimum χ^2 value for the first parameter, using the three most recent χ^2 determinations, as shown in Figure A.1. The minimum in the parabola, a_{min}, may be obtained from the following equation:

$$a_{min} = a_3 - DA\left[\frac{\chi^2(3) - \chi^2(2)}{\chi^2(3) - 2\chi^2(2) + \chi^2(1)} + 0.5\right] \qquad (A.8)$$

Having optimised the value of "a" in this way, the procedure is repeated for the remaining parameters (b, c and d in the case of equation (A.7)). Finally, the entire sequence of optimising all the parameters is repeated until only very small changes in χ^2 are observed.

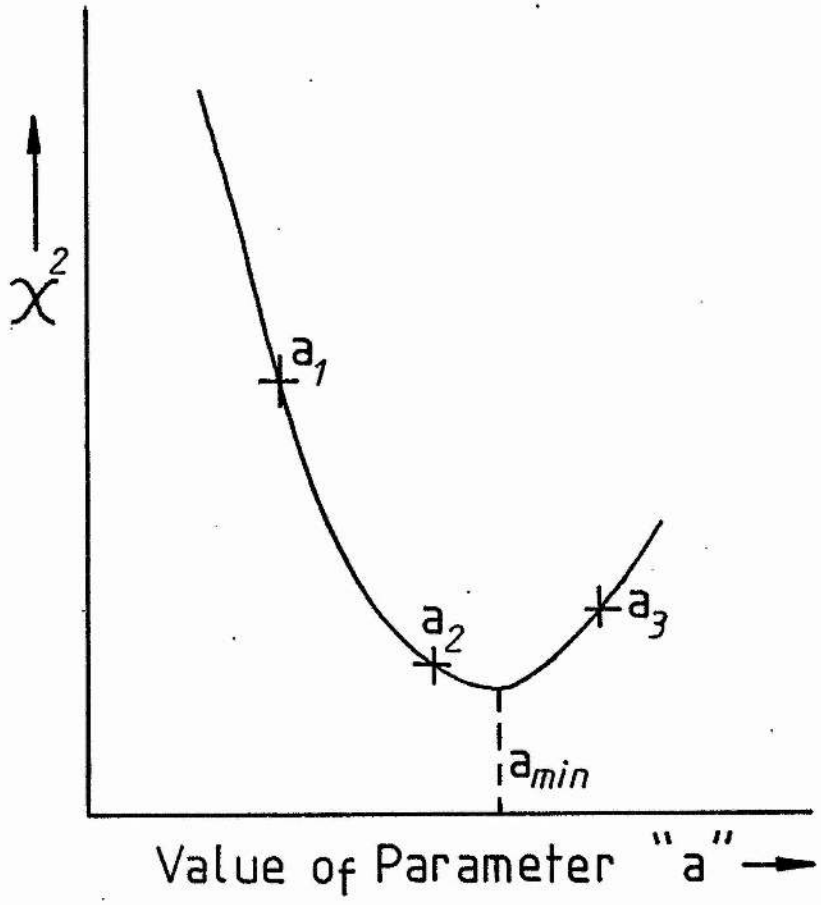

Figure A.1 Optimisation of unkown "a" by Parabolic Interpolation

Implementation of the Grid-Search Program

The Grid-Search program was written for the Apple II microcomputer using the BASIC programing language. A listing of this program is provided on page 204. Although slow in operation, the computational speed may be improved considerably by employing a BASIC compiler.

Unknown parameters are input into an array (A(I), where I = 1 up to the total number of parameters). Obviously, the greater the number of unknowns in the fitting function, the slower the program operation. The increment/decrement variable, DA, initially has a value of 1, but this is altered under program control to select the appropriate value for a given situation. The program itself is completely general; the only line which need be altered in order to fit data to a different test function is line 820. (The listing shown is set up for biexponential fitting). Finally, the program contains facilities for display of both the experimental and theoretical data on a VDU and for hard copy output of the optimised parameter and χ^2 values.

```
10 HOME
20 PRINT
30 XMAX=0:YMAX=0:CALCS=0
40 PRINT:INPUT"ENTER TOTAL NO. OF DATA PTS. ";MAX
50 DIM X(MAX),Y(MAX),C(35)
60 DIM XN(MAX),YN(MAX),F(MAX),FS(MAX)
70 FOR I=1 TO MAX
80   PRINT:INPUT"ENTER X COORD ";X(I)
90   INPUT"ENTER Y COORD ";Y(I)
100   IF X(I)>XMAX THEN XMAX=X(I)
110   IF Y(I)>YMAX THEN YMAX=Y(I)
120 NEXT I
130 REM NOW SCALE X AND Y COORDS
140 XSCALE=240/XMAX:YSCALE=70/YMAX
150 FOR I=1 TO MAX
160   XN(I)=INT(X(I)*XSCALE):YN(I)=INT(Y(I)*YSCALE)
170 NEXT I
180 PRINT:INPUT"ENTER TOTAL NO. OF UNKNOWN COEFFICIENTS ";AMAX
190 DIM A(AMAX)
200 FOR I=1 TO AMAX
210   PRINT:INPUT"ENTER ESTIMATE OF UNKNOWN(S) ";A(I)
220 NEXT I
230 PRINT:INPUT"ENTER THE ERROR LIMIT FOR CHI SQUARE ";BOUND
240 HOME:PRINT:PRINT
250 PRINT"PASS      CHI SQUARE"
260 P=0:DA=1
270 CSUM=100000!
280 IF CSUM<=BOUND THEN END
290   FOR J=1 TO AMAX
300     AHOLD=A(J)
310     GOSUB 780
320     REM J$=STR$(J)
330     REM PLOT 20,5,J$
340     REM HAVE NOW COMPUTED CHISQ
350     REM FOR INITIAL PARAMS->C(0)
360     C(0)=CSUM
370     TEST=A(J)
380     A(J)=A(J)+DA
390     GOSUB 780
400     DIRECT=CSUM
410     A(J)=TEST-DA
420     GOSUB 780
430     IF CSUM<DIRECT THEN DA=-DA
440     A(J)=TEST
450     REM SELECTS DIRECTION OF DECREASING CHI SQUARE
460     REM NOW MINIMISE THE CURRENT "A" PARAMETER
470     N=0
480     FLAG=0
490     IF FLAG=1 THEN N=0
500       REM D$=STR$(DA):PLOT 20,9,D$
510       N=N+1
520       A(J)=A(J)+DA
530       GOSUB 780
```

```
540        IF N>25 THEN DA=DA*2:A(J)=AHOLD:FLAG=1
550        IF N<=25 THEN FLAG=0
560       C(N)=CSUM
570      IF C(N)<=C(N-1) THEN GOTO 490
580      REM NOW TEST TO ENSURE >3 READINGS
590      REM OF CHI SQUARE TAKEN
600      IF N<3 THEN DA=DA/2:A(J)=AHOLD:GOTO 470
610      REM NOW CALCULATE THE OPTIMUM "A" VALUE
620      H1=C(N)-C(N-1)
630      H2=C(N)-2*C(N-1)+C(N-2)
640      HOLD=.5+(H1/H2)
650      MINA=A(J)-(DA*HOLD)
660      A(J)=MINA
670      DA=1
680    NEXT J
690    P=P+1
700    GOSUB 780
710    REM HAVE NOW COMPLETED ONE PASS
720    REM OF MINIMISATION W.R.T. EACH OF THE UNKNOWNS
730    PRINT P;"      ";CSUM
740    IF G>0 THEN GOSUB 1140
750    G=0
760    GOSUB 870
770 GOTO 280
780 REM SUBROUTINE TO CALCULATE
790 REM CHI SQUARE
800 CSUM=0
810 FOR I=1 TO MAX
820    F(I)=A(1)*EXP(-A(2)*X(I))+A(3)*EXP(-A(4)*X(I))
830    CSUM=CSUM+(Y(I)-F(I))^2
840 NEXT I
850 IF J>AMAX THEN GOTO 860
860 RETURN
870 REM GRAPHICS SUBROUTINE
880 REM TO PLOT CURRENT FIT (IF POSS.)
890 FOR I=1 TO MAX
900    FS(I)=INT(F(I)*YSCALE)
910    IF FS(I)>120 THEN RETURN
920    IF FS(I)<-35 THEN RETURN
930 NEXT I
940    HGR
950    HCOLOR=3
960    HPLOT 10,10 TO 10,158
970    HPLOT 0,120 TO 260,120
980    HCOLOR=9
990 FOR I=1 TO MAX
1000    HPLOT XN(I)+10,120-YN(I)
1010 NEXT I
1020 FOR I=1 TO 50
1030    PRINT
1040 NEXT I
1050 PRINT:PRINT"PASS=";P;"    CHI SQUARE=";CSUM
1060 HCOLOR=3
1070 HPLOT XN(1)+10,120-FS(1)
1080 FOR I=1 TO MAX-1
1090    HPLOT TO XN(I+1)+10,120-FS(I+1)
1100 NEXT I
1110 IF G>0 THEN LPRINT CHR$(25);"GM"
1120 G=0
1130 RETURN
```

```
1140 REM PRINT-OUT OF CURRENT BEST FIT
1150 HOME:TEXT:PRINT:PRINT
1160 PRINT"CURRENT BEST FIT COORDS ARE:"
1170 PRINT:PRINT"XCOORD","YCOORD","FIT-Y COORD"
1180 PRINT"-----------------------------------"
1190 FOR I=1 TO MAX
1200   PRINT X(I),Y(I),F(I)
1210 NEXT I
1220 PRINT:PRINT"CURRENT VALUE OF CHI SQUARE IS ";CSUM
1230 PRINT"CURRENT VALUES OF UNKNOWNS:"
1240 FOR I=1 TO AMAX
1250   PRINT"UNKNOWN";I;"=";A(I)
1260 NEXT I
1270 PRINT:PRINT"PLEASE PRESS ANY KEY TO CONTINUE"
1280 GET A$
1290 RETURN
```

APPENDIX II

```
10 REM A PROG. TO OPTIMISE K1 TO
20 REM CALCULATE THE CORRECTED UPTAKE DATA
90 DIM R(5),C(5),CA(5),H(5)
95 HOME
100 FOR X=1 TO 5
110   PRINT:PRINT:INPUT"ENTER MEASURED RATE VALUE ";R(X)
120   PRINT:INPUT"ENTER CYCLOHEX. CONCN. ";C(X)
130   PRINT:INPUT"ENTER C* VALUE ";CA(X)
140   PRINT:PRINT
150 NEXT X
170 K1=3.2E-11
180 GOSUB 1000
190 GOSUB 2000:I1=STORE
195 IF I1<0 THEN I1=I1*(-1)
200 K1=K1-(K1*.00001):REM SUBTRACT 0.001%
210 GOSUB 1000:GOSUB 2000
220 I2=STORE:IF I2<0 THEN I2=I2*(-1)
230 IF I2>I1 THEN PRINT"OPTIMUM VALUE OF K1=";K1+(K1*.001):END
240 IF I2<1E-15 THEN GOSUB 3000:END
250 GOTO 180
1000 FOR X=1 TO 5
1010   H(X)=R(X)-(K1*C(X))
1020 NEXT X
1030 RETURN
2000 REM LINEAR REGRESSION SUBROUTINE
2010 REM FIRST CALCULATE SXX,SYY AND SXY
2020 SUMX=0:SUMSQX=0:SUMY=0:SUMSQY=0:SUMXY=0
2030 FOR X=1 TO 5
2040   SUMX=SUMX+CA(X)
2050   SUMSQX=SUMSQX+(CA(X)*CA(X))
2060   SUMY=SUMY+H(X)
2070   SUMSQY=SUMSQY+(H(X)*H(X))
2080   SUMXY=SUMXY+(CA(X)*H(X))
2090 NEXT X
2100 SXX=SUMSQX-(SUMX*SUMX/5)
2110 SYY=SUMSQY-(SUMY*SUMY/5)
2120 SXY=SUMXY-(SUMX*SUMY/5)
2130 MEANX=SUMX/5
2140 MEANY=SUMY/5
2150 REM NOW CALCULATE REGRESSION PARAMETERS
2160 GRADIENT=SXY/SXX
2170 INTERCEPT=MEANY-(GRADIENT*MEANX)
2180 CORR=SXY/(SQR(SXX*SYY))
2190 STORE=INTERCEPT
2200 PRINT:PRINT K1,STORE,CORR
2210 RETURN
3000 LPRINT:LPRINT:LPRINT"C*","R(CORRECTED)"
3010 FOR X=1 TO 5
3020   LPRINT CA(X),H(X)
3030 NEXT X
3040 RETURN
```

APPENDIX III

```
 1: C
 2: C A PROG. WHICH FITS EXPTL.
 3: C DATA TO A T-T ANNIHILATION
 4: C MODEL
 5: C
 6: C CREATED BY IAN M. FRASER
 7: C ON 14/1/83
 8: C
 9:          DIMENSION YLN(110),T(110),FUNCT(110),Y(110)
10:          WRITE(3,110)
11:  110     FORMAT(1X,'T-T ANN. PROGRAM',/)
12:  140     FORMAT(F9.6)
13:          WRITE(3,145)
14:  145     FORMAT(1X,'ENTER (REAL) ESTIMATE OF KT ')
15:          READ(3,150) A
16:  150     FORMAT(F12.6)
17:          WRITE(3,155)
18:  155     FORMAT(1X,'ENTER (REAL) ESTIMATE OF KTT ')
19:          READ(3,150) B
20:          WRITE(3,160)
21:  160     FORMAT(1X,'ENTER TOTAL NO. OF EXPTL. PTS. ')
22:          READ(3,180) M
23:  180     FORMAT(I2)
24:          WRITE(3,185)
25:  185     FORMAT(1X,'ENTER TIME INTERVAL IN SECS ')
26:          READ(3,190) TIME
27:  190     FORMAT(F7.4)
28:          WRITE(3,193)
29:  193     FORMAT(1X,'ENTER THE SCALE FACTOR ')
30:          READ(3,140) SF
31:          WRITE(3,162)
32:  162     FORMAT(1X,'ENTER ESTIMATE OF I0 ')
33:          READ(3,150) T0
34:          WRITE(3,191)
35:  191     FORMAT(1X,'ENTER ERROR BOUND EG"0.01" ')
36:          READ(3,192) ERROR
37:  192     FORMAT(F7.4)
38:
39: C INITIAL PARAMS SET UP NOW INPUT INTENSITY DATA
40: C AND SCALE BACK LN(INT) VALUES TO THE ACTUAL LN(INT) VALUES
41:
42:          CALL OPEN (5,'DATA1   DAT',0)
43:          DO 10 I=1,M
44:            READ(6,140) YLN(I)
45:            YLN(I)=YLN(I)-ALOG(SF)
46:            Y(I)=EXP(YLN(I))
47:  10      CONTINUE
48:
49: C NEXT OBTAIN EXPTL. TIMES
50:
51:          CALL OPEN(7,'TIME1   DAT',0)
52:          DO 20 I=1,M
53:            READ(7,152) T(I)
54:  152       FORMAT(F14.10)
55:  20      CONTINUE
56:
57: C NOW START CURVE FITTING ROUTINE
58:
59:  24      K=0
60:          S1=0
```

```
      S2=0
      S3=0
      S4=0
      S5=0

 31   DO 40 I=1,M
        HOLD=EXP(-A*T(I))
        DUMP=1.00+((T0*B/A)*(1.00-HOLD))
        STORE=1.00/DUMP
        FUNCT(I)=STORE*(T0*HOLD)

C MODEL FUNCTION NOW SET UP
C NEXT,OBTAIN PARTIAL DERIV.
C OF FUNCT(I) W.R.T. KT

        DY=Y(I)-FUNCT(I)

        ST1=-1.00*(1.00/(DUMP**2))
        ST2=T0*HOLD*ST1
        ST3=(T0*B/A)*(T(I)*HOLD)
        ST4=(1.00-HOLD)*((-T0)*B*T0
     1  *B/(A*A))
        YA=((ST1*ST3)+ST4)*(T0*HOLD)
        ST5=STORE*((-T(I))*T0*HOLD)
        YA=YA+ST5

C NOW OBTAIN PARTIAL DERIV. OF FUNCT(I) W.R.T. KTT

        ST6=(T0/A)*(1.00-HOLD)
        YB=ST2*ST6

        S1=S1+(YA*YA)
        S2=S2+(YA*YB)
        S3=S3+(YB*YB)
        S4=S4+(YA*DY)
        S5=S5+(YB*DY)
 40   CONTINUE

C NOW CALCULATE INCREMENTS IN A AND B

      D=(S1*S3)-(S2*S2)
      DA=((S3*S4)-(S2*S5))/D
      DB=((S1*S5)-(S2*S4))/D

      A=A+DA
      B=B+DB
      X=ABS(DA/A) + ABS(DB/B)
      WRITE(3,463) X
 463  FORMAT(F10.4)

C IE DOES THE ERROR FALL WITHIN REASONABLE LIMITS?

      IF(X.LE.ERROR) GO TO 50
      IF(K.LT.1000) GO TO 60
      ICATCH=1

C IE CONVERGENCE CANNOT BE ACHIEVED

      GO TO 100
 60   K=K+1
```

```
121:
122: C IE NOT ACHIEVED CONVERGENCE YET
123:
124:          GO TO 31
125:  50      CONTINUE
126:
127: C MADE IT!->CONVERGENCE ACHIEVED
128:
129:          ICATCH=0
130:
131: C NOW NORMALISE MODEL COORDS AND TAKE LOGS
132:
133:          STORE=Y(1)/FUNCT(1)
134:          DO 70 I=1,M
135:            FUNCT(I)=STORE*FUNCT(I)
136:            IF(FUNCT(I).LE.0) GOTO 102
137:            FUNCT(I)=ALOG(FUNCT(I))
138:  70      CONTINUE
139:
140: C NOW OUTPUT THE RESULTS
141:
142:          IOPT=3
143:  72      WRITE(IOPT,220)
144:  220     FORMAT(1X,16X,'TRIPLET-TRIPLET ANNIHILATION FIT',/)
145:          WRITE(IOPT,240)
146:   240    FORMAT(1X,64('-'))
147:          WRITE(IOPT,260)
148:  260     FORMAT(1X,'!',5X,'TIME(SECS)',5X,'!',
149:      1   3X,'LN(EXPTL(INT))',3X,'!',4X,'LN(FIT(INT))',
150:      2   4X,'!')
151:          WRITE(IOPT,240)
152:
153: C NOW FILL IN THE TABLE
154:
155:          DO 83 I=1,M
156:            WRITE(IOPT,280) T(I),YLN(I),FUNCT(I)
157:  280       FORMAT(1X,'!',5X,F10.6,5X,'!',5X,
158:       1     F10.6,5X,'!',5X,F10.6,5X,'!')
159:            IF(IOPT.EQ.2) GOTO 83
160:            WRITE(IOPT,240)
161:  83      CONTINUE
162:          WRITE(IOPT,240)
163:
164: C NOW OUTPUT THE MODEL FIT PARAMS
165:
166:          WRITE(IOPT,300)
167:  300     FORMAT(/,10X,'T-T FIT DATA:',/)
168:          WRITE(IOPT,320)K
169:  320     FORMAT(5X,'CONVERGENCE AFTER ',I3,' ITERATION(S)',/)
170:          WRITE(IOPT,340)A
171:  340     FORMAT(5X,'COMPUTED VALUE OF KT=',F12.4,/)
172:          WRITE(IOPT,360)B
173:  360     FORMAT(5X,'COMPUTED VALUE OF KTT=',F11.4,/)
174:  100     IF(ICATCH.EQ.0) GO TO 73
175:  102     WRITE(3,520)
176:  520     FORMAT(1X,'FAILED TO GAIN CONVERGENCE',/)
177:
178: C NOW HAVE THE OPERTUNITY TO TRY AGAIN
179:
180:  73      IOPT=3
```

```
181:           WRITE(3,378)
182:  378      FORMAT(1X,'DO YOU WANT A COPY OF
183:       1   THESE RESULTS?->1=YES;0=NO ')
184:           READ(3,400) IPT
185:           IF(IPT.EQ.1) IOPT=2
186:           IF(IOPT.EQ.2) GOTO 72
187:           WRITE(3,380)
188:  380      FORMAT(1X,'ANOTHER RUN WITH DIFFERENT KT
189:       1   AND/OR DIFFERENT KTT ESTIMATES?->1=YES
190:       2   ;0=NO ')
191:           READ(3,400)ICHOSE
192:  400      FORMAT(I1)
193:           IF(ICHOSE.EQ.0) GO TO 170
194:
195: C ANOTHER RUN REQUESTED
196:
197:           WRITE(3,420)
198:  420      FORMAT(1X,'ANOTHER RUN REQUESTED',/)
199:           WRITE(3,440)
200:  440      FORMAT(1X,'INPUT NEW ESTIMATE FOR KT ')
201:           READ(3,150) A
202:           WRITE(3,460)
203:  460      FORMAT(1X,'INPUT NEW ESTIMATE FOR KTT ')
204:           READ(3,150) B
205:           WRITE(3,442)
206:  442      FORMAT(1X,'INPUT NEW IO ESTIMATE ')
207:           READ(3,150) TO
208:           GO TO 24
209:
210:  170      CONTINUE
211:
212: C IE NO NEW RUN REQUESTED,HENCE
213: C END THE PROGRAM
214:
215:           STOP
216:           END
```

REFERENCES

REFERENCES

1. B.I. Marshall, Pigments in Plastics, (Tioxide International).

2. J. Woning and R.A. Van Santen, Chem. Phys. Lett., 1983, 101(6), 541.

3. R.W.G. Wyckoff, Crystal Structures, (Interscience, New York, 1963).

4. H.G. Volz, G. Kampf and H.G. Fitzky, Farbe + Lack, 1972, 78, 1037.

5. N.S. Allen and J.F. McKellar, Photochemistry of Dyed and Pigmented Polymers, (Applied Science Publishers Ltd., London, 1980).

6. H.G. Volz, G. Kampf and A. Klaeren, XV Fatipec-Congress, Congressbook, (N.V.V.T., Amsterdam, 1980).

7. H.G. Volz, G. Kampf and A.Klaeren, Farbe + Lack, 1976, 82, 805.

8. H.G. Volz, G. Kampf, H.G. Fitzky and A. Klaeren, A.C.S. Symp. Ser., 1981, 151, 163.

9. R.B. Fox and T.R. Price, J. Appl. Polym. Sci., 1967, 11, 2373.

10. S.K.L. Li and J.E. Guillet, J. Polym. Sci., Polym. Chem. Ed., 1980, 18, 2221.

11. A.M. Trozzolo and F.H. Winslow, Macromolecules, 1968, 1, 98.

12. J.F. Rabek, XXIII IUPAC Congress, Boston USA, (Butterworths, London, 1971, 8).

13. C.E.H. Bawn and S.A. Chaudhri, Polymer, 1968, 9, 81.

14. J. Kresta and J. Majer, J. Appl. Polym. Sci., 1969, 13, 1859.

15. S.H. Zeronian, J. Textile Res., 1971, 41, 184.

16. N.S. Allen, D.J. Bullen and J.F. McKellar, J. Mater. Sci., 1979, 14, 759.

17. T.A. Skowronski, J.F. Rabek and B. Ranby, Polym. Deg. Stab., 1984, 8, 37.

18. C. Gottfried and M.J. Dutzer, J. Appl. Polym. Sci., 1961, 5, 612.

19. P.J. Papillo, J. Paint Technol., 1968, 40, 359.

20. W.L. Hawkins, Polymer Stabilization, (Wiley, New York, 1972).

21. J.B. Howard and H.M. Gilroy, Polym. Eng. Sci., 1969, 9, 286.

22. V. Schafer, Appl. Polym. Symp., 1967, 4, 111.

23. G. Irick, J. Appl. Polym. Sci., 1972, 16, 2387.

24. C.H. Rochester, J. Graham and R. Rudham, J. Chem. Soc., Faraday Trans. 1, 1984, 80, 2459.

25. G. Munuera and F.S. Stone, Disc. Faraday Soc., 1971, 52, 205.

26. R.B. Cundall, R. Rudham and M.S. Salim, J. Chem. Soc., Faraday Trans. 1, 1976, 1642.

27. P.R. Harvey, R. Rudham and S. Ward, J. Chem. Soc., Faraday Trans. 1, 1983, 79, 1381.

28. P.R. Harvey, R. Rudham and S. Ward, J. Chem. Soc., Faraday Trans. 1, 1983, 79, 2975.

29. A.R. Gonzalez-Elipe, G. Munuera and J. Soria, J. Chem. Soc., Faraday Trans. 1, 1979, 75, 748.

30. N. Grassie and N.A. Weir, J. Appl. Polym. Sci., 1965, 9, 963.

31. E.F. Caldin, Fast Reactions in Solution, (Blackwell Scientific Publications, Oxford, 1964).

32. J.L. Latham, Elementary Reaction Kinetics, (Butterworths, London, 1964).

33. R.J. Wilcock and R.Battino, J. Chem. Therm., 1978, 10, 817.

34. J.G. Calvert and J.N. Pitts, Photochemistry, (Wiley, New York, 1967).

35. T.A. Egerton and C.J. King, J. Oil Col. Chem. Assoc., 1979, 62, 386.

36. M.D. Lumb, Luminescence Spectroscopy, (Academic Press, London, 1978).

37. F. Wilkinson, Chemical Kinetics and Reaction Mechanisms, (Van Nostrand, New York, 1980).

38. D. Piszkiewicz, Kinetics of Chemical and Enzyme Catalyzed Reactions, (Oxford University Press, New York, 1977).

39. P.F. Cornaz et al., Disc. Faraday Soc., 1966, 41, 290.

40. R.D. Iyengar et al., J. Am. Chem. Soc., 1966, 88, 5055.

41. H.P. Boehm, Disc. Faraday Soc., 1971, 52, 264.

42. S.P. Fairgrieve and J.R. MacCallum, Polymer Comm., 1984, 25(2), 44.

43. P.W. Atkins, Physical Chemistry, (Oxford University Press, Oxford, 1978).

44. G.C. Pimentel and A.L. McClellan, The Hydrogen Bond, (W.H. Freeman and Co., New York, 1960).

45. A.N. Fletcher and C.A. Heller, J. Phys. Chem., 1967, 71(12), 3742.

46. S. Krimm, J. Chem. Phys., 1955, 23, 1371.

47. A. Reiser, A. Kimla and J. Hajek, Collec. Czech. Chem. Comm., 1954, 19, 4.

48. B. Ya. Levin, Zhur. Fiz. Khim., 1954, 28, 1399.

49. J.D. Lambert, Disc. Faraday Soc., 1953, 15, 226.

50. N.H. Fletcher, The Chemical Physics of Ice, (Cambridge University Press, Cambridge, 1970).

51. P.Hobza and C. Sandorfy, Proc. Natl. Acad. Sci. USA, 1983, 80(10), 2859.

52. N.D. Coggeshall and E.L. Saier, J. Am. Chem. Soc., 1951, 73, 5414.

53. N.D. Coggeshall, J. Chem. Phys., 1950, 18, 980.

54. P. Traynard, Bull. Soc. Chim. France, 1947, 316.

55. W.M. Latimer, Chem. Rev., 1949, 44, 59.

56. J.D. Lambert and E.D.T. Strong, Proc. Royal Soc. (London), 1950, 200A, 566.

57. J.A. Davison, J. Am. Chem. Soc., 1945, 67, 228.

58. M. Puchalik, Acta Phys. Polon., 1954, 13, 159.

59. G.J. Korinek and W.G. Schneider, Canad. J. Chem., 1957, 35, 1157.

60. J.C. Davis, K.S. Pitzer and C.N.R. Rao, J. Phys. Chem., 1960, 64, 1744.

61. J.A. Pople, W.G. Schneider and H.J. Bernstein, Nuclear Magnetic Resonance Spectroscopy, (McGraw Hill, New York, 1959).

62. T.M. Connor and C. Reid, J. Molec. Spec., 1961, 7, 32.

63. M. Martin, J. Chim. Physique, 1962, 59, 736.

64. A.B. Littlewood and F.W. Willmott, Trans. Faraday Soc., 1966, 62(12), 3287.

65. R.E. Day, G.D. Parfitt and J. Peacock, Disc. Faraday Soc., 1971, 52, 264.

66. P.F. Tiley, Chem. Br., 1985, 21, 162.

67. G. Svehla, Vogel's Textbook of Macro and Semmimicro Qualitative Inorganic Analysis, (Longman, London, 1979).

68. J. Muhlebach, K. Muller and G. Schwarzenbach, Inorg. Chem., 1970, 9(11), 2381.

69. D. Schwarzenbach, Inorg. Chem., 9(11), 2391.

70. W.A. Noyes, G.S. Hammond and J.N. Pitts, Advances in Photochemistry, Vol I, (Wiley, New York, 1963).

71. L.E. Orgel, Introduction to Transition Metal Chemistry: Ligand Field Theory, (Methuen, London, 1966).

72. R.O.C. Norman and P.R. West, J. Chem. Soc. (B), 1969, 389.

73. A.R. Gonzalez-Elipe, J. Soria and G. Munuera, Chem. Phys. Lett., 1978, 57(2), 265.

74. M.A. Malati and N.J. Seager, J. Oil Col. Chem. Assoc., 1981, 64, 231.

75. P.C. Gravelle et al., Disc. Faraday Soc., 1971, 52, 264.

76. N.F. Mott and R.W. Gurney, Electronic Processes in Ionic Crystals, (Dover Publications, New York, 1964).

77. H.W. Gundlack and K.E. Heisler, Z. Phys. Chem. (Wiesbaden), 1978, 112, 101.

78. M.A.J. Rodgers and E.L. Powers, Oxygen and Oxy Radicals in Chemistry and Biology, (Academic Press, 1981).

79. H. Courbon et al., J. Phys. Chem., 1977, 81(6), 550.

80. A. Tkac, Int. J. Radiat. Phys. Chem., 1975, 7, 457.

81. A.E. Cahill and T. Taube, J. Am. Chem. Soc., 1952, 74, 2312.

82. M.V. Rao et al., J. Phys. Chem., 1980, 84, 1987.

83. E.M. Ceresa et al., J. Mater. Sci., 1983, 18(1), 289.

84. D.M. Griffiths and C.H. Rochester, J. Chem. Soc., Faraday Trans. 1, 1977, 73, 1510.

85. G. Kaempf et al., Adv. Org. Coat. Sci., Technol. Ser., 1982, 4, 239.

86. R.D. Wieting, M.D. Fayer and D.D. Dlott, J. Chem. Phys., 1978, 69(5), 1996.

87. D.D. Dlott, M.D. Fayer and R.D. Wieting, J. Chem. Phys., 1978, 69(6), 2752.

88. S. Coluccia and A.J. Tench, J. Chem. Soc., Faraday Trans. 1, 1983, 79, 1881.

89. J.Guillet, Polymer Photophysics and Photochemistry, (Cambridge University Press, Cambridge, 1985).

90. K.T. Moran, Ph.D. Thesis, University of St. Andrews, 1982.

91. M.E. Green and A. Turk, Safety in Working with Chemicals, (MacMillan, New York, 1978).

92. R.A.Smith, Semiconductors, (Cambridge University Press, Cambridge, 1959).

93. W.O. Lundberg, Autoxidation and Antioxidants, (Wiley, New York, 1962).

94. G.A. Russell and R.F. Bridger, J. Am Chem. Soc., 1963, 85, 3765.

95. D.G. Hendry and G.A. Russell, J. Am. Chem. Soc., 1964, 86, 2371.

96. Yu. A. Ershov et al., Kinet. Kataliz., 1964, 5, 752.

97. Yu. A. Ershov et al., Kinet. Kataliz., 1966, 7, 597.

98. S.S. Stivala and L. Reich, Polym. Eng. Sci., 1965, 5, 179.

99. L. Reich and S.S. Stivala, J. Polym. Sci. (B), 1965, 227.

100. J.L.R. Williams, Fortschr. Chem. Forsch., 1969, 13, 227.

101. R.E. Brown, L.A. Singer and J.H. Parks, Chem. Phys. Lett., 1972, 14(2), 193.

102. M.W. Wolf et al., J. Am. Chem. Soc., 1975, 97(16), 4490.

103. H.L.J. Backstrom and K. Sandros, Acta Chem. Scand., 1958, 12, 823.

104. P.W. Shallis, Proc. SAC Conf., Nottingham, (Heffer, Cambridge, 1965).

105. E.D. Owen and R.J. Bailey, J. Polym. Sci., A1, 1972, 10, 113.

106. C.A. Parker, Photoluminescence of Solutions, (Elsevier, Amsterdam, 1968).

107. J.N. Pitts et al., Photochem. Photobiol., 1965, 4, 305.

108. J.M. Morris and D.F. Williams, Chem. Phys. Lett., 1974, 25, 312.

109. J.A. Bell, M. Berger and C. Steel, Chem. Phys. Lett., 1974, 28(2), 205.

110. Th. Forster, Disc. Faraday Soc., 1959, 27, 7.

111. D.L. Dexter, J. Chem. Phys., 1953, 21(5), 836.

112. M. Inokuti and F. Hirayama, J. Chem. Phys., 1965, 43(6), 1978.

113. I.M. Fraser, J.R. MacCallum and K.T. Moran, Eur. Polym. J., 1984, 20(5), 425.

114. A. Salmassi and W. Schnabel, Polym. Photochem., 1984, 5, 215.

115. R. La Fara, Computer Methods for Science and Engineering, (Intertext, London, 1973).

116. S. Boudin, J. Chim. Phys., 1930, 27, 285.

117. C.A. Parker and C.G. Hatchard, Trans. Faraday Soc., 1963, 59, 284.

118. P.F. Jones and A.R. Calloway, Chem. Phys. Lett., 1971, 10(4), 438.

119. C.A. Parker and C.G. Hatchard, Trans. Faraday Soc., 1961, 57, 1894.

120. J.B. Birks, Organic Molecular Photophysics, Vol. 2, (Wiley, London, 1975).

121. R.B. Fox et al., J. Chem. Phys., 1972, 57, 534.

122. P.R. Bevington, Data Reduction and Error Analysis for the Physical Sciences, (McGraw-Hill, New York, 1969).